**CZECH TECHNICAL UNIVERSITY IN PRAGUE**

**Faculty of Civil Engineering**
**Department of Hydraulics and Hydrology**

# Experimental evaluation of precipitation estimates from commercial microwave links for rainfall-runoff modelling in a small urban catchment

## DOCTORAL THESIS

**Ing. Jaroslav Pastorek**

Doctoral study programme: Stavební inženýrství (Civil Engineering)
Branch of study: Vodní hospodářství a vodní stavby
(Water Engineering and Water Management)

Doctoral thesis tutor: Ing. Vojtěch Bareš, Ph.D.

**Prague, 2022**

# Declaration

I hereby declare that this thesis has been composed by myself under the guidance of the tutor Ing. Vojtěch Bareš, Ph.D.

I confirm that the thesis submitted is my own work and effort, except where work which has formed part of jointly-authored publications is included. Any additional sources of information from which I have quoted or drawn reference have been referenced fully in the text and in the list of references.

In Prague, on 22nd April 2022

.....
Jaroslav Pastorek

https://doi.org/10.14311/dis.fsv.2022.001

# Acknowledgements

I would like to thank everyone who supported my work on this project. In particular, I would like to thank Vojtěch Bareš, Martin Fencl, and David Stránský from CTU in Prague, and also Jörg Rieckermann, Andreas Scheidegger, and others from Eawag.

I would also like to thank T-Mobile Czech Republic, a.s., for providing the CML data, and especially Pavel Kubík for assisting with our numerous requests. I would also like to thank Pražská vodohospodářská společnost, a.s., for providing rainfall data from their rain gauge network, and Pražské vodovody a kanalizace, a.s., for carefully maintaining the flow meter and the rain gauges inside the experimental catchment.

I would like to thank the team around the ctuthesis LaTeX package which provided a template for this document.

The work on the thesis was supported by:

- the Czech Science Foundation (GAČR) under the projects no.
  - 14-22978S
  - 17-16389S
  - 20-14151J
- the Grant Agency of the Czech Technical University in Prague under the projects no.
  - SGS16/057/OHK1/1T/11
  - SGS17/064/OHK1/1T/11
  - SGS18/053/OHK1/1T/11
  - SGS19/045/OHK1/1T/11
  - SGS20/050/OHK1/1T/11

I owe a special thank you to Deep Thought for the answer to the ultimate question of life, the universe, and everything.

# Abstract

Quantitative precipitation estimates (QPEs) from commercial microwave links (CMLs) represent a promising source of innovative rainfall data which, however, has not been yet extensively investigated in hydrological modelling. We mean to experimentally evaluate the potential of CML QPEs for rainfall-runoff modelling in small urban catchments. We address the ability of individual CMLs of various characteristics to provide relevant QPEs for urban hydrology. We analyze how wet-antenna attenuation, a major source of bias in CML QPEs, can be adequately estimated without dedicated rainfall monitoring. Using discharge observations, we evaluate the performance of rainfall-runoff modelling with state-of-the-art CML QPEs and compare it with the performance of traditional rain gauge data. We employ stochastic error model calibrated by Bayesian inference to quantify uncertainties of the runoff predictions. The presented results show that QPEs from CMLs spatially corresponding to the catchment area can very well reproduce runoff dynamics. However, the bias common in QPEs from short CMLs, typically best fitting small urban catchments, has to be reduced to make the best use of this data. It is then presented how high-quality QPEs can be derived from CMLs of all path lengths, even when no additional rainfall data are available. Lastly, it is shown that, for rainfall-runoff modelling in small urban catchments covered by 1 rain gauge per roughly 20–25 km$^2$, CML QPEs represent a notable improvement. For networks with 1 gauge per 0.5–1 km$^2$, CML QPEs are a satisfying alternative.

**Keywords:** commercial microwave links, rainfall-runoff modelling, uncertainties, urban hydrology, wet-antenna attenuation

# Abstrakt

Kvantitativní srážkové odhady (QPE) z komerčních mikrovlnných spojů (CML) představují slibná inovativní srážková data, která však dosud nebyla intenzivněji prozkoumána v hydrologickém modelování. Cílem této práce je experimentálně vyhodnotit potenciál CML QPE pro srážko-odtokové modelování v malých městských povodích. Zabýváme se schopností jednotlivých CML různých charakteristik poskytovat relevantní QPE pro městskou hydrologii. Analyzujeme, jak lze útlum na mokré anténě, jeden z hlavních zdrojů chyb v CML QPE, věrohodně kvantifikovat bez monitorování srážek speciálně pro tento účel. Pomocí měření průtoků vyhodnocujeme kvalitu srážko-odtokového modelování za použití CML QPE odvozených nejaktuálnějšími metodami a porovnáváme ji s kvalitou modelování za použití tradičních dat ze srážkoměru. Ke kvantifikaci nejistot předpovězených průtoků používáme stochastický model chyb kalibrovaný pomocí Bayesovské inference. Prezentované výsledky ukazují, že QPE z CML které prostorově odpovídají ploše povodí, mohou velmi dobře reprodukovat dynamiku odtoku. Nicméně, aby se tato data co nejlépe využila, systematické chyby běžné v QPE z krátkých CML, které typicky nejlépe vystihují velikost malých městských povodím, musí být korigovány. Dále je prezentováno, jak lze získat vysoce kvalitní QPE z CML všech délek, i za okolností kdy nejsou k dispozici žádné další údaje o srážkách. Nakonec je ukázáno, že CML QPE mají potenciál značně vylepšit výsledky srážko-odtokového modelování v malých městských povodích pokrytých 1 srážkoměrem na přibližně 20–25 km$^2$. V porovnáni se srážkoměrnými sítěmi o hustotě 1 srážkoměr na zhruba 0,5–1 km$^2$, CML QPE představují uspokojivou alternativu.

**Klíčová slova:** komerční mikrovlnné spoje, městská hydrologie, nejistoty, srážko-odtokové modelování, útlum na mokré anténě

**Překlad názvu:** Experimentální vyhodnocení srážkových měření z komerčních mikrovlnných spojů pro srážko-odtokové modelování v malém městském povodí

# Contents

# Chapter 1

# Introduction

## 1.1 Motivation and goals

As the driving phenomenon of runoff mechanisms, rainfall plays an essential role in urban hydrology (Berne et al., 2004). Due to high degrees of imperviousness, relatively small scales, and high land-use spatial variability in urban areas, small-scale spatial and temporal rainfall variability can affect the hydrological response in terms of the hydrograph shape, peak flows, and their timing (Cristiano et al., 2017; Rico-Ramirez et al., 2015). Thus, when used as input for urban hydrological models, rainfall data represent one of the most prominent sources of uncertainty in the modelling process (Schellart et al., 2012; Thorndahl et al., 2008). Therefore, there are high requirements on the resolution of rainfall data for urban hydrology.

Berne et al. (2004) found that hydrological applications in urban catchments of the order of 1 $km^2$ require a resolution of about 3 min and 2 km. Moreover, the growing interest in fully distributed and grid-based models (Ochoa-Rodriguez et al., 2015; Ichiba et al., 2018), developments in geographic information systems, ever increasing data availability and computational power is expected to further strengthen the need for high-resolution rainfall data in urban hydrology (Ochoa-Rodriguez et al., 2019; Salvadore et al., 2015).

Operational management of the quantity and quality of urban stormwater runoff is a serious concern nowadays as excessive amounts of stormwater can overload drainage systems and cause urban pluvial flooding and health risks due to pathogens, decrease the efficiency of wastewater treatment plants, or impact the aquatic biota of receiving waters through hydraulic stress and pollution (Tsihrintzis & Hamid, 1997). The mitigation of such negative effects often relies on methods and concepts requiring operational rainfall products which are not only available in high spatiotemporal resolution, but also in

real time (Einfalt et al., 2004). However, standard rainfall observations are often not available online and/or in adequate resolutions. Therefore, much effort has been invested in investigating alternative rainfall sensors.

Commercial microwave links (CMLs) are pairs of telecom antennas which operate at frequencies where radio signal is attenuated by rainfall droplets. The difference between the transmitted and received signal levels can be used to derive path-integrated quantitative precipitation estimates (QPEs). About five million CMLs were operated worldwide in 2018 as a crucial part of telecom networks (Ericsson, 2018), covering urbanized areas especially densely. Moreover, CMLs can provide data in sub-minute temporal resolutions which are accessible in (near) real time from network operation centers either through network monitoring systems or specifically designed server-sided applications (Chwala et al., 2016). Therefore, QPEs derived from CMLs represent a very promising rainfall data source for urban hydrological modelling.

Thanks to the innovations introduced over the last decade, CML QPEs have proven to provide valuable rainfall information which could complement traditional observations with rain gauges and weather radars (Chwala & Kunstmann, 2019; Imhoff et al., 2020; Rios Gaona et al., 2018; Uijlenhoet et al., 2018). Nonetheless, to date, only a few studies investigated the ability of QPEs derived from real-world CML networks for quantitative hydrology, either for rural (Brauer et al., 2016; Cazzaniga et al., 2020; Smiatek et al., 2017) or urban catchments (Disch et al., 2019; Stránský et al., 2018). Therefore, many questions regarding their hydrological applications remain unanswered.

It has been shown that, if available in high temporal resolutions, CML QPEs could be conveniently used for urban hydrological modelling, and can lead to very well predicted temporal dynamics of runoff from a small urban catchment (Disch et al., 2019; Stránský et al., 2018). However, these findings are based on continuous adjusting of CML QPEs to reference data from traditional rain gauges, as systematic errors (bias) often associated with CML QPEs (Fencl et al., 2017; Chwala & Kunstmann, 2019) compromise their potential for hydrological applications where precipitation or runoff volume is of high importance. This is unfortunate because CML QPEs could be especially helpful in regions where the availability of long-term rainfall monitoring networks is limited (Gosset et al., 2016). Yet, it is not clear how to make the best use of the CML QPEs under such conditions.

The bias in QPEs is especially common for CMLs with short (ca. $< 2$ km) path lengths (Leijnse et al., 2008). Nevertheless, such QPEs could be particularly useful for urban hydrology as they often represent well the typical scales of small urban catchments. Moreover, shorter CMLs are better suited to capture small-scale rainfall spatial variability which is of high importance for urban hydrology. Uncertainties associated with such errors thus represent a major challenge to be overcome in order to maximize the benefits of the CMLs as a promising source of QPEs for urban hydrology.

It has also been argued that ignoring the uncertainty, particularly related to input rainfall data, compromises hydrological modelling (Beven, 2006; Kavetski et al., 2006), or similarly, that quantification of uncertainties associated with urban rainfall-runoff modelling is a must (Dotto et al., 2012). However, extensive quantification of the uncertainties related to applying CML QPEs in urban hydrology, and a comparison with traditional rainfall data uncertainty, has not been presented yet in relevant literature.

The main goal of the work presented in the thesis is to evaluate the potential of QPEs retrieved from CMLs for rainfall-runoff modelling in small urban catchments. This is to be accompanied by a robust quantification of uncertainties in the runoff predictions, both for traditional rain gauge data and for CML QPEs. In order to make the best use of these innovative rainfall data, we also investigate the following subsidiary research questions:

- Which factors (e.g. position relative to the catchment of interest, sensitivity to rainfall) most affect the suitability of individual CMLs to be used as a source of rainfall data for rainfall-runoff modeling?
- How can the CML QPE pre-processing routine be optimized to reduce the bias common in CML QPEs?
- Can high-quality CML QPEs be retrieved also when the availability of auxiliary rainfall data, e.g. from traditional rainfall monitoring networks, is considerably limited, which is a common challenge in urban hydrology?

## 1.2 Thesis outline

This thesis is an extensive but not exhaustive presentation of research efforts conducted by Jaroslav Pastorek as part of his doctoral studies, following the above defined research goals. Selected most relevant studies are presented in four individual chapters. However, these are preceded by an elaboration of the ideas and problems briefly introduced above.

First, in chapter 2, the thesis provides an overview of recent developments and the current state of rainfall monitoring in urban areas for quantitative hydrological purposes. Retrieving QPEs from CMLs is introduced as a promising way of obtaining high-resolution rainfall measurements, which, however, is associated with considerable uncertainties. Recent approaches to reducing these uncertainties are reviewed while acknowledging space for further improvements.

Different approaches to assessing the value of given rainfall data for urban hydrology are analyzed in chapter 3. A special attention is payed to the

importance of robust uncertainty evaluation when performing hydrological modelling. The model output uncertainty quantification method which is to be applied within the presented research is introduced and put in perspective.

Material used when performing simulations and analyses which resulted in this thesis is presented in chapter 4. This includes an extensive data set spanning over three years and containing both rainfall and runoff observations as well as a calibrated well-performing rainfall-runoff model.

Chapter 5 presents a first study exploring whether QPEs obtained from CMLs can be regarded as a viable source of rainfall data in the field of urban rainfall-runoff modelling. This study can be understood as "the pilot study" which has foreshadowed the direction of the subsequent research endeavors. This chapter represents a synthesis of two studies first published in Pastorek et al. (2017) and Pastorek et al. (2018).

Chapter 6 presents a study which addresses the ability of individual CMLs to provide relevant QPEs for urban rainfall-runoff modelling. It investigates in how far CML instrumental parameters (path length, transmission frequency) and network topology influence the rainfall-runoff modelling performance. This study was first published in Pastorek et al. (2019b).

Chapter 7 contains a study which analyzes how, when deriving CML QPEs, WAA can be estimated without dedicated rainfall monitoring. Various WAA estimation models, including a newly proposed one, based on considerably different assumptions are tested. The transferability of WAA model parameters among CMLs of various characteristics is also addressed. This study was first published in Pastorek et al. (2022)

Chapter 8 introduces a study exploring the possibilities to calibrate WAA estimation models using data that could be commonly available to urban hydrology specialists. This investigation is then leveraged to derive state-of-the-art CML QPEs, the suitability of which for urban rainfall-runoff modelling is then to be evaluated by means of model output uncertainty quantification.

Finally, in chapter 9, the most relevant findings from all the presented research are summarized and put to mutual perspective.

The bulk of the research presented in this thesis has been originally published in peer-reviewed journal or conference papers over the course of the past few years. The thesis thus partially documents the progress made within the research area. Therefore, although valid when first published, some statements, especially regarding the state of knowledge at the period, are outdated from the today's point of view. Thus, especially when chapters 5 and 6 are considered, the reader is kindly asked to perceive the presented research in the context of the time when it was first published.

# Chapter 2

# Rainfall monitoring for urban hydrology

## 2.1 Requirements on rainfall data for urban hydrology

From the hydrological point of view, urban catchments differ from natural ones in two fundamental aspects. Firstly, scales of areas examined in urban and natural catchment hydrology typically differ in orders of magnitude. Secondly, urban areas are covered by a high ratio of impermeable surfaces that not only limit rainfall infiltration, but also lead to more surface runoff (e.g. causing higher peak flows) and a faster response of the runoff process. Therefore, requirements on both temporal and spatial resolution of rainfall data are notably higher in urban catchments (e.g. Schilling, 1991; Berne et al., 2004). These requirements will further vary depending on the catchment size (Ochoa-Rodriguez et al., 2015), the climatic region (Berne et al., 2004), intended application (e.g. long-term analysis vs. online nowcasting Einfalt et al., 2004), or hydrological model complexity (semi- vs. fully-distributed Gires et al., 2015).

Berne et al. (2004) found that hydrological applications in urban catchments of the order of 1 $km^2$ require a resolution of about 3 min and 2 km. Notaro et al. (2013) concluded that temporal resolutions below 5 min and spatial resolutions of one rain gauge for each 1.7 $km^2$ is required. Ochoa-Rodriguez et al. (2015) recommended using rainfall temporal resolutions below 5 min and spatial resolution about 500 m for drainage areas between 1 ha and 100 ha, whereas 1-km resolution is recommended for drainage areas larger than 100 ha. Moreover, the growing interest in fully distributed and grid-based models (Ochoa-Rodriguez et al., 2015; Ichiba et al., 2018), developments in geographic information systems, ever increasing data availability and computational

power is expected to further strengthen the need for high-resolution rainfall data (Ochoa-Rodriguez et al., 2019; Salvadore et al., 2015).

Mitigation of the negative effects of urban drainage on society and the environment is nowadays often related to methods and concepts requiring operational rainfall products which are not only available in high spatial and/or temporal resolutions but as well in (near) real time (Einfalt et al., 2004). Such rainfall observations are employed in real-time control strategies to optimize treatment processes at wastewater treatment plants (Schütze et al., 2004), or to minimize the impacts of sewer overflows (Vezzaro & Grum, 2014). Furthermore, these data are used for extreme event analyses, e.g. for the evaluation of insurance damage claims (Spekkers et al., 2013) or for operational warnings (Montesarchio et al., 2009). Operational rainfall data are becoming increasingly important because of the ongoing climate change (van der Pol et al., 2015) as the intensity and frequency of heavy rainfall in many areas around the world are expected to increase (Willems et al., 2012).

## 2.2 Rainfall data retrieval and availability

Tipping bucket rain gauges represent the traditional way of retrieving precipitation measurements in urban areas. These devices provide relatively accurate rainfall estimates near the ground surface. On the other hand, they are prone to considerable uncertainties due to wind (Nešpor & Sevruk, 1999) and, especially relevant in urban conditions, obstructions by surrounding objects. Moreover, rain gauge records are in general representative only for a limited spatial extent. For instance, in a case study in northern Israel, Peleg et al. (2013) found that at least three rain stations in a specific configuration are needed to represent the rainfall data from a radar pixel of roughly 1.5 $km^2$ with a temporal resolution of about 3 min. Thus, due to their low densities, rain gauge networks very often fail to provide sufficient information on the rainfall with high spatiotemporal variability (Villarini et al., 2008). Moreover, these errors resulting from approximating an areal estimate using point measurements increase substantially with the decreasing aggregation time (Wood et al., 2000).

The development and use of weather radar quantitative precipitation estimates (QPEs) for hydrological applications has increased in recent decades (Berne & Krajewski, 2013; Thorndahl et al., 2017). Radars can survey large areas while providing rainfall data in resolutions of 500–2000 m every 5–15 min (Thorndahl et al., 2017). New generation X-band radars (e.g. Chen & Chandrasekar, 2015; Schleiss et al., 2020) can measure at even higher resolutions, but with a shorter range. However, weather radars provide indirect rainfall estimates measured hundreds of meters above ground relatively far away from the radar itself. Due to these inherent limitations of radar as a

rainfall measurement tool, the accuracy of radar measurements is in general insufficient, particularly in the case of extreme rainfall magnitudes (Bárdossy & Pegram, 2017; Thorndahl et al., 2017). Therefore, radar QPEs require adjustment to ground observations obtained typically from rain gauge networks (Harrison et al., 2009), although other data including urban stormwater runoff measurements have been employed as well (Ahm & Rasmussen, 2017).

The usage of weather radars for urban water management applications has been extensively investigated in the past decades and substantial progress has been made towards reliable high-quality data, however, many challenges remain unresolved. For example, adjusting radar data in an operational mode is both a methodological and technical challenge because rain gauge data are often delivered with a delay. Similarly, it is difficult to quantify uncertainty arising from the discrepancy between the catch area of a rain gauge (in the order of $10^{-2}$ m$^2$) and the area of a radar pixel (in the order of $10^4$–$10^6$ m$^2$) (e.g. Anagnostou et al., 1999). Nevertheless, many innovative radar-rain gauge merging techniques, which aim at combining the advantages while partially overcoming the individual weaknesses of the two data sources, have been recently developed (McKee & Binns, 2016). Such methods seem to have the potential to significantly improve the quality and applicability of radar and rain gauge rainfall estimates for hydrological tasks, however, there are still considerable challenges specific to urban applications, such as the availability of rain gauge data (or other ground truth) in adequate resolutions (Ochoa-Rodriguez et al., 2019). Next, the small-scale spatial structure reflecting local rainfall extremes, critical for urban hydrology applications, is often not preserved after the adjustment (Wang et al., 2013; Borup et al., 2016; Ochoa-Rodriguez et al., 2019).

Lastly, the availability of weather radars is mostly limited to most developed countries, where, however, there are still observational gaps with radar observations not available in the desired spatiotemporal resolution (Heistermann et al., 2013; Saltikoff et al., 2019). The same holds also for the traditional rain gauge data, for which, moreover, a decrease in their availability has been observed in many areas around the world (Lorenz & Kunstmann, 2012; Sun et al., 2018). Actually, adequate rainfall data are in general lacking for most of the Earth's land surface. Global precipitation data sets can be obtained from satellite missions, but the accuracy and spatiotemporal resolution of these observations are still insufficient to be used in the hydrological modelling of small, mountainous or urban catchments (Kidd & Huffman, 2011). Thus, in order to increase the quality and availability of rainfall data, much effort has been invested in investigating alternative innovative data sources.

One possibility to overcome the above challenges regarding the rainfall data retrieval could be to make use of the recent development of various accessible hardware and software solutions which has made measurements with special purpose sensors widely available throughout many different fields (Swan,

2012). For example, there are numerous online amateur weather networks that aggregate and visualize citizen-contributed weather observations (Gharesifard et al., 2017; de Vos et al., 2017). However, quality control of such crowdsourced data (and associated metadata) from amateur weather stations is extremely challenging since these devices are often uncalibrated or irregularly maintained. Furthermore, as with radar rainfall observations, this kind of data is primarily available in developed regions only.

Rainfall data from new types of devices which could conveniently complement traditional precipitation observation networks and, thus, improve rainfall data availability, can also be obtained using so-called "opportunistic sensing" (Tauro et al., 2018). Opportunistic precipitation sensing can be performed using devices which are not constructed primarily for rainfall observation, e.g. telecommunication infrastructure or building automation sensors. Such devices are often connected to centralized communication infrastructure, so the data can be queried in (sub-)minute intervals. This is also the case of commercial microwave links whose millimeter-wave radio signal is attenuated by rainfall droplets and which densely cover urban areas worldwide and could, thus, provide urban hydrologists with rainfall data of high spatiotemporal resolutions.

## 2.3 Rainfall retrieval from commercial microwave links

Commercial microwave links (CMLs) are point-to-point radio connections widely used as cellular backhaul. A substantial part of CML networks is operated at frequencies between 20 and 40 GHz where radio wave attenuation caused by raindrops is almost proportional to rainfall intensity. These CMLs can, therefore, be used as unintended rainfall sensors providing path-integrated quantitative precipitation estimates (QPEs). Although deriving precipitation estimates from the attenuation of microwaves was originally suggested several decades ago (Atlas & Ulbrich, 1977), the idea has experienced a renaissance in recent years, thanks to the extensive growth of cellular networks (Messer et al., 2006; Leijnse et al., 2007) which frequently incorporate CMLs.

The relationship between raindrop-induced attenuation $A_r$ [dB] and rainfall intensity $R$ [mm/h] is robust and well-understood. For a given rainfall intensity, $A_r$ is proportional to CML path length and frequency. The relation can be expressed using the following approximation:

$$R = \alpha(A_r/L)^\beta \tag{2.1}$$

where $L$ [m] is the length of a given CML, and $\alpha$ [mm/h km$^\beta$ dB$^{-\beta}$] and $\beta$ [-] are empirical parameters dependent upon CML frequency and polarization,

and drop size distribution (Olsen et al., 1978). The fraction $A_r/L$ can be expressed as a single variable – specific raindrop attenuation $\gamma$ [dB/km].

Nonetheless, $A_r$ must be separated from other components of the difference between the transmitted and received signal levels *TRSL* [dB], for whose purposes the following relation is often used:

$$TRSL = B + A = B + A_{wa} + A_r \tag{2.2}$$

where $B$ [dB] represents baseline attenuation consisting of, e.g., free space loss and gaseous attenuation, $A$ [dB] stands for observed attenuation after baseline separation, and $A_{wa}$ [dB] represents wet antenna attenuation (WAA). Imprecise quantification of the raindrop-induced attenuation $A_r$ due to CML rainfall retrieval uncertainties such as WAA estimation represents a considerable source of errors in CML QPEs (Chwala & Kunstmann, 2019) and a major challenge to their hydrological applications.

## 2.4 CML QPE uncertainties

Most uncertainties associated with the retrieval and application of CML QPEs could be categorized as either:

- Uncertainties associated with rainfall retrieval from individual CMLs; or
- Uncertainties associated with spatial information processing and its representativeness in relation to the location/area of interest.

### 2.4.1 Uncertainties in QPE retrieval from individual CMLs

Uncertainties in QPE retrieval from individual CMLs can be linked with *TRSL* measurements (quantization, hardware imperfections), with the separation of raindrop-induced attenuation $A_r$ from other sources of attenuation (Eq. 2.2), and with the transformation of the attenuation data into rainfall intensities (Eq. 2.1). The most prominent error sources include in particular: too coarse temporal sampling, quantization of *TRSL* values, uncertainty regarding the baseline level and regarding the WAA estimation, with the latter two being most important for systematic errors (bias) in the estimated rain rates (Leijnse et al., 2010; Zinevich et al., 2010; Chwala & Kunstmann, 2019).

Baseline $B$ can be identified by interpolating from dry-weather attenuation levels (Overeem et al., 2011; Schleiss & Berne, 2010). Alternatively, a low-pass filter of the *TRSL* time series can be applied (Fenicia et al., 2012). Although

the latter approach has shown to improve CML QPEs when compared to using a constant baseline, it "might produce dynamics similar to the temporal evolution of an anticipated rain-rate-dependent WAA effect" (Chwala & Kunstmann, 2019), and thus interfere with the WAA estimation. Nevertheless, the baseline is relatively stable, whereas antenna wetting is a complex dynamic process which has not been yet completely understood (Schleiss et al., 2013, more in next subsection).

QPEs are more prone to be contain systematic errors for CMLs with shorter path lengths and lower frequencies (Leijnse et al., 2008). These CMLs are less sensitive to rainfall, and raindrop-induced attenuation $A_r$ thus constitutes only a relatively small part of the observed *TRSL* (Eq. 2.2). In other words, QPEs from these CMLs are more sensitive to errors in the process of $A_r$ estimation. Let us illustrate this problem with a brief didactic example.

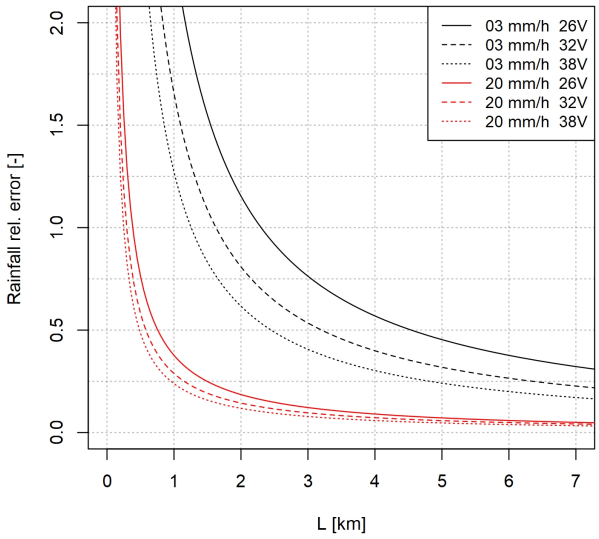


**Figure 2.1:** The relative error in QPEs from CMLs with vertical polarization in relation to CML path length for two rainfall intensities (3 and 20 mm/h) and three CML frequencies (26, 32, 38 GHz) as caused by an error of 1 dB in the estimate of $A_r$ due to intrumental uncertainties.

For a 1-km-long CML working at a frequency of 32 GHz, the raindrop attenuation $A_r$ caused by the rainfall of 20 mm/h is about 4 dB. However, for a CML with the same frequency and a path length of 4 km, $A_r$ equals roughly 15 dB. If $A_r$ is overestimated by 1 dB, a common value due to the instrumental uncertainties, the derived precipitation rate is overestimated by approximately 30% for the 1-km CML, and by 10% for the 4-km one (see Fig. 2.1). This becomes worse if the rainfall intensity is only 3 mm/h, because the relative errors in CML QPEs rise to 175% and 40% for the 1-km and 4-km CMLs respectively. Furthermore, for low rainfall rates, the derived rainfall is very sensitive to the CML frequency, and thus higher errors are associated with lower frequencies.

### Wet antenna attenuation

Wet antenna attenuation (WAA) is, in contrast to raindrop-induced attenuation $A_r$ and baseline $B$, independent of CML path length. Previous studies (Leijnse et al., 2008; Overeem et al., 2011) have also suggested that it is relatively insensitive to CML frequency at bands suitable for rainfall retrieval (20–40 GHz). However, antenna wetting is influenced not only by rainfall, but by other atmospheric conditions (e.g. wind, temperature, humidity or solar radiation) and also antenna hardware properties (e.g. antenna radome material or coating; van Leth et al., 2018). Due to this complexity of the antenna wetting process, reliable WAA estimation remains to be challenging (Chwala & Kunstmann, 2019).

To date, there is no unified approach to estimate WAA and reported WAA models are often based on different assumptions and result in considerably different estimates. For example, drying times of up to several hours have been reported (Schleiss et al., 2013), whereas other studies have not considered any wetting or drying dynamics at all, relating WAA only to rainfall intensity (Valtr et al., 2019; Kharadly & Ross, 2001).

It has also been suggested to estimate WAA based on water quantity and distribution (droplets, rivulets, water film) on antenna radomes (Leijnse et al., 2008; Mancini et al., 2019). Recently, it has been shown that WAA can be estimated using antenna reflectivity acting as a proxy variable for water film thickness (Moroder et al., 2019). However, applying this model is significantly limited by the unavailability of the required antenna reflectivity measurements.

Since having a globally valid WAA model only depending on known CML characteristics such as frequency does not seem possible, optimal WAA models should ideally be determined for each individual CML. This is especially true for models whose parameters depend on CML path length (e.g. Kharadly & Ross, 2001). However, optimal WAA model identification (e.g. for calibration purposes) on the level of individual CMLs is challenging, especially for real-world application with networks consisting of a high number of CMLs. As noted by (Ostrometzky et al., 2018), maintenance of dedicated equipment for the retrieval of the needed reference rainfall observations is impractical for such networks.

Due to all the above-discussed issues, application-focused studies with city or regional-scale CML networks have often not applied any WAA correction at all (Chwala et al., 2012; Smiatek et al., 2017) or have used only a simple constant offset model (Overeem et al., 2011; Roversi et al., 2020; Fencl et al., 2020). Although the latter approach may be a reasonable choice when only 15-min *TRSL* maxima and minima are available (Chwala & Kunstmann, 2019),

it can introduce considerable bias in the resulting CML QPEs (Fencl et al., 2019).

Adopting a different approach to the challenge of WAA estimation, Fencl et al. (2017) proposed continuous adjusting of $A_{wa}$ representing WAA and $\alpha$ (Eq. 2.1, 2.2) to measurements from traditional rain gauges, if these are available in the vicinity of CMLs. They have shown that such adjusted high-resolution CML QPEs can, in spite of underestimating peak rainfalls, outperform the gauge data used as the adjusting reference.

Alternatively, prior calibration to reference rainfall data seems to be a reasonable way to achieve reliable WAA models. However, reference rainfall retrieval approaches employed in research studies which include intensive monitoring campaigns (e.g. Schleiss et al., 2013; van Leth et al., 2018) are impractical for high numbers of CMLs due to the costs associated with the dedicated equipment needed. Alternatively, already existing rain gauge networks or high-resolution weather radars might be used to calibrate the WAA models. However, as discussed above, such rainfall data sources are often not readily available to urban hydrologists. Moreover, the potential usefulness of CML QPEs increases with the decreasing availability of other rainfall (or other reference) data. Thus, it would come handy if WAA models could be calibrated using better available data and tools, such as low resolution rainfall measurements or stormwater discharge observations in combination with a rainfall-runoff model.

### 2.4.2 Spatial uncertainties

Other uncertainty type arises from the spatial processing of rainfall information, e.g. algorithms used to transform path-integrated QPEs from individual CMLs to spatially distributed (typically gridded) rainfall maps (e.g. Overeem et al., 2013; Rios Gaona et al., 2018), and from the rainfall data representativeness in relation to the location/area of interest, given by the spatial relations between the CMLs and the area of interest and by the spatiotemporal rainfall variability. It has been observed that spatial (or mapping) uncertainties are relatively small compared to rainfall retrieval uncertainties (Rios Gaona et al., 2015). Nonetheless, the role of these uncertainties should not be ignored, especially if QPE retrieval uncertainties are successfully reduced.

Several more or less sophisticated methods of rainfall field reconstruction from the path-integrated CML QPEs have been introduced (e.g. Goldshtein et al., 2009; D'Amico et al., 2016; Haese et al., 2017). Nevertheless, spatial rainfall field reconstruction remains unappealing for some CML QPE hydrological applications, e.g. when using lumped or semi-distributed models and/or modelling hydrological processes in a catchment the size of which is similar to (or smaller than) the size of a rainfall grid cell.

For such tasks where areal rainfall estimates are satisfying and several CMLs are at hand, the influence of different CML topologies on the estimated areal rainfall has been investigated (Fencl et al., 2015) with a conclusion that combining QPEs from all available CMLs can very well capture the rainfall and is recommended when no prior information on CML data quality is available. However, at the same time, only a few very precise (i.e. least biased) CMLs are expected to deliver the most accurate areal rainfall data and, thus, CMLs used to derive areal rainfall should be ideally selected very carefully (Fencl et al., 2015). However, if the bias in QPEs is relatively comparable among the available CMLs, it is not clear how to identify optimal subsets of CMLs in such conditions; whether, for substance, the CML spatial relations with the area of interest can be used as the only decisive criteria.

## 2.5 Potential of CML QPEs for hydrological modelling

CML QPEs have a path-integrated character which makes them better suited for capturing rainfall spatial variability over a catchment than rain gauges. Moreover, unlike weather radars, they observe rainfall close to the ground. Recently, there were about five million CMLs being used worldwide within cellular networks and the number has been increasing (Ericsson, 2018). Exploiting this infrastructure for rainfall detection does not necessitate substantial additional investments. Moreover, CML data can be accessed online in high temporal resolutions and in (near) real time from network operation centers either through network monitoring systems or specifically designed server-sided applications (Chwala et al., 2016). Thanks to the dense coverage of urban areas, CMLs represent very promising rainfall sensors for urban hydrological modelling.

In fact, thanks to the intensive recent research, especially regarding the uncertainties in their retrieval, CML QPEs have proven to provide valuable rainfall information which could complement traditional observations with rain gauges and weather radars (Chwala & Kunstmann, 2019; Imhoff et al., 2020; Rios Gaona et al., 2018; Uijlenhoet et al., 2018). However, despite the high potential and recent advances, only a few studies have investigated the ability of QPEs derived from real-world CML networks for quantitative hydrology, either for rural (Brauer et al., 2016; Cazzaniga et al., 2020; Smiatek et al., 2017) or urban catchments (Disch et al., 2019; Stránský et al., 2018). Therefore, many questions remain unresolved.

The studies from urban environments (Disch et al., 2019; Stránský et al., 2018) have suggested that, if available in high temporal resolutions, CML QPEs in combination with other rainfall data could be conveniently used to

predict rainfall runoff. Nevertheless, CML QPEs could be particularly useful in regions where long-term rainfall monitoring networks are not available, or available only in resolutions which do no not suffice for most purposes of urban hydrological modelling (Gosset et al., 2016). Yet, it is not clear how to make the best use of CML QPEs under such conditions, as their potential of a stand-alone rainfall sensors for hydrological applications is compromised by systematic errors common in the QPEs, especially those from shorter CMLs (Leijnse et al., 2008).

# Chapter 3

# Evaluation of rainfall data by rainfall-runoff modelling

It is a common approach (e.g. Fencl et al., 2015, 2017; Rios Gaona et al., 2015; Graf et al., 2020) to evaluate and benchmark rainfall data by a direct comparison with a reference rainfall data set. However, weather radars are often not available in adequate spatial resolutions (Heistermann et al., 2013; Saltikoff et al., 2019) and have intrinsic problems with reflecting local rainfall extremes (Wang et al., 2013; Borup et al., 2016). Records from rain gauges, other common type of rainfall reference, are in general representative only for a limited spatial extent. Therefore, the limited or unknown representativeness of the reference rainfall data, compared to the true incident rainfall, represents a major uncertainty of direct comparison to reference rainfall observations. If one was about to evaluate a data set which would better describe the ground-truth precipitation than the reference rainfall data, the potential improvement could not be discovered.

River and drainage system discharges closely reflect transformed rainfall aggregated for a whole given catchment. Especially in urban areas, stormwater runoff can be considered as a proxy variable of the catchment areal rainfall. Furthermore, stream discharges are typically measurable more reliably than the true incident precipitation over the corresponding catchment. This can be especially useful in the case of convective precipitation commonly associated with high spatiotemporal rainfall variability, which is difficult to capture with traditional reference rainfall measurements. Therefore, when evaluating the suitability of rainfall data sets for purposes of rainfall-runoff modelling, using a rainfall-runoff model and runoff observations as the reference is a valid approach which has been commonly applied. This was done in the studies of Obled et al. (1994), Segond et al. (2007), or Sikorska & Seibert (2018) which investigated natural catchments. Focusing specifically on urban rainfall-runoff modelling, Goormans & Willems (2013) and Wang et al. (2015) evaluated the suitability of weather radar data sets, and Kleidorfer et al.

(2009) studied the impact of artificially created imperfections in rainfall data on model parameters.

A similar approach to rainfall data evaluation has been employed by Ochoa-Rodriguez et al. (2015) who analyzed the impact of spatial and temporal resolution of rainfall inputs on urban hydrodynamic modelling. In this study, model outputs obtained using various rainfall data sets were evaluated using, as the reference, model outputs associated with the finest resolution rainfall estimates. This approach was also applied by Disch et al. (2019) when comparing the impact of different sources of rainfall data on urban rainfall-runoff predictions. Nevertheless, when using this approach, similar issues as discussed above, regarding the representativeness of the reference, can arise. Furthermore, it is unclear whether the best-quality rainfall data lead to the best model performance in some circumstances, e.g. when the model used was calibrated using another rainfall data set.

Alternatively, Berne et al. (2004) investigated spatiotemporal rainfall-runoff dynamics in Mediterranean urban areas in relation to, among others, rainfall data integration to various temporal resolutions. The relation between the precipitation and runoff was quantified without rainfall-runoff modelling, only using the lag time, i.e. "the time difference between the gravity centre of the mean rainfall over the catchment on one hand and the gravity centre of the generated hydrograph on the other hand".

## 3.1 Quantification of prediction uncertainty in hydrological modelling

When hydrological modelling is employed for rainfall data evaluation, additional uncertainties are introduced into the process, which should be taken account for. It has been argued that ignoring the uncertainty, particularly related to input data, compromises (not only) hydrological modelling (Beven, 2006; Kavetski et al., 2006), or similarly, that quantification of the uncertainty associated with the models in urban stormwater modelling is a must (Dotto et al., 2012). However, quantifying the effect of all principal uncertainty sources (or, specifically, the effect of uncertainty related to rainfall data) on rainfall-runoff modelling results is a complex and challenging task. Therefore, though conceptually desirable, it is rarely practiced (Dotto et al., 2012). Researchers have often decided, instead, to put effort to maximize the reliability of modelling results, e.g. by using data measured over a long period of time (Segond et al., 2007), or by employing "verified and operational models" (Ochoa-Rodriguez et al., 2015).

Deletic et al. (2012) reviewed studies investigating uncertainty in urban hydrological modelling and identified the following key uncertainty sources:

1. Model input (measured input data and parameters) uncertainties;
2. Calibration (calibration data measuring, availability, and choices; calibration algorithms and objective functions used in the calibration process) uncertainties;
3. Model structure (conceptualisation errors, equations and numerical methods) uncertainties.

Many published urban drainage modelling studies have dealt with uncertainties associated with model parameters, often producing parameter probability distributions and estimating confidence intervals around the model's outputs (e.g. Thorndahl et al., 2008; Dotto et al., 2012). However, Deletic et al. (2012) recognized that the uncertainty sources are highly interlinked, suggesting that assessing the impact of a single source is not going to be adequate and that simultaneous propagation of key sources of uncertainties is required.

Dotto et al. (2012) observed that a common approach when trying to estimate the total uncertainty (related to parameters and all other sources) is adding a Gaussian error term to the model predictions. This approach is based on the assumption that the residuals between the measured and modelled values are normally distributed (i.e. only due to white measurement noise). However, the deviations of model outputs from observed data are usually considerably larger than random observation errors, typically due to a simplified description of the system by the deterministic model and due to input data imperfections (Reichert & Schuwirth, 2012). When ignored, such systematic deviations can lead to unrealistic (usually too narrow) uncertainty bounds of model parameters and model predictions (Reichert & Schuwirth, 2012).

Systematic deviations of model predictions from observed data, or model bias, can by addressed by increasing the complexity of the model to reduce bias or by trying to find a statistical description of the bias in model outputs. Reichert & Schuwirth (2012) adapted a statistical technique of Kennedy & O'Hagan (2001), accounting for bias in model outputs, for purposes of environmental modelling and extended it with a framework enabling for multiobjective model calibration. Sikorska & Seibert (2018) used this approach to asses the value of different precipitation data for flood prediction in an alpine catchment. Del Giudice et al. (2013) applied this technique to urban drainage modelling while proposing various formulations of the stochastic process representing the model bias (more in section 3.2). Their results showed that runoff simulations are much more reliable when bias is accounted for than when it is neglected.

While approaches based on explicit model bias consideration can improve the reliability of hydrological predictions, they only provide limited information

about the causes of model bias and, therefore, do not help much to distinguish imperfections in input rainfall data from model structural errors (Del Giudice et al., 2013). A conceptually more satisfying approach is to make the input uncertain and to propagate it through the model. This can be done by using so-called rainfall multipliers (Kavetski et al., 2006; Vrugt et al., 2008). These random variables multiply observed rainfall rates (1 multiplier per event) before feeding it into the model. They are estimated together with other model parameters and allow to quantify the rainfall-related uncertainty directly in input data. Sikorska et al. (2012) combined a stochastic error model with rainfall multipliers to separate the effect of uncertainty in the rainfall data from other erorrs sources. However, the rainfall multiplier approach fails when the observed precipitation has a different temporal pattern from the true one or if the true nonzero rainfall is not detected (Del Giudice et al., 2016).

To overcome the above problem, Del Giudice et al. (2016) introduced a method where the average precipitation over a given catchment is formulated as a stochastic process, parameters of which are inferred together with other model parameters during calibration. They showed that, even when starting with inaccurate precipitation data, this approach can accurately reconstruct the whole-catchment precipitation and reliably quantify the related uncertainty. However, their results suggested that even a simpler approach (e.g. Del Giudice et al., 2013) can lead to similar model parameters and prediction intervals. Therefore, if precipitation reconstructing is not of major interest, the novel approach is not appealing, given its high computational requirements.

## 3.2 Explicit statistical consideration of model bias

Herein we describe the framework of Kennedy & O'Hagan (2001) as formulated by Reichert & Schuwirth (2012) and first used in the context of urban hydrology by Del Giudice et al. (2013). The basic principle of the method is extension of a deterministic (e.g. rainfall-runoff) model by a stochastic error model. However, a commonly used error model considering only independent and identically distributed (i.i.d.) errors is adjusted to explicitly account for the systematic model errors (bias) of the deterministic model, acknowledging the fact that simulators cannot describe the true behavior of a system (Del Giudice et al., 2013). Using this approach, the extended model can be formulated using the equation

$$Y_o(x, \theta, \psi) = y_M(x, \theta) + B(\psi) + E(\psi) \tag{3.1}$$

where variables in capitals represent random variables and those in lowercase are deterministic functions. $Y_o$ represents the observed system output, $y_M$ stands for the deterministic model output. To better fulfill the underlying

statistical assumptions and thus obtain more reliable predictions, a transformation (details in 3.2.1) should be applied on both $Y_o$ and $y_M$ (Del Giudice et al., 2013). Next, $B$ and $E$, respectively, stand for the bias and measurement noise in the system output. Precipitation as the external driving force is represented by $x$, whereas $\theta$ and $\psi$ respectively represent the deterministic and error model parameters. The measurement noise of the system response $E$ is sampled from a multivariate normal distribution with mean 0 and a diagonal covariance matrix

$$\Sigma_E = \sigma_E^2 \mathbb{1} \tag{3.2}$$

Del Giudice et al. (2013) investigated various formulations of the model bias $B$ and presented a structured approach to select the optimal bias description for a given case study. In general, it is an autoregressive term which can be dependent on the input (rainfall) or/and output (runoff) of the system. For more details, see Del Giudice et al. (2013).

By combining the deterministic hydrological and the stochastic error models, we can quantify the probability that the observed runoffs can be explained by given predicted runoffs and error model. This can be formally expressed by a likelihood function describing the joint probability density $f(Y_o|\theta, \psi, x)$ of observed system response $Y_o$ for given $\theta$, $\psi$, and $x$. It can be written as

$$f(Y_o|\theta,\psi,x) = \frac{(2\pi)^{-\frac{n}{2}}}{\sqrt{\det(\Sigma(\theta,\psi,x))}}$$

$$. \exp\Big(-\frac{1}{2}[\tilde{Y}_o - \tilde{y}_M(\theta,x)]^T \Sigma(\theta,\psi,x)^{-1}[\tilde{Y}_o - \tilde{y}_M(\theta,x)]\Big) \prod_{i=1}^{n} \frac{\mathrm{d}g}{\mathrm{d}y}(Y_{o,i},\psi), \tag{3.3}$$

where $n$ is the number of observations (i.e. the dimension of $Y_o$ and $y_M$) and $\Sigma(\theta, \psi, x)$ stands for a covariance matrix of the residuals transformed by a function $g()$. Similarly, $\tilde{y}_M = g(y_M)$.

To achieve accurate rainfall-runoff predictions and reliable quantification of their uncertainty, the extended model should be calibrated. In theory, this could be done by optimizing the likelihood function as the objective function. However, there is "a severe identifiability problem" between the deterministic model $y_M$ and bias $B$ "as the two components cannot be observed separately" (Reichert & Schuwirth, 2012). By implementing the Bayesian approach, i.e. combining the likelihood with prior knowledge (belief) about the extended model, we can specify that we are seeking for the smallest bias possible when calibrating the model. Although somewhat subjective choices regarding the amount of bias acceptable are required, this approach at least makes them transparent (Reichert & Schuwirth, 2012).

### 3.2.1 Output transformation

Because of the statistical assumptions of homoscedasticity and normality of calibration residuals, a transformation $g()$ should be applied on simulation and observed output data (i.e., in our case, runoff discharges). It is a common way in hydrological modelling how to account for increasing variance with increasing discharge and thus reduce the residual heteroscedascity. Moreover, it is expected to reduce the proportion of negative flow predictions by making error distributions asymmetric (Del Giudice et al., 2013).

According to Del Giudice et al. (2013), two most promising variance stabilization techniques for urban drainage applications are the Box–Cox (Box & Cox, 1964) and the log-sinh (Wang et al., 2012) transformation. The Box-Cox transformation has been used more often in hydrological studies than the log-sinh alternative, primarily due to the date of its first introduction. The two-parameter Box–Cox transformation can be written as

$$g(y) = \begin{cases} log(y + \lambda_2), & \text{if } \lambda_1 = 0 \\ \frac{(y+\lambda_2)^{\lambda_1}-1}{\lambda_1}, & \text{otherwise} \end{cases} \tag{3.4}$$

and holds for $y > -\lambda_2$. The one-parameter version would need only $\lambda_1$ while keeping $\lambda_2 = 0$. Del Giudice et al. (2013) used the one-parameter version of the transformation with the parameter value $\lambda_1 = 0.35$, which had already been proven to perform satisfactorily in the past (e.g. Honti et al., 2013; Wang et al., 2012).

The log-sinh transformation was introduced for hydrological purposes only recently by Wang et al. (2012). Del Giudice et al. (2013) proposed its modification which would result in a "reparameterised form with parameters that have a more intuitive meaning". The formula would be

$$g(y) = \beta\, log\Big(sinh\big(\frac{\alpha + y}{\beta}\big)\Big), \tag{3.5}$$

where $\alpha$ and $\beta$ represent lower and upper reference outputs. This means that "$\alpha$ controls how the relative error increases for low flows" and "for outputs larger than $\beta$, the absolute error gradually stops increasing" (Del Giudice et al., 2013).

## 3.3 Rainfall-runoff modelling performance assessment

Whether the uncertainty analysis is employed or not, there are various methods to evaluate the performance of a rainfall-runoff model. The primary output

of a rainfall-runoff model is a time series of simulated discharges at a given location. Such a time series is well suited to be evaluated visually, creating a hydrograph. However, for numerical evaluation, it is preferable to summarize the performance in a single metric (or a small number of metrics). Many metrics often represent only a specific part (e.g. maximal discharge) or only a certain aspect (e.g. temporal precision, total volume discharged) of the hydrograph. If multiple rainfall-runoff events or even various catchments are to be compared, it is preferable to use standardized dimensionless criteria, e.g. the relative error of maximal discharges. Alternatively, there are metrics which take into account the whole time series and are often applied when trying to summarize the overall model performance, such as the mean squared error (*MSE*) or Nash-Sutcliffe efficiency (*NSE*). These two metrics are used very commonly in hydrological modelling although it has been shown that there are systematic problems inherent with their usage (Gupta et al., 2009; Ehret & Zehe, 2011).

When dealing with interval predictions, it is common to evaluate two aspects of the predictive performance – its precision and accuracy. The prediction precision can be quantified by the width of the determined confidence interval, referred to also as interval sharpness (e.g. Breinholt et al., 2012). The prediction accuracy can be understood as the position of observed value(s) in relation to the confidence bound(s). Time series predictions such as hydrographs can also be assessed in this manner, e.g. by calculating the prediction reliability, i.e. the share of observed data points within the predicted bounds, and the "average bandwidth" – the interval widths averaged over the entire prediction period (Del Giudice et al., 2013).

Gneiting & Raftery (2007) proposed a metric which combines the two above aspects – the interval score $S_\alpha$. For a single interval prediction at a confidence level $1-\alpha$ (determined by the prediction quantiles at levels $\frac{\alpha}{2}$ and $1-\frac{\alpha}{2}$), the interval score is defined as

$$S_\alpha(l,u,x) = (u-l) + \frac{2}{\alpha}(l-x)\mathbb{1}\{x<l\} + \frac{2}{\alpha}(x-u)\mathbb{1}\{x>u\}, \qquad (3.6)$$

where $l$ and $u$ stand for lower and upper interval bounds. This metric is supposed to allow for intuitive comprehension as "the forecaster is rewarded for narrow prediction intervals and incurs a penalty, the size of which depends on $\alpha$, if the observation misses the interval" (Gneiting & Raftery, 2007).

For time series predicition, the idea of $S_\alpha$ can be extended and the mean interval scores (*MIS*) for a given period can be quantified. Bourgin et al. (2015) further developed the concept and, "to ease comparison between catchments and evaluate the skill of the prediction bounds", proposed to benchmark the prediction confidence bounds by *MIS* for reference bounds ($MIS_{ref}$) obtained e.g. from long term climatological data. The mean interval skill score *MISS* would be computed as

$$MISS = 1 - (MIS/MIS_{ref}), \qquad (3.7)$$

high values of which indicate greater prediction skill, with positive scores indicating that evaluated predictions are more skillful than the reference.

# Chapter 4

# Material

Data used in this thesis originate from an experimental urban catchment (Fig. 4.1) with an area of 1.3 km$^2$ which lies in Prague-Letňany, Czech Republic, and is drained by a separate stormwater drainage system. Approximately 35% of the catchment area is covered by impervious surfaces. The catchment is slightly inclined to the north, with the altitude gradually declining from roughly 280 to 250 m above sea level (Baltic 1957 height, EPSG:8357). The lag time between rainfall peak and runoff peak observed at the outlet from the catchment's drainage system is approximately 20 minutes.

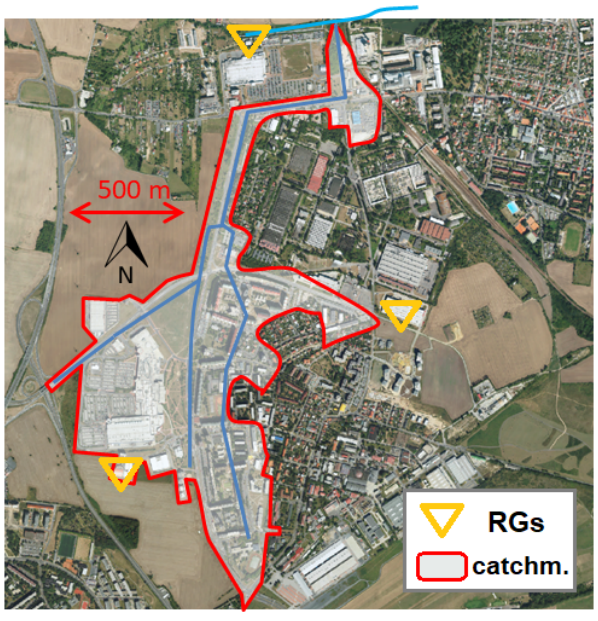


**Figure 4.1:** Aerial view of the urban catchment studied with the main sewers and receiveing water body as well as the position of the local rain gauges (RGs).

## 4.1 Data retrieval and availability

A set of 19 CMLs (Table 4.1; Fig. 4.2) and several rain gauges located in the catchment's surroundings (Figs. 4.1 and 4.2) were monitored over the period between July 2014 and October 2016, excluding the winter months (December–March) as CML signal attenuation by frozen precipitation, occurring in winter periods, is considerably different than that of liquid precipitation. Moreover, our monitoring setup is designed for periods with liquid precipitation only, as the rain gauges (see below) are not heated.

The CMLs (Mini-Link, Ericsson) broadcast at frequencies from 25 to 39 GHz, their lengths are between 611 and 5795 m, and they are operated by a major telecommunication service provider. Long CMLs extend out of the catchment for several kilometers. Signal-level data from CMLs, featuring a common quantization of 1 dB and 0.33 dB for the transmitted and received signal power, were retrieved at a 10-s resolution with a custom-made logging script (Fencl et al., 2015) and then aggregated to a 1-min resolution.

All tipping bucket rain gauges in the area (Figs. 4.1 and 4.2) were produced by the same manufacturer (MR3, Meteoservis) and feature the same characteristics: A funnel area of 500 $cm^2$, a bucket volume of 5 ml, and a single tip corresponding to 0.1 mm of rainfall. They are all dynamically calibrated (Humphrey et al., 1997) every year and the rainfall data they provide is stored at a 1-min resolution. However, the rain gauges make part of two different networks. Those located one km or more outside of the catchment (Fig. 4.2) are operated and maintained by the municipal sewer authority as a part of their long-term monitoring network with a density of one gauge per 20—25 $km^2$. These gauges are further referred to as "municipal". In contrast, rain gauges temporarily installed for research purposes at three locations at the catchment boundaries (Fig. 4.1) are referred to as "local".

In addition, discharges were measured roughly 100 m upstream from the stormwater drainage system outlet (50°9'7.572", 14°30'44.800"E; Fig. 4.2) using an area-velocity flow meter (Triton, ADS). The flow meter is located in a concrete pipe of a circular shape with the diameter of 1.5 m and horizontal inclination of 0.86%. The device was calibrated in a standard way using stream gauging and the velocity-area method employing an electromagnetic velocity probe. The temporal resolution of these measurements is 2 min for wet periods and 10 min for dry periods. Observed discharge values range from approximately 2 to 2000 l/s. Uncertainty of these observations is estimated in chapter 6.2.4.

During the observation period, more than 100 relevant rainfall events with depths exceeding 2 mm were registered. However, due to outages in data from the monitoring devices, it was possible to analyze data from only a

| ID | FreqA [GHz] | FreqB [GHz] | Polarization | Length [m] |
|---|---|---|---|---|
| 1 | 31.82 | 32.63 | V | 611 |
| 2 | 32.63 | NA | H | 645 |
| 3 | NA | 32.63 | V | 816 |
| 4 | 38.88 | 38.60 | V | 911 |
| 5 | 24.55 | 25.56 | V | 1022 |
| 6 | 37.62 | 37.62 | V | 1086 |
| 7 | 37.62 | 38.88 | V | 1396 |
| 8 | 37.62 | 38.88 | V | 1584 |
| 9 | 31.82 | 32.63 | V | 1858 |
| 10 | 24.55 | 25.56 | H | 1953 |
| 11 | 38.88 | NA | V | 1979 |
| 12 | 31.82 | 32.63 | V | 2611 |
| 13 | 24.55 | 25.56 | V | 2957 |
| 14 | 24.55 | 25.56 | V | 3000 |
| 15 | 24.55 | 25.56 | V | 3195 |
| 16 | 24.55 | 25.56 | V | 3432 |
| 17 | 25.56 | 24.55 | V | 4253 |
| 18 | 24.55 | 25.56 | V | 4523 |
| 19 | 24.55 | 25.56 | V | 5795 |

**Table 4.1:** Characteristics of the CMLs observed. FreqA and FreqB are CML frequencies for the two directions. The NA values indicate that records are not available. Polarization (Vertical/Horizontal) is the same for both directions.

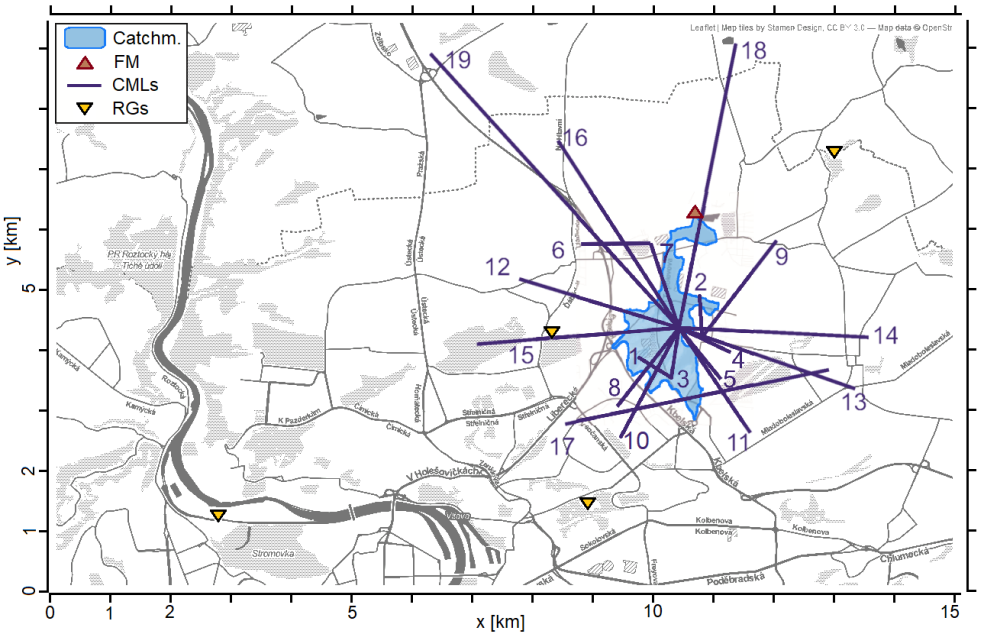


**Figure 4.2:** Spatial relations of the catchment, the flowmeter (FM), the CMLs (with IDs denoted), and the monitored municipal rain gauges (RGs).

considerably lower number of events. The exact number differs for each study presented due to using data from various sets of devices, the availability of the data at a given time, or differences in event definition. Details on rainfall characteristics for events as used in the study presented in chapter 6 (see 6.2.1) are provided in Appendix (Table A.1).

An overview of CML data availability during the monitoring period is shown in Appendix (Fig. A.1). Data from each CML were available, on average, during 80% of the events. Six CMLs had data availability higher than 95% and only two of them lower than 50%. Due to long-term outages, data from CMLs #1, #2, and #10 are analyzed only in the study presented in chapter 5, which investigates only a shorter period for which the data from these CMLs are available.

## 4.2 Rainfall-runoff model and its reliability

To simulate discharges at the drainage system outlet, a rainfall-runoff model built in the EPA-SWMM software is used. It was constructed using detailed information about the catchment (e.g. the ratio of impervious areas for individual subcatchments) and the drainage system (e.g. pipe materials and diameters) provided by the municipal water management authority. The model was calibrated for rainfall measurements obtained from the three local rain gauges (Fig. 4.1), however, using an independent data set collected before the above specified observation period (Pastorek, 2014). The process of runoff generation is formulated empirically and separately for each model subcatchment (195 in total) using the respective surface-depression-storage-depth parameters. The subsequent runoff itself is modeled as one-dimensional flow expressed by Saint-Venant equations. These are numerically solved in an approximated form of a kinematic wave for surface runoff and in the full form of a dynamic wave for the following runoff in the drainage network.

In the cases of all rainfall data sets (observation layouts) studied within the thesis, except for the local rain gauges, the rainfall model input is always implemented as areal rainfall in the model, meaning that rainfall intensity in a given time step has a constant value over all model subcatchments. For the local rain gauges, the catchment is divided into three Thiessen polygons, corresponding to the local gauges at three locations. This means that every subcatchment is assigned the same rainfall intensity as measured at the closest local rain gauge.

The reliability of model predictions was tested using rainfall data from the three local rain gauges, i.e. the same devices that were used for the model calibration. This verification was performed for 56 rainfall-runoff events (see section 6.2.1) from the observed period between July 2014 and October 2016.

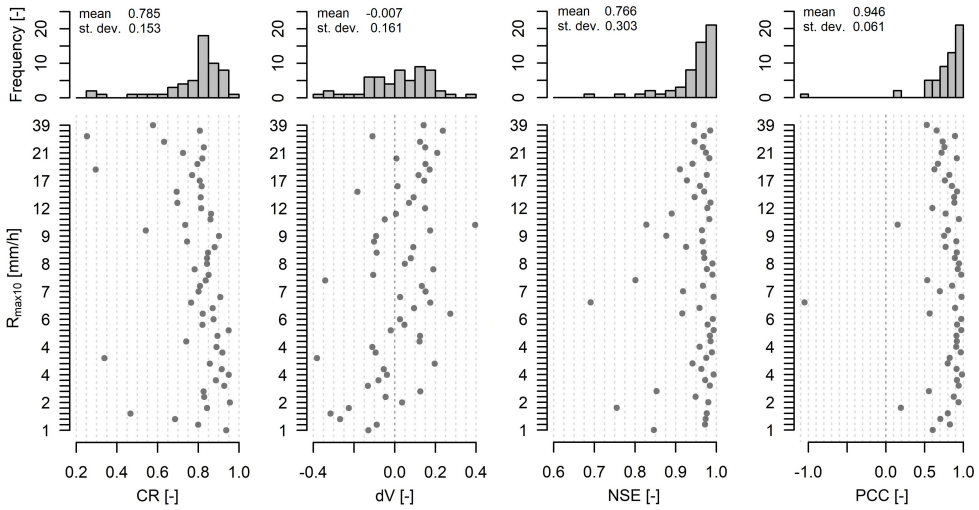


**Figure 4.3:** Results of the rainfall-runoff model verification. Top: Histograms of the statistics for all evaluated events. Bottom: Scatter plots showing the statistics for single events with respect to the maximal 10-minute rainfall intensity ($R_{max,10}$) observed by the local rain gauges during these events.

Hydrographs for all analyzed events are provided in the Supplementary Data appended to the study of Pastorek et al. (2019b). Results of this verification are summarized in Fig. 4.3. These results suggest that the model predicts very realistic rainfall runoff. First, on average 78% of simulated discharges fall within the 95% confidence bands of observed runoff defined by 2.5% and 97.5% quantiles of observation errors (see section 6.2.4), i.e. the mean containing ratio $CR$ [-] is 0.78, and its st. dev. is 0.15. Second, the relative error in volume on average is only -0.7%, and modelled discharge shows a 0.95 Pearson's correlation coefficient in relation to the observed values. The Nash–Sutcliffe efficiency is also high (mean 0.77 and st. dev. 0.3). The model performs less satisfactorily in terms of predicting peak flows during heavy rainfalls, they are often substantially overestimated (on average by 40%). This is probably related to errors associated with the rainfall measurement or strong assumptions regarding rainfall spatial variability over the catchment area. For some of the heaviest rainfalls, peak flows are overestimated by more than 100%, which is probably also due to the model structural deficiencies, e.g. unmodelled overland flows during extreme events. In summary, the rainfall-runoff model performs very well except for extreme events.

# Chapter 5

# Assesing CML QPEs by quantifying uncertainties in runoff predictions in a small urban catchment: The pilot study

This study represents a first assessment of applying quantitative precipitation estimates (QPEs) retrieved from commercial microwave links (CMLs) for hydrological modelling in urban catchments. We compare rainfall data from CMLs with more conventional observations from rain gauges by evaluating rainfall-runoff modelling predictions against observed runoffs. We employ a method based on Bayesian inference to calibrate our rainfall-runoff model and to estimate the uncertainty of modelling outputs. Results of the performed analyses show that CML rainfall data, when a suitable adjustment is applied (e.g. using information from nearby rain gauges), allow for better detection of dynamics of precipitation and subsequent runoff than data from rain gauges alone, especially in the case of heavy rainfalls which are highly variable in space and time. Thus, CMLs seem to represent a relevant rainfall data source, which can conveniently complement existing rainfall monitoring networks.

The bulk of this chapter was originally published in:

Pastorek, J., Fencl, M., Stránský, D., Rieckermann, J., & Bareš, V. (2017). **Reliability of microwave link rainfall data for urban runoff modelling**. In *Proceedings of the 14th IWA/IAHR International Conference on Urban Drainage* (pp. 1340–1343). Prague, Czech Republic.

Pastorek, J., Fencl, M., Rieckermann, J., Sýkora, P., Stránský, D., Dohnal, M., & Bareš, V. (2018). **Posouzení srážkových dat z mikrovlnných spojů v městském povodí pomocí analýzy nejistot hydrologického modelu**. [The Evaluation of CML Rainfall Data in Urban Catchment by Means of Hydrologic Model Uncertainty]. *SOVAK: Časopis oboru vodovodů a kanalizací* 27, 16–22.

## 5.1 Introduction

Reliable rainfall data are crucial when performing urban rainfall-runoff modelling. Nevertheless, high spatial variability of rainfall during convective events negatively affects the representativeness of point precipitation measurements from rain gauges. This could be avoided by employing commercial microwave links (CMLs), which allow for indirect path-averaged precipitation detection and are typically very dense in urban areas. However, to date, only a few studies have investigated the ability of quantitative precipitation estimates (QPEs) from CMLs for quantitative hydrology.

Smiatek et al. (2017) investigated the potential of QPEs from CMLs for streamflow prediction in an orographically complex mountainous region. In urban settings, Fencl et al. (2013) assessed the potential of CMLs to capture spatiotemporal rainfall dynamics and thus improve urban rainfall-runoff modelling, however, using only virtual rainfall fields. In a similar analysis, Fencl et al. (2015) evaluated QPEs derived from real-world CML data, however, without using these for hydrological modelling. Thus, to the best of our knowledge, no research has been presented yet in relevant literature where real-world CML QPEs would be applied for urban rainfall-runoff modelling.

In this study, we target the above research gap and analyze whether QPEs obtained from CMLs can be regarded as a viable alternative for rainfall data in the field of urban rainfall-runoff modelling. As CML QPEs are often highly biased, what limits their usability for practical purposes, we analyze CML QPEs derived using both a standard approach and a recently proposed (Fencl et al., 2017) method for adjusting the QPEs to existing rain gauges.

The CML QPEs, as well as traditional data from rain gauges, are propagated through a calibrated rainfall-runoff model and evaluated against observed discharges. Since additional uncertainties are introduced into the process of rainfall data evaluation by employing the rainfall-runoff modelling, we use a thorough statistical method which allows for reliable quantification of the runoff prediction uncertainty associated with various rainfall observation layouts.

## 5.2 Methods

The defined problem is addrresses using rainfall and runoff data collected in a small urban catchment in Prague-Letňany, Czech Republic (details in chapter 4) during three months (August – October) of 2014. Precipitation

time series from six rainfall observation layouts are propagated through a rainfall-runoff model (chapter 4.2) and evaluated against observed runoffs. In order to quantify the associated uncertainties, the hydrological model is operated by means of prediction uncertainty quantification as first used in an urban hydrology context by Del Giudice et al. (2013) and theoretically introduced in chapter 3.2.

### 5.2.1 Rainfall observation layouts

We investigate rainfall data observed during 15 rainfall-runoff events from the summer season of 2014 using the six following observation layouts:

1. Measurements from three local rain gauges

   Rainfall data from three local rain gauges installed for research purposes (Fig. 4.1) around the catchment of interest. This data set represents rainfall information observed on site which, however, in the context of the Czech Republic, is available only for short term experimental purposes. In this study, this data set is considered as the best-case-scenario reference.

2. Measurements from a single local rain gauge

   Rainfall data at a 1-min resolution from the local rain gauge located at the south-west catchment boundary (Fig. 4.1). This data set represents rainfall information observed on site which could be available more commonly than the data above, however typically also only for a limited period of time, e.g. in order to evaluate the effect of (re)construction works in the catchment.

3. Measurements from three municipal rain gauges

   Rainfall data from the three municipal rain gauges closest to the catchment (Fig. 4.2). Due to their 1-min resolution, for which correlations are low for the given distances (Villarini et al., 2008), only a single time series, constructed as the mean of the instantaneous $R$ [mm/h] values of the three gauges, is evaluated. This data set represents rainfall data standardly available in long-term perspectives in urbanized areas of the Czech Republic.

4. QPEs from four CMLs adjusted by the local rain gauge,

   Data from the single local rain gauge specified above, aggregated to 15-min time steps, is used to adjust (Fencl et al., 2017) CML QPEs with a 1-min resolution. In particular, wet

antenna attenuation ($A_{wa}$ from Eq. 2.2) and $\alpha$ (Eq. 2.1) are adjusted, while keeping $\beta = 1$. Only short CMLs (path length $< 1500$ m) located close to the catchment center are used (#1, #2, #5, #7; Fig. 4.2; #3 and #4 are excluded due to outages and erratic behavior, respectively). Only a single time series, constructed as the mean of the instantaneous $R$ [mm/h] values of the four CMLs, is evaluated. This rainfall data set showcases application of CML QPEs when traditional rainfall information is available directly in the catchment area, however, not in a satisfying spatial resolution.

5. QPEs from four CMLs adjusted by the municipal rain gauges

   The instantaneous mean of the QPEs from the same four CMLs as above, adjusted in the same way, however, using the mean of the data from the three municipal rain gauges (specified above). This rainfall data set showcases application of CML QPEs in situations when rainfall is not measured directly in the catchment, but there are gauges in the distance of 2 – 3 km, which, however, provide data in lower temporal resolutions (e.g. 15, 30, or 60 min).

6. Unadjusted QPEs from all CMLs available (Fig. 4.2).

   The instantaneous mean of QPEs derived, using a standard approach, from all 19 CMLs available in the area in a given time. $A_{wa}$ is estimated as a constant offset with the value of 2.5 dB, which was determined by comparing the specific raindrop attenuation $\gamma$ [dB/km] of short and long CMLs. The rainfall intensity $R$ [mm/h] is calculated with parameter values $\alpha$ and $\beta$ chosen in accordance with ITU Radiocommunication Sector (2005). This data set represents a situation when traditional rainfall information is not available in the catchment's surroundings.

In the cases of all CML data, prior to applying the correction for $A_{wa}$, baseline $B$ [dB] (Eq. 2.2) is separated in the same manner as in Fencl et al. (2017). In particular, the unprocessed data are first classified into dry and wet periods according to Schleiss & Berne (2010) using a moving window of the length of 15 min. The baseline for a given wet period is then assumed to equal the 10% quantile in the preceding dry weather period.

### 5.2.2 Rainfall-runoff modelling and uncertainty analysis

Rainfall time series retrieved using all the five observation layouts are propagated through a rainfall-runoff model (4.2) and evaluated against discharges

observed at the outlet from the local stormwater drainage system. When using rainfall data from the three local rain gauges, the rainfall input is implemented in the model using three Thiessen polygons. This means that the rainfall intensity above a given model subcatchment is assumed to be the same as measured at the closest gauge. In all other cases, rainfall input is implemented as areal rainfall, meaning that rainfall intensity in a given time step has a constant value over all subcatchments of the model.

In order to acknowledge uncertainties of the rainfall-runoff model predictions, we employ uncertainty analysis framework of Kennedy & O'Hagan (2001) as formulated by Reichert & Schuwirth (2012) and first used in a context similar to ours by Del Giudice et al. (2013), as introduced in chapter 3.2. This method, among other features, enables quantification of uncertainties in model output, i.e. in discharge predictions. By varying the input rainfall data while keeping the rainfall-runoff model structure unchanged, we are able to trace the associated changes in the prediction uncertainty back to the respective rainfall data. Details regarding the application of this framework in the presented study are provided below.

### 5.2.3 Uncertainty analysis implementation

The basic idea behind this uncertainty analysis method is the extension (Eq. 3.1) of a deterministic (i.e., in our case, rainfall-runoff) model by a stochastic error model which explicitly accounts not only for the random errors ("white noise"), but also for systematic model errors, i.e. bias. Del Giudice et al. (2013) investigated various formulations of the model bias. Based on their recommendations and our previous analyses (Pastorek, 2016), we formulate the bias $B(\psi)$ (Eq. 3.1) as an autoregressive stationary random process with a long-term equilibrium value of zero and a constant variance. It is a mean-reverting Ornstein–Uhlenbeck process (Uhlenbeck & Ornstein, 1930), "the discretisation of which would be a first-order autoregressive process with Gaussian independent and identically distributed noise" (Del Giudice et al., 2013). It can be expressed using the following differential equation:

$$dB(t) = -\frac{B(t)}{\tau}dt + \sqrt{\frac{2}{\tau}}\sigma_B dW(t), \tag{5.1}$$

where $\tau$ represents the correlation time, $\sigma_B$ the asymptotic standard deviation of the random fluctuations around the equilibrium, and $dW(t)$ a Wiener process, i.e. standard Brownian motion. The following steps are then required to calibrate the extended (deterministic + stochastic) model formulated as described above, and to perform the subsequent uncertainty analysis (Del Giudice et al., 2013):

1. Definition of marginal distributions of the prior joint probability distribution of the both the deterministic rainfall-runoff model parameters $\theta$ and the stochastic error model parameters $\psi$.

   Del Giudice et al. (2013) suggest that completely uninformative prior distributions should not be used for parameters of neither the deterministic rainfall-runoff model ($\theta$) nor the stochastic error model ($\psi$). Considering the chosen error model (Eq. 5.1), $\sigma_B$ is unlikely to be higher than the variability of observed discharge, $\tau$ should represent the characteristic correlation length of the residuals, and $\sigma_E$ should mirror the measurement noise of the system output Del Giudice et al. (2013). The priors are, thus, chosen based on our knowledge of the urban catchment and on consultations with experts who have already used the method.

   For all the parameters, marginals of the prior joint distribution are defined (Table 5.1) as truncated normal distributions with four defining parameters - mean ($\mu$), standard deviation ($\sigma$), minimum, and maximum. When $\theta$ parameters are concerned, they represent multiplicative (scaling) values of the actual model parameters. This means that when a given parameter, e.g. *imp*, is set to 1.1, the respective *imp* values for all 195 subcatchments are multiplied by 1.1.

   Before the next step, a transformation $g()$ should be applied on simulation results and output data to account for the variance increasing with the discharge and to reduce the heteroscedascity of residuals (details in 3.2.1). Thus, $\psi$ parameters $\sigma_B$ and $\sigma_E$ are also defined in the transformed space. Based on our previous analyses (Pastorek, 2016), as transformation $g()$, we use the Box-Cox transformation (Box & Cox, 1964) with parameters $\lambda_1 = 0.45$ and $\lambda_2 = 1$.

2. Bayesian inference of the posterior parameter distribution.

   The extended model is calibrated by the means of Bayesian inference. To obtain posterior parameter distribution, the joint probability density, a product of the prior $f(\theta, \psi)$ and the likelihood function $f(Y_o|\theta, \psi, x)$ (Eq. 3.3), gets conditioned on the observed discharge data:

$$f(\theta, \psi|Y_o, x) = \frac{f(\theta, \psi)\, f(Y_o|\theta, \psi, x)}{\iint f(\theta', \psi')\, f(Y_o|\theta', \psi', x)\mathrm{d}\theta'\mathrm{d}\psi'} \,. \tag{5.2}$$

   Solving this problem analytically would include dealing with multidimensional integrals. This can be avoided by employing a numerical method such as Markov Chain Monte Carlo (MCMC) to approximate properties of the posterior distribution.

   Although the determinstc rainfall-runoff model has been calibrated in the past, we optimize its parameters also here, together with the stochastic error model parameters, as we aim to maximize both the discharge prediction accuracy and precision. Data from five out of the 15 available rainfall-runoff events are used to calibrate the extended model.

| parameter | abbrev. | $\mu$ | $\sigma$ | min. | max. |
|---|---|---|---|---|---|
| Percentage of impervious areas [%] | $imp$ | 1 | 1 | 0.8 | 1.2 |
| Width of overland flow path [m] | $wid$ | 1 | 1 | 0.3 | 1.7 |
| Manning's N for impervious areas | $N_{im}$ | 1 | 1 | 0.3 | 1.7 |
| Surface depression storage for impervious areas [mm] | $S_{im}$ | 1 | 1 | 0.3 | 1.7 |
| Percentage of impervious areas with no depression storage [%] | $pc0$ | 1 | 1 | 0.3 | 1.7 |
| Manning's N for drainage pipes | $N_{co}$ | 1 | 1 | 0.3 | 1.7 |
| Correlation time [h] | $\tau$ | 0.5 | 0.25 | 0.01 | 3 |
| Asymptotic stand. dev. of independent errors [$g$(l/s)] | $\sigma_E$ | $g(0.5)$ | g(0.25) | 0.01 | 1.5 |
| Asymptotic stand. dev. of the random fluctuations around the equilibrium [$g$(l/s)] | $\sigma_B$ | $g(50)$ | g(25) | 0 | 10 000 000 |

**Table 5.1:** Summary of the prior marginal distributions.

The calibration itself is performed in two steps. First, we use a generalized simulated annealing function which was designed to "search for a global minimum of a very complex non-linear objective function with a very large number of optima" (Xiang et al., 2013). Second, we use a numerical Monte Carlo Markov Chain sampler which "achieves often a high efficiency by tuning the proposal distributions to a user defined acceptance rate" as implemented by Scheidegger (2012) according to the proposal of Vihola (2012).

3. Probabilistic predictions for the data set used for calibration

   Samples from the joint posterior parameter distribution are taken and used to obtain predictions from the extended model. We re-use the last 2000 samples from the calibration. Probabilistic predictions for multivariate normal distributions related to the random variables of this type are performed as recommended by Kendall et al. (1994) and Kollo & von Rosen (2006).

4. Probabilistic predictions for unseen temporal points (validation)

   It is possible to proceed above. However, Del Giudice et al. (2013) suggest to take advantage of using bias formulated as an Ornstein–Uhlenbeck process and to "draw a realization for the entire period by iteratively drawing the realization for the next time step at time $t_j$ from that of a previous time step at time $t_{j-1}$ from a normal distribution".

5. Verification of the statistical assumptions

   In many similar cases, it is usual to confirm the statistical assumptions of the error model by residual analysis (Reichert & Schuwirth, 2012).

However, the Bayesian approach implemented in this method allows us to test only the observation error $E$, which is the only purely frequentist term. However, since these errors are likely to constitute only a small portion of the residuals of the deterministic simulator, the informative value of this analysis might be limited.

### 5.2.4 Performance assessment

After performing the extended model calibration, data from the ten remaining rainfall-runoff events are used to analyze the model predictions. To evaluate the rainfall-runoff predictions visually, we produce hydrographs for each of the ten events and rainfall data from each of the five observation layouts. We do not the evaluate the prediction performance by examining separately the uncertainty intervals for the deterministic rainfall-runoff model output. This is in accordance with Del Giudice et al. (2013), who see this approach as "not conclusive because the field observations are not realisations of the deterministic model but of the model plus the errors". Instead, we only evaluate the total uncertainty intervals associated with the extended model, i.e. the deterministic and the stochastic model together.

We also employ common summary hydrological metrics such as the Nash-Sutcliffe efficiency *NSE* [-], the total discharged volume during a whole given event, or the discharged volume during peak flow period. In particular, we compute relative errors of the total discharged volume $dV$ [-] and of the volume during peak flow $dV_{peak}$ [-] for every single prediction of the extended model. When calculating $dV_{peak}$, the time step with the maximal discharge observed is identified first and the volume discharged during eight minutes around the time step (four minutes before and four after) is computed afterwards. The difference between the modelled time with the maximal discharge and the observed one $dt_{Qmax}$ [h] is another metric we quantify for every model prediction.

The uncertainty in the metrics *NSE*, $dV$, $dV_{peak}$, and $dt_{Qmax}$ is evaluated by calculating the median and other quantiles for the whole set of predictions associated with a given rainfall observation layout, which are then graphically presented in boxplots. This is in accordance with Fencl et al. (2013) who also used the relative error of the total discharged volume and interpreted its mean $\overline{dV}$ as the volume prediction bias and its standard deviation $sd(dV)$ as the prediction uncertainty. Moreover, the discharge prediction reliability associated with a given observation layout is quantified as the fraction of discharge observations falling into the predicted 90% confidence intervals.

To better interpret the results, we classify the rainfall events as either light or heavy, based on the maximal 10-minute precipitation rate.

## 5.3 Results

First, we present hydrographs showing observed and modelled discharges for a heavy and a light rainfall event which characterize well typical features of the overall results. Next, a summary of the results for all 10 events used, as well as only those classified as heavy (maximal 10-min rainfall intensity $R_{max,10} > 12$ mm/h), and those classified as light ($R_{max,10} \leq 12$ mm/h), is presented in boxplots, with a special attention on the heavy rainfalls.

Hydrographs of a chosen light rainfall event (Fig. 5.1 top) show that the prediction performance during such an event is very similar for five out of the six evaluated rainfall observation layouts. The runoff dynamics as well as volumes are captured very well in all cases and errors occur in the same part of the hydrographs - the rising limbs. In contrast, results for the unadjusted CML QPEs present different characteristics. There is a tendency to notably underestimate the discharges. The runoff dynamics feature similar trends as before, however, not as precisely. Interestingly, many observations are out of the prediction bounds, meaning that the prediction reliability is low for this rainfall observation layout.

Hydrographs of a chosen heavy rainfall event (Fig. 5.1 bottom) present a slightly different picture than the light rainfalls above. The worst runoff prediction was obtained using rainfall data from three municipal rain gauges. In particular, the peak flows were considerably underestimated in this case. Rainfall data from all other observation layouts, including unadjusted CML QPEs, reproduced well the peaks as well as all other hydrograph features.

Summary results presented in Fig. 5.2 confirm the previously mentioned tendencies. First of all, unadjusted CML QPEs feature remarkably different results than other five observation layouts which quite resemble each other. The unadjusted QPEs considerably underestimate the runoff volumes for light rainfalls, circa by 75% in median. However, for heavy rainfall events, the bias is at the same level as in other cases. This is also reflected in the associated *NSE* values, which are around -0.5 in median for light and around 0.7 for heavy rainfalls. A certain level of bias is present as well in result for the five other observation layouts, roughly between -10% and -20% in median. Interestingly, in the cases of both the single local rain gauge and the three municipal gauges, CML QPEs adjusted using the gauge data feature smaller bias than the gauge data used alone. This also affects the associated *NSE* values, which are higher for the adjusted CML QPEs than for the rain gauge data, especially when the heavy rainfalls are considered.

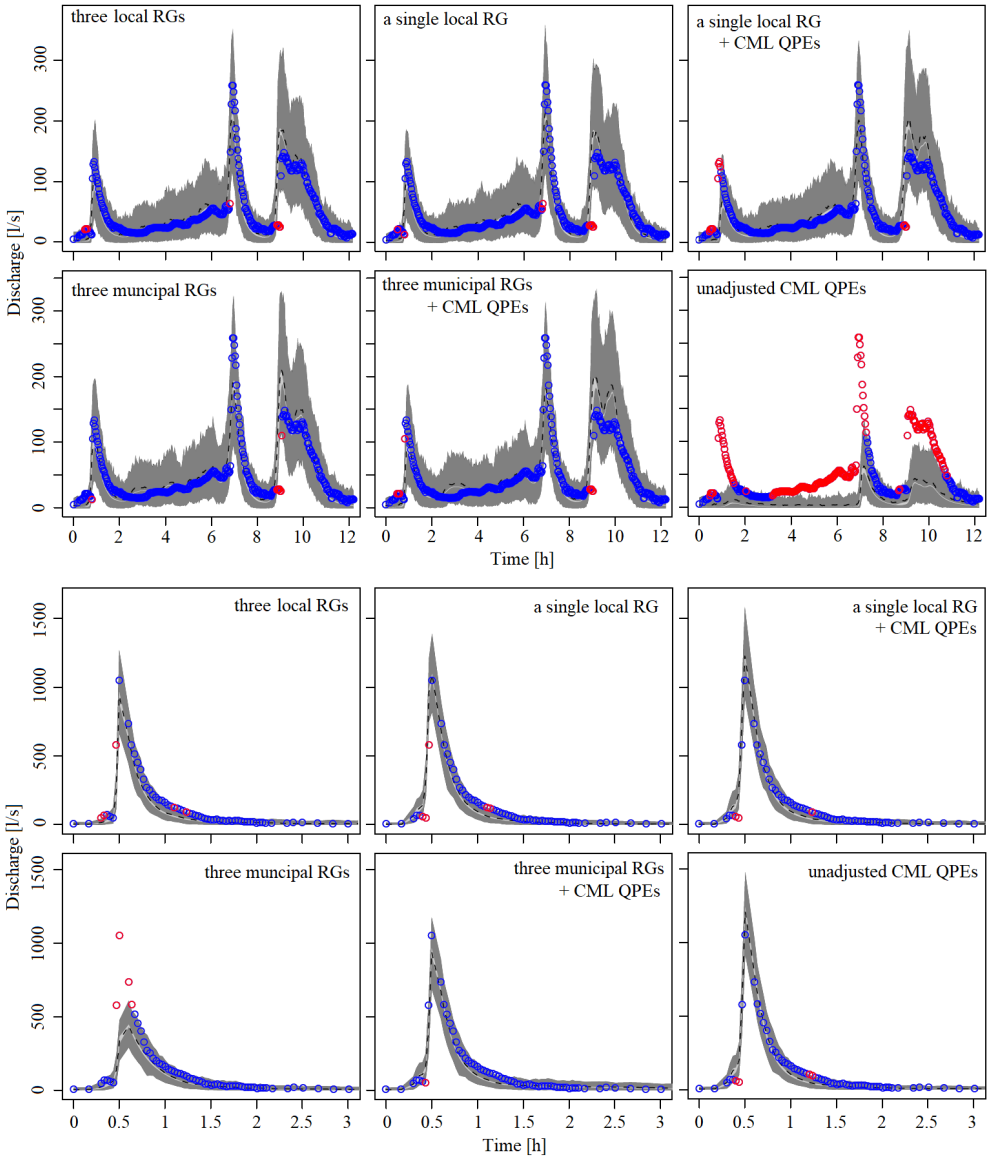


**Figure 5.1:** Hydrographs associated with a light rainfall observed on 11th August 2014 with a start at 02:24 am (top) and a heavy rainfall observed on 29th August 2014 with a start at 02:56 pm (bottom). Predicted discharges at a confidence level of 90% are shown as grey bands. The dashed line represents median prediction for a given timestep. Observed discharges are shown as circles (blue if within the prediction bounds, red if outside).

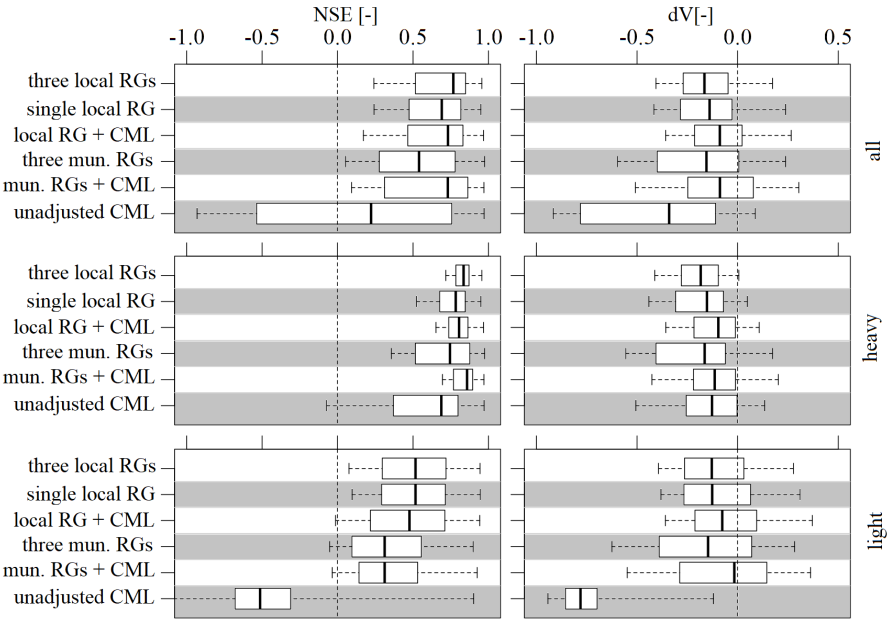


**Figure 5.2:** Boxplots showing prediction performance summaries in terms of *NSE* (left) and *dV* (right) for all 10 events (top), heavy rainfalls (center), and light rainfalls (bottom). Boxplot whiskers extent from the 10th to 100th percentile for *NSE* and from the 5th to 95th percentile for *dV*.

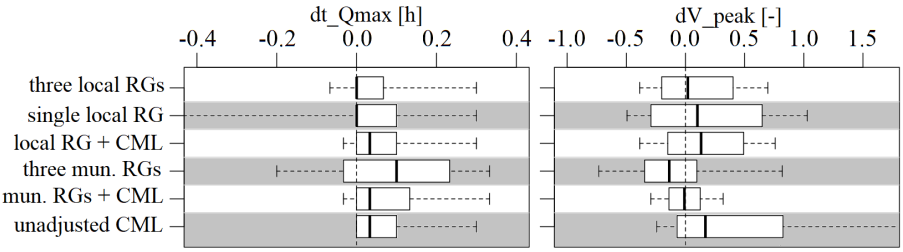


**Figure 5.3:** Boxplots showing prediction performance summaries in terms of $dt_{Qmax}$ (left) and $dV_{peak}$ (right) for heavy rainfalls. Boxplot whiskers extent from the 5th to 95th percentile.

Heavy rainfall events are analyzed in more detail in terms of their peak flows in Fig. 5.3. This shows that unadjusted CML QPEs most overestimate the peak discharges. However, adjusting CML QPEs to rain gauge data reduces the variance in $dV_{peak}$ values, even when compared to the rain gauge data themselves. In fact, most accurate and precise peak flows are obtained using the QPEs adjusted to the three municipal rain gauges. When timing of the discharge maximum is considered, the worst results in terms of precision are obtained using the single local rain gauge, and in terms of accuracy using the

three municipal gauges. CML QPEs, both adjusted and unadjusted, perform very similarly as the best-case-scenario three local rain gauges.

## 5.4 Discussion

The main findings of the study are that CML QPEs derived using a standard approach, which are often biased, lead to biased rainfall-runoff predictions, especially their underestimation during light rainfall events. However, for heavy rainfalls, which are often associated with convective events, the bias is notably lower, and runoff temporal dynamic are captured similarly well as when using high-resolution local rain gauge data. Moreover, compared to traditional rain gauge data (a single local rain gauge or three municipal gauges) used alone, adjusting CML QPEs to these gauge data has lead to an improvement in the reproduction of peak discharges and the overall modelling performance in terms of *NSE* for heavy rainfalls, for which CMLs play out the advantage of excellent spatial coverage.

These findings suggest that CML QPEs can be regarded as a viable additional rainfall data source for the field of urban rainfall-runoff modelling, especially for the monitoring of heavy rainfalls when the availability of traditional rain gauge data is limited. This is in agreement with Smiatek et al. (2017) who investigated the potential of CML QPEs for streamflow prediction in an orographically complex mountainous region. They found that, during an extreme flooding period with many local heavy rainfall events, a considerable improvement in hydrograph reproduction can be achieved when CML QPEs are employed. Our findings are also in agreement with those of Fencl et al. (2017), who found that adjusting CML QPEs to rain gauge data reduces the bias in the QPEs, which can then outperform each of the rainfall data types used individually.

Nevertheless, the relevance of our findings should be subject to further research using more extensive data sets ideally from multiple locations, since our data set only covers three consecutive months in the area of a single urban catchment. Next, it should be stressed out that the observation layouts of unadjusted CML QPEs consists of data from all 19 CMLs available in the area in that time. However, due to high computational demands, the CML QPEs adjusting to rain gauge data has been done only for four rather short CMLs which were assumed to correspond well to the catchment topology. Therefore, a similar analysis should be performed where data from CMLs of more variable path lengths and other relevant characteristics (e.g. frequency) would be evaluated, and the potential role of these characteristics on the results would be studied.

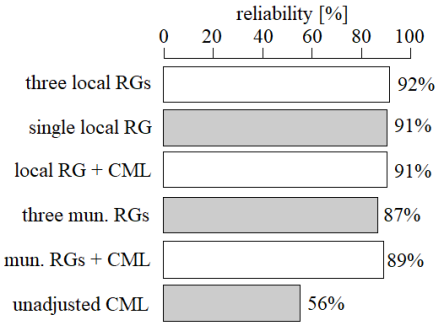


**Figure 5.4:** Discharge prediction reliability for all 10 events evaluated as a whole.

Next, the bias in simulated runoffs when using the unadjusted CML QPEs, especially pronounced during light rainfall events, has not been adequately compensated for by extending the prediction intervals (see e.g. Fig. 5.1 top) which has also lead to low overall prediction reliability as presented in Fig 5.4. For all other observational layouts, the prediction reliability at the declared 90%-confidence level is very close to 90%, however, it is only 56% for the unadjusted CML QPEs. This behavior, which could be explained by an inappropriately calibrated stochastic error model, does not compromise the main findings regarding rainfall data from this observational layouts Nevertheless, it should be analyzed what factors ( e.g. the definition of the parameter prior distributions, or the choice of meta-parameters necessary for the calibration process) have caused this effect so that similar erratic behavior could be avoided in future analyses.

It should also be noted that, during the extended model calibration, the internal structure of the deterministic rainfall-runoff model stays unchanged for a given $\theta$ parameter, which is used only as a scaling factor affecting all sub-parts of the model in the same way (see **??**). This could be avoided by employing additional stochastic parameters which would introduce random changes into the internal proportions of the $\theta$ parameters and might, in theory, improve the model structure and thus reduce the associated uncertainties. However, we have chosen not to implement this, for the sake of modelling simplicity (lower number of parameters) and results interpretability.

## 5.5 Conclusions

This study has presented the first analysis of using QPEs from real-world CMLs for rainfall-runoff modelling in a small urban catchment. This has included a comparison of the modelling performance with traditional rain gauge data and a robust statistical analysis of the model prediction uncertainty.

Our results have shown that stormwater discharges modelled using CML QPEs derived using a standard approach are often considerably biased, especially during light rainfall events. On the other hand, these QPEs can very well reproduce the runoff temporal dynamics. Moreover, adjusting the CML QPEs to traditional rain gauge data in sub-optimal resolutions has lead to an improvement in the reproduction of peak discharges and the overall modelling performance in terms of *NSE* for heavy rainfalls, compared to using the rain gauge data alone. Such adjusted CML QPEs can even lead to the same rainfall-runoff modelling performance as high-resolution rain gauge data during heavy precipitation events.

The above findings suggest that CML QPEs can be regarded as a viable additional rainfall data source for the field of urban rainfall-runoff modelling, especially for monitoring of heavy rainfalls, if local rain gauge data in high spatial resolution are not available in a given catchment. In such cases, adjusting CML QPEs to gauges from a low-density network, e.g. operated by national meteorological service or similar institutions, could provide rainfall information of adequate quality, especially when heavy rainfalls, crucial for design and operation of urban drainage systems, are considered.

Using CML QPEs in situations when other rainfall data are not available, i.e. when adjusting is not an option, would be complicated by the systematic errors in these data. However, more advanced pre-processing of CML QPEs could in theory reduce these errors in the future.

Future studies should also assess the validity of our findings using more extensive data sets which would cover longer time periods and ideally various experimental areas with CMLs of various relevant characteristics (path length, frequency), and could thus evaluate the potential role of these various factors for the CML QPE suitability for urban rainfall-runoff modelling.

# Chapter 6

# The effect of link characteristics and their position on runoff simulations

This study addresses the ability of individual commercial microwave links (CMLs) to provide relevant quantitative precipitation estimates (QPEs) for urban rainfall-runoff simulations and specifically investigates the influence of CML characteristics and position on the predicted runoff. QPEs from real world CMLs are used as inputs for urban rainfall-runoff predictions and subsequent modelling performance is assessed by comparing simulated runoffs with measured stormwater discharges. The results show that model performance is related to both the sensitivity of CML to rainfall and CML position. The bias propagated into the runoff predictions is inversely proportional to CML path length. The effect of CML position is especially pronounced during heavy rainfalls, when QPEs from shorter CMLs, located within or close to catchment boundaries, better reproduce runoff dynamics than QPEs from longer CMLs extending far beyond the catchment boundaries. Interestingly, QPEs averaged from all available CMLs best reproduce the runoff temporal dynamics. Adjusting CML QPEs to three rain gauges located 2–3 km outside of the catchment substantially reduces the bias in CML QPEs. Unfortunately, this compromises the ability of the CML QPEs to reproduce runoff dynamics during heavy rainfalls.

The bulk of this chapter was originally published in:

Pastorek, J., Fencl, M., Rieckermann, J., & Bareš, V. (2019). **Commercial microwave links for urban drainage modelling: The effect of link characteristics and their position on runoff simulations**. *Journal of Environmental Management* 251, 109522. https://doi.org/10.1016/j.jenvman.2019.109522.

## 6.1 Introduction

Inaccuracies in quantitative precipitation estimates (QPEs) from commercial microwave links (CMLs) are very much dependent on CML's sensitivity to inaccurate estimation of raindrop-induced attenuation $A_r$ [dB] which is largely determined (see 2.4.1) by its characteristics such as transmission frequency and path length (Leijnse et al., 2008).

Path lengths of CMLs typically range from a few hundred meters up to a few kilometers. Longer CMLs are less prone to bias in CML QPEs caused by inaccurate $A_r$ estimation due to, e.g., imprecise correction for wet antenna attenuation (WAA). However, their path lengths often do not correspond well to relatively small scales of urban (sub)catchments and, thus, they cannot capture rainfall spatial variability at corresponding scales. On the other hand, shorter path lengths, fitting the typical urban catchment scale well, make CMLs more prone to bias. Nonetheless, shorter CMLs usually operate at higher frequencies which are associated with a lower liability to bias.

Unfortunately, very little is known about the combined effect of the CML characteristics and their spatial representativeness on efficient use of CML QPEs for hydrological applications such as rainfall-runoff modeling. This study addresses the above knowledge gap and investigates in how far CML instrumental parameters and network topology influence the performance of CMLs as rainfall sensors for hydrological modelling. This complex problem is addressed in three steps:

1. The sensitivity of QPEs to the CML path length and transmission frequency is analyzed.
2. The CML spatial representativeness related to their path length, position, and the spatial structure of the rainfall event are investigated.
3. As, in theory, CML QPEs should outperform point measurements from rain gauges during extreme or heavy rainfall, we analyze the performance of CML QPEs in such conditions in greater detail.

In our view, main innovations of the study include also the following:

1. It is among the very first which investigate the potential of CML QPEs for urban rainfall-runoff modelling at catchment scales;
2. It employs a unique real-world data set which was collected over three consecutive summer seasons and which contains comprehensive, high-resolution data from a dense network of 19 CMLs; and
3. It provides specific recommendations on how to select CMLs suitable for urban rainfall-runoff modelling.

## 6.2 Methods

QPEs from real-world CMLs (4.1) are used as inputs in a calibrated urban rainfall-runoff model (4.2). The model performance is evaluated for CML QPEs from various observation layouts by comparing the simulated runoffs with those observed at the stormwater drainage system outlet. Next, we perform an exploratory data analysis on CML attributes to better understand their influence on volumes and temporal dynamics of the simulated runoff.

### 6.2.1 Data availability

Due to outages in data from the monitoring devices, it was possible to perform and evaluate rainfall-runoff simulations for 71 events from the monitoring period (section 4.1). For each of the events, there were data available from between 9 and 17 CMLs (47%–89%). To improve the robustness of the statistical evaluation, we have excluded from the analysis 12 rainfall events with less than two thirds of the CMLs available. Also, we excluded three extreme rainfall events for which runoff predictions were unsatisfactory, i.e. maximal discharges were overestimated by more than 100% when modelled using high-quality rainfall data from the three local rain gauges (Fig. 4.1). Similarly, three CMLs (#1, #2, #10), which experienced long outages during the experimental period, are not analyzed in the study. In summary, after rigorous quality control, the analysis is performed for 16 CMLs and 56 events. Details on the rainfall characteristics are provided in Appendix (Table A.1).

### 6.2.2 From signal levels to QPEs

Although we deliberately chose a pragmatic approach to derive CML QPEs, several steps are necessary to estimate precipitation-induced attenuation for a given CML and to derive the associated precipitation rates:

1. The difference between the transmitted and received signal level $TRSL$ [dB] is calculated for each of two CML channels.
2. A quality check is performed to identify erratic CML behavior which has to be filtered out. The following behavior is regarded as erratic:
   - Sudden peaks where, within two time steps, $TRSL$ increases and then decreases (or vice versa) by more than 5 dB,
   - Longer periods (days) with no signal fluctuation, and
   - Periods with random noise larger than 2 dB.

3. $TRSL$ data are aggregated to regular 1-min time series by averaging values within 1-min intervals.
4. $TRSL$ time series from the two CML channels are averaged.
5. Baseline attenuation $B$ is estimated with a low-pass filter parameter $m = 0.00145$ (Fenicia et al., 2012) and separated from $TRSL$ (Eq. 2.1).

After the baseline separation, we proceed by applying WAA correction ($A_{wa}$ from Eq. 2.2) and calculating the rainfall intensity $R$ [mm/h] (Eq. 2.1) in two different ways:

- WAA $A_{wa}$ is modelled as a constant offset with values suggested by Overeem et al. (2011). Parameters $\alpha$ and $\beta$ are chosen in accordance with ITU Radiocommunication Sector (2005).
- The mean of the instantaneous $R$ values of the three municipal rain gauges closest to the catchment (Fig. 4.2), aggregated to 15-min time steps, is used for adjusting $A_{wa}$ and $\alpha$, while keeping $\beta = 1$ , as proposed by Fencl et al. (2017).

### 6.2.3 Observation layouts and their evaluation

Rainfall data from 18 different observation layouts are used as precipitation inputs into the rainfall-runoff model. The rainfall model input is in all cases implemented as areal rainfall in the model meaning that rainfall intensity in a given time step has a constant value over all subcatchments of the model.

Firstly, we employ QPEs derived from only a single CML at a time, using each of the 16 CMLs consecutively. Next, we construct a time series calculated as the arithmetic mean of all available CML QPEs (not weighted) for every time step. These 17 observational layouts based on the CML data are used for both methods of deriving CML QPEs (see the end of section 6.2.2). Additionally, to compare CML QPEs with a traditional way of rainfall monitoring, the mean of the three rain gauges from the municipal network is used as the model input. These are the same rain gauges as those used for CML adjusting, but the original 1-min resolution is used in this case.

The rainfall-runoff simulations are not performed continuously for the whole observation period, but only for individual rainfall-runoff events. The model performance is evaluated, for the 18 studied observation layouts, both CML QPE deriving methods, and each of the 56 events, by comparing the simulated runoffs and observed stormwater discharges. Performance metrics are Nash–Sutcliffe efficiency $NSE$ [-], the Pearson correlation coefficient $PCC$ [-], and the relative error of the total runoff volume $dV$ [-].

The model performance for the rainfall observation layouts is analyzed also with respect to rainfall intensities of evaluated events. For these purposes, we classify the events into “light”, “moderate” and “heavy” (Table 6.1). Runoff simulations for heavy rainfalls are investigated in more detail to demonstrate the ability of CMLs for capturing heavy rainfalls, which are often characterized by high spatial variability and thus difficult to measure reliably with point rain gauge observations. However, we expect that location and spatial scale of CMLs might play a larger role than their instrumental errors when used for modelling runoff generated by heavy (spatially variable) rainfalls.

| | **Light** | **Moderate** | **Heavy** |
|---|---|---|---|
| Defining $R_{max,10}$ [mm/h] | $x \leq 5$ | $5 < x < 12$ | $12 \leq x$ |
| Number of events | 20 | 20 | 16 |

**Table 6.1:** Categorization of rainfall events. The defining maximal 10-min rainfall intensity $R_{max,10}$ as measured by the three local rain gauges temporarily installed around the catchment. For detailed info, see Appendix (Table A.1).

### 6.2.4 Data uncertainty

To interpret correctly the study results, it is crucial to estimate expected errors of both CML QPEs and discharge measurements. The errors in CML QPEs are addressed in section 2.4.1. The uncertainty of the measured discharges at the outlet of the catchment are estimated following the suggestions of Muste et al. (2012). The discharge is computed from pipe radius $R$ [m], measured flow depth $h$ [m], and measured cross sectional velocity $V$ [m/s], which are assumed to have uncorrelated errors. The following values of input variables are propagated: $R = 0.75$ m with a standard uncertainty (at a 68% level of confidence) $u(R) = 0.0015$ m. The discharge uncertainty is estimated only for periods with stormwater runoff, therefore, we assume that the standard uncertainty of measured flow depth $h$ is $u(h) = 0.015$ m. The standard uncertainty of the flow velocity $V$ in the cross section is estimated as $u(V) = 0.05V$. Finally, the expanded uncertainty (at a 95% level of confidence) of measured discharge $U(Q)$ is estimated for all discharge measurements. The expanded uncertainty $U(Q)$ varies for different flow depths, e.g. for 10% pipe filling, $U(Q) = \pm\ 0.0282$ m$^3$/s, what is equivalent to $\pm$ 31.0% of the total value $Q = 0.091$ m$^3$/s. For 50% pipe filling, the uncertainty $U(Q) = \pm\ 0.245$ m$^3$/s, corresponding to ($\pm$ 11.0%) of the discharge $Q = 2.17$ m$^3$/s.

## 6.3 Results

Firstly, typical features of simulated discharge are illustrated on a hydrograph of one of the 56 events. Secondly, the performance of the rainfall-runoff model

is investigated in relation to the CML lengths and frequencies. Afterwards, the model performance is evaluated separately for heavy rainfalls to understand the effect of CML lengths and positions during spatially more variable rainfalls. Finally, runoff simulations for CML QPEs adjusted to rain gauges are presented.

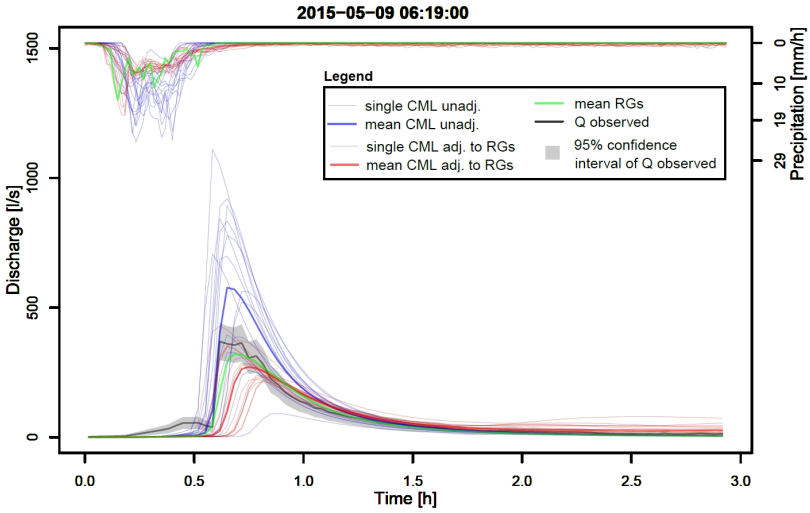


**Figure 6.1:** Modelled and observed discharges for a selected rainfall-runoff event and all examined rainfall observation layouts: QPEs from individual CMLs both unadjusted ("single CML unadj.") and adjusted to rain gauges ("single CML adj. to RGs"); The mean of both unadjusted and adjusted QPEs from all available CMLs ("mean CML unadj." and "mean CML adj. to RGs"); The mean of the three municipal rain gauges ("mean RGs").

### 6.3.1 Characteristic features of simulated hydrographs

A hydrograph which illustrates well typical features of the rainfall-runoff process is shown in Fig. 6.1. Firstly, one can see that discharge simulations using unadjusted CML QPEs (in blue) can be highly biased, however, this bias varies substantially for various individual CMLs ($dV$ between -0.709 and 0.823). In contrast, the correlation with the observed runoff is relatively high ($PCC$ 0.878 in mean) and much more stable among various CMLs (0.15 in st. dev.). Secondly, the efficiency of adjusting CML QPEs to rain gauge observations (in red) is highly conditional on the rain gauge data. The adjustment reduces the bias in simulated discharges ($dV$ between -0.280 and 0.066), but it does not always outperform simulations based on the mean of the rain gauges ($dV$ -0.152).

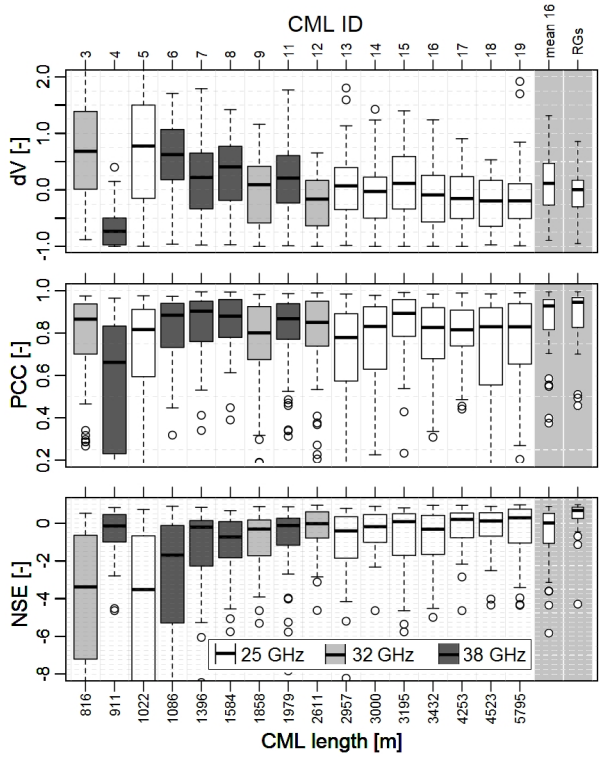


**Figure 6.2:** Boxplots of performance metrics (see 6.2.3) obtained using unadjusted CML QPEs, summarized for all available rainfall-runoff events. "Mean 16" stands for the mean of all QPEs from all 16 individual CMLs, "RGs" stands for the mean of the three municipal rain gauges. Boxes represent the interquartile range, whiskers extend to the most extreme data point which is no more than 1.5 times the interquartile range from the box, and circles represent outliers.

### 6.3.2 Performance in relation to CML lengths and frequencies

Fig. 6.2 shows boxplots of the model performance when using unadjusted CML QPEs for all 56 rainfall-runoff events, where each boxplot belongs to one observation layout. The layouts are sorted by the CML path length. Predicted discharges are on average highly biased and the large whiskers indicate substantial inter-event variability outside the upper and lower quartiles for all metrics. The largest $dV$ values tend to be associated with unadjusted QPEs from short CMLs (the exception of CML #4 is discussed below). Similarly, the inter-event variability in $dV$ is largest for simulations with short unadjusted CMLs. Such positive bias linked to the high sensitivity of short CMLs to wet antenna attenuation has been observed in the past (e.g. Fencl et al., 2019).

CML #4 is a distinctive exception to the observations formulated above. Although it is very short, unadjusted QPEs from this CML lead to substantially

underestimated runoff volumes. Additional analyses identified malfunction in one of the two channels of this CML causing unusually low values of observed attenuation. Since we use the mean of the observed attenuation of the two channels to estimate rainfall intensity, the intensities derived from this CML, and consequently the simulated runoffs, are systematically underestimated.

The model performance in terms of $PCC$ (Fig. 6.2, middle), which is insensitive to linear bias, does not show a clear dependence on CML path lengths. Better-than-average values are obtained using QPEs from 38 GHz CMLs. This is probably because these CMLs cover the catchment relatively well while being more sensitive to rainfall than lower frequency CMLs. Interestingly, the best performing CML QPEs, with $PCC$ values similar to the rain gauges, are those derived from the mean of all available CMLs. $NSE$ values (Fig. 6.2, bottom) are generally unsatisfactory, due to the high bias in the unadjusted CML QPEs. As expected, $NSE$ values are better for longer CMLs and for the mean of QPEs from all 16 CMLs.

Using the given CML network topology, the relation between the CML frequency and its performance cannot be studied completely independently of the CML path length. Nevertheless, results of CMLs #9 and #11 or #12 and #13, which have similar lengths but different frequencies, indicate that higher frequencies (which are more sensitive to raindrop attenuation) tend to provide better results, especially in terms of better correlations.

In general, when evaluating discharge simulations using volume-related performance metrics ($dV$ and $NSE$), instrumental errors seem to dominate over errors related to CML spatial representativeness. The longest least biased CMLs distinctively outperform shorter CMLs. The short CMLs are within or close to the catchment boundaries, and their lengths correspond better to the catchment scale (Fig. 4.2), but they are more prone to bias due to wet antenna attenuation (see 2.4.1). On the other hand, correlations are slightly better for shorter 38 GHz CMLs than for longer 26 GHz CMLs. However, the spatial representativeness of CMLs in relation to the catchment area might be more pronounced during heavy rainfalls, which are typically highly spatially variable and during which we can expect CMLs to be relatively less prone to instrumental errors (see 2.4.1). This is investigated in greater detail in the following subsection.

### 6.3.3 Performance during heavy rainfalls

Fig. 6.3 summarizes the rainfall-runoff modelling performance for heavy rainfalls. General tendencies for volume-related statistics are similar as when summarizing for all available events. It can be seen that there is still a considerable dependence between the CML path length and the bias in simulated discharges ($dV$, Fig. 6.3, top), which also affects the performance

in terms of $NSE$ (Fig. 6.3, bottom). Interestingly, the temporal dynamics ($PCC$, Fig. 6.3, middle) are now best reproduced (median $PCC$ 0.94, st. dev. 0.04) by the mean of all CML QPEs. This suggests that such averaged data contain valuable information about the rainfall spatiotemporal dynamics above the catchment. For the individual CML QPEs, the highest $PCC$ values are reached by QPEs from relatively short 38 GHz CMLs (#6, #7, #8) located in the western part of the catchment. This demonstrates that even biased CML QPEs can very well reproduce runoff dynamics if the CMLs cover the catchment area well. Nevertheless, the bias in the QPEs from short CMLs considerably limits their performance in terms of volume-related performance metrics, which are important for applications such as modelling of water balance or designing large retention tanks. Elimination of the bias in CML QPEs by adjusting to rain gauges is presented in the next section.

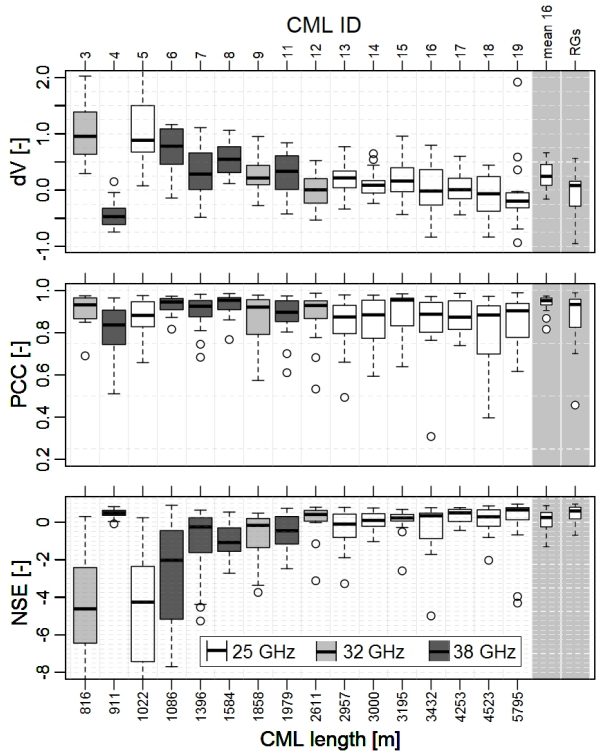


**Figure 6.3:** Boxplots of performance metrics obtained using unadjusted CML QPEs, summarized only for heavy rainfalls. "Mean 16" stands for the mean of all QPEs from all 16 individual CMLs, "RGs" stands for the mean of the three municipal rain gauges. Boxes represent the interquartile range, whiskers extend to the most extreme data point which is no more than 1.5 times the interquartile range from the box, and circles represent outliers.

### 6.3.4 Discharge simulations from adjusted CML QPEs

Although the adjustment of CML QPEs to rain gauges greatly reduces the bias (median $dV$ between 0.01 and 0.12; Fig. 6.4), it does not outperform the rain gauge data (median $dV$ 0.01). There are no clear trends associated with CML path length, neither in terms of the $dV$ median nor the $dV$ inter-event variability (st. dev. between 0.37 and 0.61). Similarly, for all CML QPEs, correlations of simulated and observed discharges are in similar ranges as for the rain gauges used alone ($PCC$ medians around 0.9, st. dev. around 0.27). For six of the individual CMLs (including short ones) and for the mean of all CMLs, the adjusted QPEs lead to slightly less variable $NSE$ values than the rain gauges (st. dev. between 0.6 and 0.73). However, no CML QPEs lead to decisively higher median $NSE$ values.

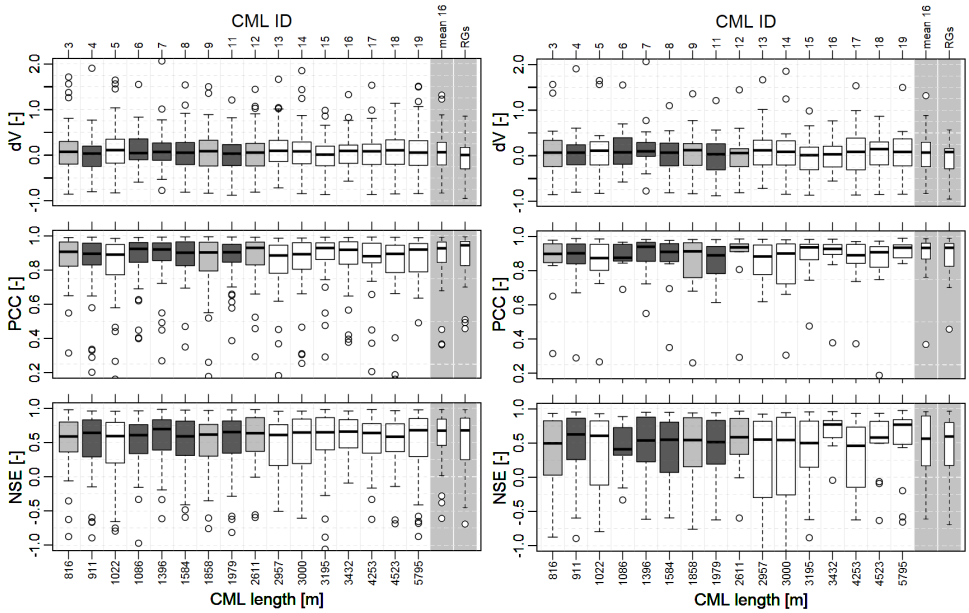


**Figure 6.4:** Boxplots of performance metrics obtained using the adjusted CML QPEs, summarized for all available rainfall events (left) and only for heavy rainfalls (right). "Mean 16" stands for the mean of all QPEs from all 16 individual CMLs, "RGs" stands for the mean of the three municipal rain gauges. Boxes represent the interquartile range, whiskers extend to the most extreme data point which is no more than 1.5 times the interquartile range from the box, and circles represent outliers.

Adjusting CML QPEs to rain gauge data effectively minimizes the bias in the CML QPEs, though it is considerably constrained by the reliability of the rain gauge data. This is especially critical during heavy rainfalls when observations from rain gauges located 2–3 km from the catchment often do not represent rainfall intensities directly in the catchment. In these cases, adjusted CML QPEs tend to be unreliable and can even worsen CML performance,

especially in terms of their ability to capture temporal dynamics of rainfall and subsequent runoff. This is demonstrated in Fig. 6.5, where discharge simulations based on *i)* only rain gauges, *ii)* the mean of all unadjusted CML QPEs, and *iii)* the mean of all adjusted CML QPEs are evaluated in terms of *PCC* and compared with each other. For heavy rainfall events, the unadjusted CML QPEs clearly outperform the rain gauge data (Fig. 6.5, left). Adjusting CML QPEs to rain gauges improves the *PCC* performance for light and moderate rainfall events, but it also worsens the results for heavy (and a few moderate) rainfall events (Fig. 6.5, right). When comparing the adjusted CML QPEs and the rain gauge data (Fig. 6.5, middle), there is no clear difference between the respective *PCC* values.

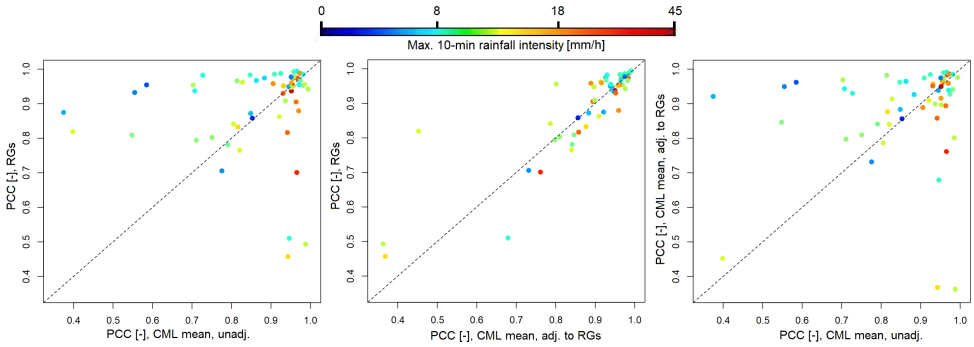


**Figure 6.5:** Scatterplots of PCC with color-coded max. 10-min rainfall intensities (Rmax,10) of individual events. Left: The mean of unadjusted CML QPEs (x axis) vs. rain gauges (y axis). Middle: The mean of adjusted CML QPEs (x axis) vs. rain gauges (y axis). Right: The mean of unadjusted (x axis) and the mean of adjusted CML QPEs (y axis).

## 6.4 Discussion

Our experimental results on using QPEs from CMLs for urban rainfall-runoff predictions suggest that CMLs can indeed provide valuable rainfall data. However, if CML QPEs are not adjusted to rain gauges, the large bias in CML QPEs leads to unsatisfactory performance, especially for short CMLs. Nevertheless, the results strongly depend on the reliability of the rainfall-runoff model and discharge observations, the pre-processing method applied

to obtain CML QPEs, and the quality and availability of the CML data. Therefore, to better interpret our results, it is necessary to discuss:

- the combined effect of uncertainty in measured discharges and the rainfall-runoff model on overall performance of CML-based discharge simulations,
- CML preprocessing with a special focus on eliminating the bias in CML QPEs, and
- the effect of the quality and availability of CML QPEs on the representativeness of the results and their transferability to different catchments.

The rainfall-runoff model was validated using independent rainfall observations from three rain gauges located within or close to the catchment boundaries (Fig. 4.1, left) for all events analyzed in this study. This enables us to directly quantify the reliability of the model (see section 4.2). The validation shows that the model reproduces runoff very well in terms of both discharge volumes ($dV$) and temporal dynamics ($PCC$, partly $NSE$). The relative error in $dV$ is small for most of the evaluated events (mean -0.007, st. dev. 0.153). These values are more than a magnitude lower than those obtained using unadjusted QPEs from short CML, and about two times lower in comparison to those of the best performing CML. Therefore, the bias in CML-based discharge simulations can be attributed mostly to the uncertainty (the bias) in CML QPEs and not to the combined uncertainty of observed discharges and the rainfall-runoff model.

The validation also shows that the simulated discharges are highly correlated with the observed ones (mean 0.95, st. dev. 0.06). The mean $PCC$ for CML-based discharge simulations is between 0.49 and 0.86, with st. dev. between 0.15 and 0.43. Thus, the deficit in reproducing runoff dynamics can also be attributed predominantly to uncertainties in CML QPEs. The only exception are discharge simulations for heavy rainfalls obtained from the mean of all unadjusted CML QPEs (Fig. 6.3, boxplot 'mean 16'), for which $PCC$ values are comparable (mean 0.94, st. dev. 0.04) to the excellent runoff predictions using the local rain gauges (mean 0.96, st. dev. 0.02). In summary, the validation of the rainfall-runoff model demonstrates that the combined uncertainty related to measured discharges and the rainfall-runoff model introduces only very little variability and, most importantly, no systematic errors into the performance assessment.

Results of this study show that bias in unadjusted CML QPEs negatively affects their usefulness for rainfall-runoff modelling, especially in terms of volume-related statistics. Most importantly, unadjusted QPEs were increasingly overestimated as CML path length decreased since shorter CMLs are relatively more sensitive to errors in $A_r$ estimation (2.4.1) due to, e.g. inaccurate WAA correction (Eq. 2.2). In our pragmatic rainfall retrieval approach,

WAA $A_{wa}$ was considered constant and its value was taken from literature (Overeem et al., 2011). It can be expected that calibrating the WAA model using independent rainfall data, or stormwater runoff measurements which reflect transformed rainfall aggregated for a whole catchment well (Pastorek et al., 2019a), would result in less biased QPEs, on average. However, the large inter-event variability indicates that the simple wet antenna correction with a constant threshold is not satisfactory, and more precise WAA models (e.g. with WAA $A_{wa}$ proportional to rainfall intensity) are necessary to obtain unbiased CML QPEs.

Adjusting CML QPEs to measurements from traditional rain gauges (Fencl et al., 2017) successfully minimizes the bias. However, using adjusted CML QPEs does not outperform predictions based on rain gauge data. Moreover, the adjustment considerably worsens the ability of CML QPEs to reproduce runoff dynamics during heavy rainfalls, except for QPEs from long individual CMLs with end nodes located further from the catchment than rain gauges. This is because the adjustment method strongly depends on the reliability of rain gauge observations which are often too far from each other to accurately observe small-scale rainfall variability. Thus, although the adjusting is conceptually promising for eliminating the bias, it requires further development. One important advantage of the adjustment suggested by Fencl et al. (2017) is that, thanks to the high temporal resolution of CML QPEs, it performs well also for rain gauge data with hourly resolution. Thus, this method can be recommended for disaggregating rainfall data in catchments where rain gauge data are available only in temporal resolutions suboptimal for urban drainage modelling.

We show that runoffs simulated using QPEs from (relatively short) CMLs located within or close to the catchment boundaries are, in spite of being biased, very well correlated with the observed runoffs. Moreover, in this respect they outperform runoffs simulated using the relatively unbiased QPEs from long CMLs, primarily during heavy rainfalls. This is probably because heavy rainfalls are often characterized by high spatial variability, and the paths of the long CMLs extend far beyond the catchment. Thus, these long CMLs cannot accurately capture areal rainfall over the catchment. For larger catchments, even relatively long CMLs might not extend out of the catchment, and thus they could be better suited to provide representative rainfall information. However, larger catchments might also require spatially distributed rainfall information, and assuming uniform rainfall, as in our study, might provide unsatisfying results. On the other hand, our results show that averaging unadjusted QPEs from all available CMLs best reproduces runoff dynamics, probably because it best captures the temporal variability of areal rainfall over the catchment, even though the averaging concerns a substantially larger area. This is in accordance with the findings of Ochoa-Rodriguez et al. (2015), who identified temporal variability of rainfall as the most sensitive attribute for urban rainfall-runoff simulations. Therefore,

it can be expected that CML QPEs will be suitable for modelling runoff dynamics also in other urban catchments where CML coverage corresponds to the spatial extent of typical rainfalls.

## 6.5 Conclusions

This study has evaluated the suitability of quantitative precipitation estimates (QPEs) from commercial microwave links (CMLs) for urban rainfall-runoff modelling. Using a unique data set from three summer seasons collected in a small (1.3 $km^2$) urban catchment in Prague-Letňany, runoff observed in the catchment was compared to runoff predicted using rainfall data from different observational layouts, in particular QPEs derived from various individual CMLs. We used a hydrodynamic model which accurately describes the rainfall-runoff process, although it underestimates flows for extreme events. The results have demonstrated that CML QPEs can be conveniently used for rainfall-runoff modeling. However, the CML data pre-processing, characteristics of the individual CMLs, such as frequency or path length, and their position influence the quality of the retrieved QPEs. The main conclusions are as follows:

- The sensitivity of CMLs to rainfall, which is given by their frequency, polarization, and length, is the most influential factor affecting the accuracy of CML QPEs, especially their bias, i.e. systematic under- or overestimation. This bias is greatest for the shortest CMLs, however, it is also variable among events. Thus, the ability of such biased CML QPEs to provide reliable flow estimates is predominantly low.

- As expected, the position of CMLs within the small urban catchment affects their ability to capture rainfall-runoff dynamics, such as the onset of a runoff event, timing of the hydrograph rising limb, runoff peak, and recession limb. The effect of CML position is especially pronounced for heavy rainfalls, when shorter CMLs with paths within or close to the catchment boundaries reproduce runoff dynamics better than longer CMLs extending far beyond the catchment.

- The best performance in terms of capturing runoff dynamics is obtained when rainfall observations of all CMLs are averaged. Notably promising results are obtained during heavy rainfall events, probably because areal rainfall from all the CMLs captures the temporal rainfall variability especially well, and runoff dynamics in small urban catchments are often more sensitive to temporal than spatial variations. Therefore, averaging of CML QPEs can be especially recommended for applications where the temporal structure of runoff and timing of peak flows is

more important than volume-related statistics, e.g. alarms during sewer construction/maintenance works.

- Adjusting the CML QPEs to data from rain gauges substantially reduces their bias while minimizing the difference among CMLs of various characteristics. Unfortunately, the adjustment also considerably worsens the ability of CML QPEs to reproduce runoff dynamics during heavy rainfalls, except for QPEs from long individual CMLs. On the other hand, the adjustment can be recommended for disaggregating rainfall data in catchments where traditional rainfall data are available only in temporal resolutions suboptimal for urban drainage modelling.
- Our experimental results demonstrate that CMLs cannot replace observation networks designed for long-term continuous hydrological monitoring. Many events had to be excluded from the analysis because of the limited CML data availability due to removal or replacement of CML units, communication outages, or hardware malfunctions, to name just a few challenges. Nevertheless, CMLs can very well complement the traditional networks and provide valuable data for operational hydrology. We expect that this is especially the case for sparsely gauged or completely ungauged regions.

Reducing systematic errors in CML QPEs remains a major challenge compromising their applications in water management tasks where runoff volume is essential, e.g. water balance modelling or designing retention capacity of drainage systems. CML QPE preprocessing methods tailored to different water management tasks, catchments, and CML networks could solve this problem. Therefore, it is necessary to better understand the interactions between the CML QPE observation errors and catchment runoff characteristics. Although modelling studies with virtual drop size distribution fields (Fencl et al., 2013) can be useful to investigate topological issues, more monitoring campaigns and experimental case studies are necessary to understand error-generating processes related to CML hardware, such as antenna wetting.

# Chapter 7

# Practical Approaches to Wet-Antenna Correction

This study analyzes how, when deriving quantitative precipitation estimates (QPEs) from commercial microwave links (CMLs), wet antenna attenuation (WAA) can be corrected without dedicated rainfall monitoring. For a set of 16 CMLs, the performance of six empirical WAA models is studied, both when calibrated to rainfall observations from a permanent municipal rain gauge network and when using model parameters from the literature. The transferability of WAA model parameters among CMLs of various characteristics is also addressed. The results show that high-quality quantitative precipitation estimates with a bias below 5% and RMSE of 1 mm/h in the median could be retrieved, even from sub-kilometer CMLs where WAA is relatively large compared to raindrop attenuation. Models in which WAA is proportional to rainfall intensity provide better WAA estimates than constant and time-dependent models. It is also shown that the parameters of models deriving WAA explicitly from rainfall intensity are independent of CML frequency and path length and, thus, transferable to other locations with CMLs of similar antenna properties.

The bulk of this chapter was originally published in:

Pastorek, J., Fencl, M., Rieckermann, J., & Bareš, V. (2022). **Precipitation Estimates from Commercial Microwave Links: Practical Approaches to Wet-Antenna Correction**. *IEEE Transactions on Geoscience and Remote Sensing* 60, 1–9. https://doi.org/10.1109/TGRS.2021.3110004.

## 7.1 Introduction

The complexity of the antenna (radome) wetting process, namely its dependence on antenna hardware properties (e.g. coating; van Leth et al., 2018) and on atmospheric conditions other than precipitation, is a major challenge to reliable estimation of wet antenna attnuation (WAA). It also negatively affects the transferability of WAA models among different commercial microwave links (CMLs) and, thus, optimal WAA models should ideally be determined for each individual CML. This is especially true for models whose parameters depend on CML path length (e.g. Kharadly & Ross, 2001). However, optimal WAA model identification (e.g. for calibration purposes) on the level of individual CMLs is challenging for real-world application with networks consisting of a high number of CMLs. As noted by Ostrometzky et al. (2018), maintenance of dedicated equipment for the retrieval of the needed reference rainfall observations is impractical for such networks. Consequently, application-focused studies with city or regional-scale CML networks have often not applied any WAA correction at all (Chwala et al., 2012; Smiatek et al., 2017) or have used only a simple constant offset model (Pastorek et al., 2019b; Overeem et al., 2011; Roversi et al., 2020; Fencl et al., 2020). Although the latter approach may be a reasonable choice when observations of the difference between the transmitted and received signal levels *TRSL* [dB] are available only as 15-min maxima and minima (Chwala & Kunstmann, 2019), it can introduce considerable bias in resulting CML quantitative precipitation estimates (QPEs) (Pastorek et al., 2019b; Fencl et al., 2019). To avoid such errors, Graf et al. (2020) recently tested a time-dependent (Schleiss et al., 2013) and a semi-empirical WAA model assuming a homogeneous water film on antenna radomes which depends on rain rate through a power law (Leijnse et al., 2008). However, in the case of both WAA models, only a single set of fixed parameters for all of around 4000 CMLs from their extensive dataset was used and this did not address the suitability of the WAA model parameters for individual CMLs.

This study analyzes, for the first time, six empirical WAA models, including a newly proposed one, based on considerably different assumptions and tests their performance in detail. In contrast to previous studies, often limited by a low number of CMLs investigated (Schleiss et al., 2013; Leijnse et al., 2008; van Leth et al., 2018), short time series of a few months (Leijnse et al., 2008; Overeem et al., 2011; Roversi et al., 2020) or 15-min CML data sampling intervals (Overeem et al., 2011; Rios Gaona et al., 2018), a rich dataset of more than two years of data retrieved from 16 CMLs with a sub-minute sampling rate is used. Motivated by the vision of reducing the costs of future studies with high numbers of CMLs, we also address the previously recognized need (Ostrometzky et al., 2018; Graf et al., 2020) to minimize the amount of auxiliary data necessary for WAA estimation without compromising the quality of retrieved QPEs and, thus, we introduce three

conceptual innovations not previously presented in relevant literature. Firstly, we show how the investigated empirical WAA models can be calibrated while notably minimizing the requirements on the reference rainfall data necessary, i.e. using only a rain gauge network with a spatial resolution of one gauge per $20-25$ km$^2$ and a temporal resolution of 15 minutes. Secondly, we analyze the variability in WAA model parameters optimized for different CMLs, thus indirectly assessing parameter uncertainties, and investigate which of the studied models can provide reliable WAA estimates without being calibrated for each individual CML. This includes a reformulation of a previously reported WAA model (Valtr et al., 2019). Thirdly, we suggest a procedure enabling the application of rainfall-dependent WAA models without any auxiliary rainfall observations, i.e. using only CML data.

## 7.2 Methods

Attenuation data from 16 CMLs collected over a 3-year period (see section 4.1) are processed (section 7.2.1) and corrected for WAA using six empirical WAA models (sections 7.2.2 and 7.2.3). The resulting CML QPEs are evaluated against the rain gauge data from the municipal network (section 7.2.4).

### 7.2.1 From signal levels to QPEs

CML data processing steps before baseline separation, including a quality check and aggregation to a 1-min resolution, are done in the same way as described in section 6.2.2. Baseline attenuation $B$ [dB] is assumed to equal $TRSL$ [dB] (Eq. 2.2) during dry periods. During wet periods, $B$ is estimated by linearly interpolating from the dry periods. Data available from both CMLs and rain gauges for the wet period identification are used. First, we identify wet timesteps for the CML data (mean $TRSL$ of all CMLs) using a climatological threshold (Schleiss & Berne, 2010) defined as the 90th percentile of the rolling standard deviation of a 60-minute window. For the rain gauge data, timesteps are identified as wet when gauge tipping is observed at one or more gauges. Subsequently, wet periods are defined for both sensor types by setting the start of a wet period to one minute before the first observed wet timestep and the end to 60 minutes after the last one to ensure that baseline interpolation is not affected by wet antennas. Afterwards, the wet periods defined by the two sensor types are merged by taking the earliest starts and the latest ends. These are then used for the baseline separation using the linear baseline model.

From the above defined wet periods, only hydrologically relevant rainfall events (total rainfall depth $H > 2$ mm) are selected for further processing.

After eliminating events with substantial data gaps, 53 events (360 hours) are available.

After the baseline separation, WAA $A_{wa}$ [dB] is estimated (details in the next section) and subtracted to obtain raindrop attenuation $A_r$ [dB] (Eq. 2.2). Then, $A_r$ is divided by the CML path length and thus transformed into specific raindrop attenuation $\gamma$ [dB/km] from which rainfall intensity $R$ [mm/h] is calculated using Eq. 2.1, with parameters $\alpha$ and $\beta$ according to ITU Radiocommunication Sector (2005). These parameter values are in very good agreement with values derived directly from drop size distribution observations (Chwala & Kunstmann, 2019; Valtr et al., 2019), however, they may not be optimal for other rain type regions (Rios Gaona et al., 2018).

### 7.2.2 Empirical WAA models

We evaluate a scenario without correcting for WAA (Zero) and six empirical models for WAA correction (overview in Table 7.1). For all models, it is assumed that WAA is estimated for two antennas, i.e. at both CML ends. The simplest approach is to model WAA $A_{wa}$ as a constant offset (O; Overeem et al., 2011). In a more complex method, we model $A_{wa}$ as time-dependent, exponentially increasing towards an upper limit during wet periods, and decreasing exponentially afterwards (S; Schleiss et al., 2013).

Next, we evaluate models where $A_{wa}$ depends on $R$. Valtr et al. (2019) proposed a model (V) where the dependence on $R$ is explicit through a power law

$$A_{wa} = 2k' R^{\alpha'} \tag{7.1}$$

where $k'$ and $\alpha'$ are the power law parameters. We also analyze a model (KR) suggested by Kharadly & Ross (2001) deriving $A_{wa}$ from observed attenuation after baseline separation $A$ [dB] (see Eq. 2.2), i.e. depending on $R$ implicitly. However, as $A$ is dependent on CML path length, optimal parameters of the KR model would differ for two CMLs with the same hardware but with different path lengths. To eliminate this feature, we propose a model (KR-alt) in which $A_{wa}$ is bounded by an upper limit, as in Kharadly & Ross (2001), but derived from $R$ explicitly through a power law

$$A_{wa} = C(1 - \exp(-dR^z)) \tag{7.2}$$

where $C$ [dB] represents the maximal $A_{wa}$ possible, and $d$ and $z$ are power law parameters. Nevertheless, as optimal $C$ and $d$ values are not independent and can compensate for each other (similar to the KR model, see Fig. 7.4), we reduce the number of parameters to two by setting $d = 0.1$.

WAA models with parameters independent of CML path length can also be formulated when $A_{wa}$ is derived explicitly from $\gamma$, not only $R$. However, it is

unclear which of the two alternatives would provide WAA model parameters independent of CML frequency. Unlike $\gamma$, $R$ is independent of CML frequency. The results from Leijnse et al. (2008) suggest that $A_{wa}$ is also considerably less sensitive to CML frequency than $A_r$ or $\gamma$. Therefore, parameters of the models deriving $A_{wa}$ from $R$ explicitly are probably more transferrable among frequencies. To confirm this hypothesis, we reformulate the model of Valtr et al. (2019) (V-alt), and replace $R$ with $\gamma$ so that:

$$A_{wa} = 2p\gamma^q \tag{7.3}$$

where $p$ and $q$ are the power law parameters.

As neither $R$ nor $\gamma$ can be observed directly using CMLs, the V, V-alt, and KR-alt model equations must be rearranged to include only one unknown variable, $A_{wa}$, which can thus be quantified from $A$ (details in the next section). The rearranged equations are then solved numerically.

| WAA model | Parameter values from the literature | Abbrev. |
|---|---|---|
| Zero WAA<br>(no WAA correction) | – | Zero |
| Constant<br>non-zero offset | $A_{wa} = 1.585$ dB<br>the mean of the optimal values<br>identified in Overeem et al. (2011) | O |
| Dynamic (time-dependent)<br>(Schleiss et al., 2013) | $W = 2.3$ dB $\quad \tau = 15$ min<br>from Schleiss et al. (2013) | S |
| Depending on $A$ explicitely<br>with an upper limit<br>(Kharadly & Ross, 2001) | $C = 8$ dB $\quad d = 0.125$<br>from Kharadly & Ross (2001); for 27 GHz | KR |
| Depending on $R$ explicitely<br>with an upper limit | – | KR-alt |
| Power-law relation to $R$<br>(Valtr et al., 2019) | $k' = 0.68 \quad \alpha' = 0.34$<br>from Valtr et al. (2019) | V |
| Power-law relation to $\gamma$<br>(reformulated V) | – | V-alt |

**Table 7.1:** Overview of the investigated WAA models and their parameters.

### 7.2.3 Practical details on WWA model equations

Herein we show how WAA models dependent on rainfall intensity can be used during the CML data processing routine without the need for auxiliary rainfall observations. In particular, we formulate single-unknown equation forms of the models which relate WAA $A_{wa}$ [dB] explicitly to the rainfall intensity $R$ [mm/h] and to the specific raindrop attenuation $\gamma$ [dB/km]. Using these rearranged equations, $A_{wa}$ can be quantified directly from the observed attenuation after baseline separation $A$ [dB], e.g. by solving the equations numerically. The relation between V and V-alt models is also provided.

### V model

The original equation of V model (Eq. 7.1; Valtr et al., 2019), where $k'$ and $\alpha'$ are the WAA model's power law parameters, requires independent observation of the rainfall intensity $R$ [mm/h] as its input. However, it holds that:

$$R = \alpha\gamma^{\beta} \tag{7.4}$$

where $\alpha$ and $\beta$ are the power law parameters with values depending on the CML frequency and polarization. Moreover, if $L$ [km] is the CML path length, then

$$\gamma = (A - A_{wa})/L. \tag{7.5}$$

Therefore, using Eq. 7.4 and 7.5, the original Eq. 7.1 can be rearranged into the following single-unknown form which can be used to quantify $A_{wa}$ from $A$:

$$A_{wa} = 2k'(\alpha((A - A_{wa})/L)^{\beta})^{\alpha'}. \tag{7.6}$$

### V-alt model

Starting from its original equation in which $A_{wa}$ is explicitly dependent on $R$ (Eq. 7.1), V model can be reformulated using Eq. 7.4 in the following manner:

$$A_{wa} = 2k'R^{\alpha'} = 2k'(\alpha\gamma^{\beta})^{\alpha'} = 2k'\alpha^{\alpha'}\gamma^{\beta\alpha'}. \tag{7.7}$$

If ($p = k'\alpha^{\alpha'}$ and $q = \beta\alpha'$), then the V-alt model (Eq. 7.3) represents a reformulation of the V model in which $A_{wa}$ is explicitly dependent on $\gamma$.

Similarly as the original V model, also the V-alt model (Eq. 7.3) can be rearranged using Eq. 7.5 into a single-unknown form which can be used to quantify $A_{wa}$ from $A$:

$$A_{wa} = 2p((A - A_{wa})/L)^{q}. \tag{7.8}$$

### KR-alt model

The following original KR model (Kharadly & Ross, 2001), where $C$ [dB] and $d$ are the model parameters, relates $A_{wa}$ explicitly to $A$:

$$A_{wa} = C(1 - \exp(-dA)). \tag{7.9}$$

However, as $A$ is affected by CML path length, optimal parameters of the KR model would differ for two CMLs with the same hardware but different path lengths. To eliminate this feature, we have proposed a WAA model (Eq.

7.2; KR-alt) in which $A_{wa}$ is, similar to Eq. 7.9, bounded by an upper limit, but derived from $R$ explicitly through a power law.

Analogically to the V model (Eq. 7.1), also the KR-alt model (Eq. 7.2) can be rearranged, by applying Eq. 7.4 and 7.5, into a single-unknown form which can be used to quantify $A_{wa}$ from $A$:

$$A_{wa} = C(1 - \exp(-d(\alpha((A - A_{wa})/L)^{\beta})^{z})). \tag{7.10}$$

### 7.2.4 Calibration and performance of WAA models

The WAA models studied are evaluated when using parameter values taken from the literature, if available, and when calibrated to rainfall data from the three municipal rain gauges. Moreover, for each WAA model, calibration is done in three scenarios:

- separately for each of the 16 CMLs;
- separately for each frequency band; and
- for all CMLs at once.

In total, data from 53 rainfall events (360 hours) are available for WAA model calibration and evaluation. From these, we randomly select 25 events (281 hours) for the calibration. Model parameters are optimized by comparing the CML QPEs with the mean $R$ of the three municipal rain gauges. Both data sets are aggregated from a 1-min to a 15-min resolution to reduce observation noise. The root mean square error (*RMSE*) is used as the objective function and optimized with simulated annealing, an optimization method designed for complicated non-linear functions with many local minima (Xiang et al., 2013). For calibration scenarios using multiple CMLs at once, the mean RMSE of the CMLs is optimized.

Once the optimal WAA model parameters are identified, they are used to derive CML QPEs for the remaining 28 events (349 hours) not used for calibration. The CML QPEs are aggregated from the 1-min to the 15-min resolution and evaluated by direct comparison with the rain gauge data (the mean of the three gauges in the 15-min resolution). The QPEs are evaluated individually for each CML using a time series consisting of all 28 events, the performance for individual events is not quantified. Performance metrics employed are:

- the relative error of the rainfall depth *dH* [%] reflecting the bias;
- the root mean square error *RMSE* [mm/h]; and
- the Spearman rank correlation coefficient SCC [-] which quantifies the strength of a monotonic relationship between two variables and is independent of both linear and non-linear bias.

## 7.3 Results

Firstly, the performance of the estimated CML QPEs summarized for all CMLs is presented (7.3.1). Secondly, the QPEs are investigated in closer detail on the level of individual CMLs (7.3.2). Parameter values used for the WAA model evaluation are also presented (7.3.3).

### 7.3.1 Summary for all CMLs

The results summarized in Fig. 7.1 show that, when calibrated individually for each CML, models in which $A_{wa}$ is proportional to $R$ (KR, V, KR-alt, V-alt) can lead to CML QPEs with a bias lower than 5% in the median (up to 10% for most CMLs) and with *RMSE* between 0.8 and 1.2 mm/h. Models explicitly relating $A_{wa}$ to $R$ (V and KR-alt) attain similarly good values (median bias less than 5%, standard deviation 18%) not only when calibrated individually for each CML, but also when calibrated for groups of CMLs with the same frequency and for all CMLs at the same time. Similarly, *RMSE* obtained using these two models is almost the same, between 0.8 and 1.2 mm/h, for all three calibration approaches. A very similar performance is reached using the V-alt model, which relates $A_{wa}$ to $\gamma$, when calibrating separately for each of the three frequency bands. However, when calibrating the V-alt model for all CMLs at once, the standard deviation of dH increases to 25% and *RMSE* values reach up to 1.4 mm/h for some CMLs. Calibrating models O and S leads to markedly underestimated *dH* values for most CMLs (around 40% in median) for all three calibration approaches. This also affects the respective *RMSE* values which are around 1.4 mm/h in the median for

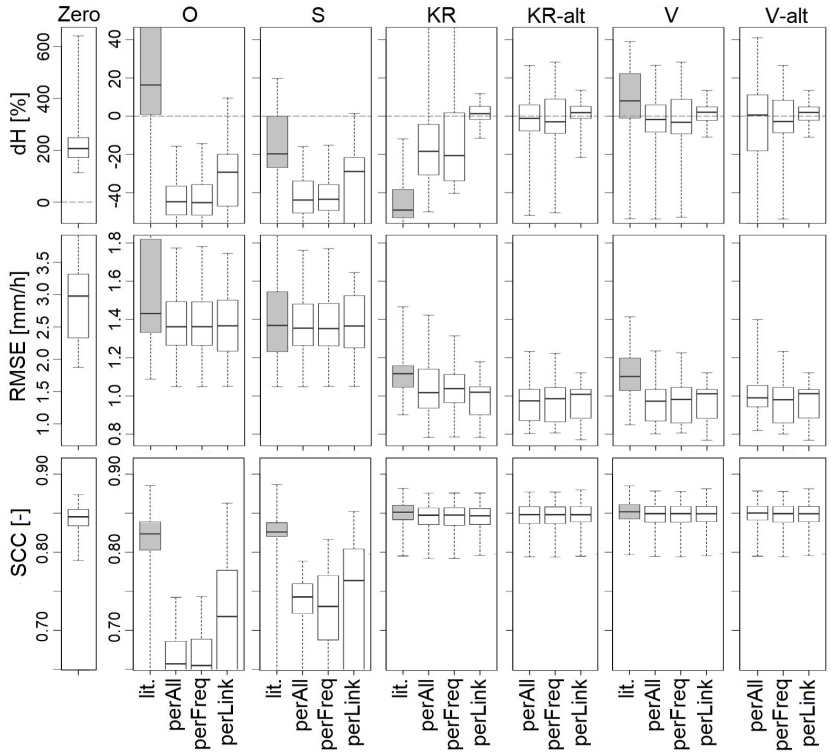


**Figure 7.1:** Boxplots showing variation in the performance of the QPEs from the 16 individual CMLs quantified by the performance metrics *dH* (top), *RMSE* (middle), and *SCC* (bottom). CML QPEs have been derived without WAA correction (Zero) and using the six WAA models. Sub-boxplots show the effect of WAA model calibration (lit. – parameter values from literature, perAll – calibrated for all CMLs at once, perFreq – calibrated separately for CMLs operating at the three various frequency bands, perLink – calibrated separately for each CML). Note the different ranges of the y-axes for the Zero model.

all calibration approaches. Interestingly, using the S model with parameter values from the literature leads to a lower bias for most CMLs (*dH* -20% in the median). However, the *RMSE* is virtually the same as for the calibrated model, with only a slightly larger variance. For other WAA models, the literature values perform, in general, worse than those optimized during the calibration, both in terms of *dH* and *RMSE*. As expected, without the WAA correction, CML QPEs are considerably overestimated (median *dH* ca. 200%, *RMSE* ca. 3 mm/h).

The correlation in terms of *SCC* (Fig. 7.1 bottom) reaches very similar values (about 0.85 in median) for all WAA models in which $A_{wa}$ is proportional to $R$ (KR, V, KR-alt, V-alt), regardless of whether/how they are calibrated. Only negligibly lower values are reached when not using any WAA model at all (scenario Zero). For most CMLs, *SCC* values between 0.8 and 0.85 are associated with the O and S models with parameter values from the

literature. Calibrating these two models has led not only to a considerable underestimation of rainfall, but also to relatively low *SCC* values (medians between 0.65 and 0.76).

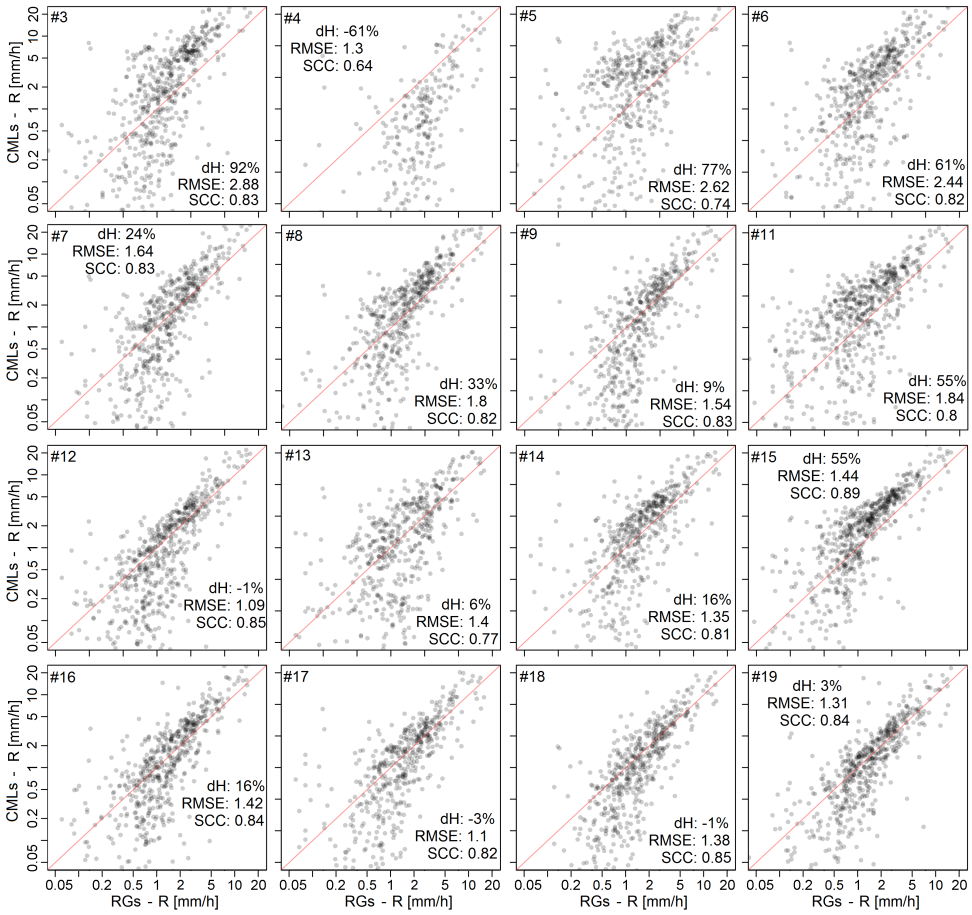


**Figure 7.2:** Scatter plots comparing rain gauge data (RGs) with CML QPEs for the O model with parameters from the literature. Note that the axes are in logarithmic scales. The presented 15-minute data from the 28 rainfall events used for the evaluation represent 349 hours of observations. In 835 out of the 1,401 time steps, rain gauge data contain non-zero records. Most points with RG rainfall intensity below 0.3 mm/h are out of the plotting range, as the respective CML QPEs are below 0.05 mm/h.

### 7.3.2 Individual CMLs

In addition, we analyze the estimated QPEs on the level of individual CMLs for two WAA modelling scenarios. First, CML QPEs derived using the commonly used O model with parameter values from literature are compared with the rain gauge data (Fig. 7.2). Next, representing the better performing WAA models from above, the same is done for the V model with parameters

optimized for all CMLs at once (Fig. 7.3). The V model leads to a distinct improvement over the O model. The V model reduces the bias for low and high $R$ and thus removes the dependence of errors in CML QPEs on $R$. Therefore, the performance metrics *dH* and *RMSE* are improved for most CMLs, however, the change of *SCC* is practically negligible. The reduction of errors is most significant for the shortest CMLs, as the relative contribution of $A_{wa}$ to $A$ decreases with the increasing path length.

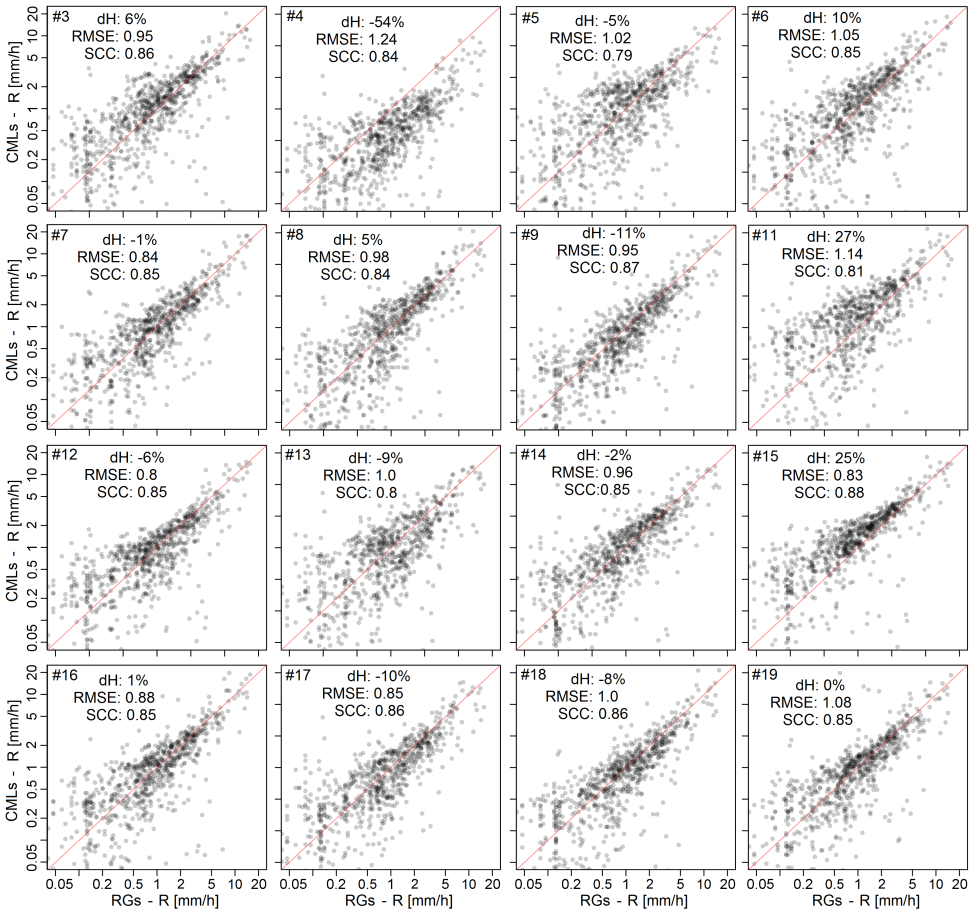


**Figure 7.3:** Scatter plots comparing rain gauge data (RGs) with CML QPEs for the V model with the same parameters used for all the CMLs (obtained by optimizing for all CMLs at once). Note that the axes are in logarithmic scales. The presented 15-minute data from the 28 rainfall events used for the evaluation represent 349 hours of observations. In 835 out of the 1,401 time steps, rain gauge data contain non-zero records.

### 7.3.3 WAA model parameters

We also present parameter values used for the WAA model evaluation, both optimized during calibration and taken from the literature (Fig. 7.4). Op-

timized parameter values of the V and KR-alt models are similarly located in their parameter spaces. Moreover, optimal parameter values for the three various frequency bands are, for these two models, located very close to the optimal values obtained when calibrating for all CMLs at once. This stands in contrast to the V-alt method for which a dependence between the frequency band and the optimal parameter values can be seen. For the KR model, the clear dependence of the two model parameters is most striking. For the S model, optimal values of the $W$ parameter are similar to the parameter values of the O model. However, there is no clear relation to the CML frequency for either of these two WAA models. Parameter values taken from the literature are, in all four cases, located relatively close to the optimized parameters.

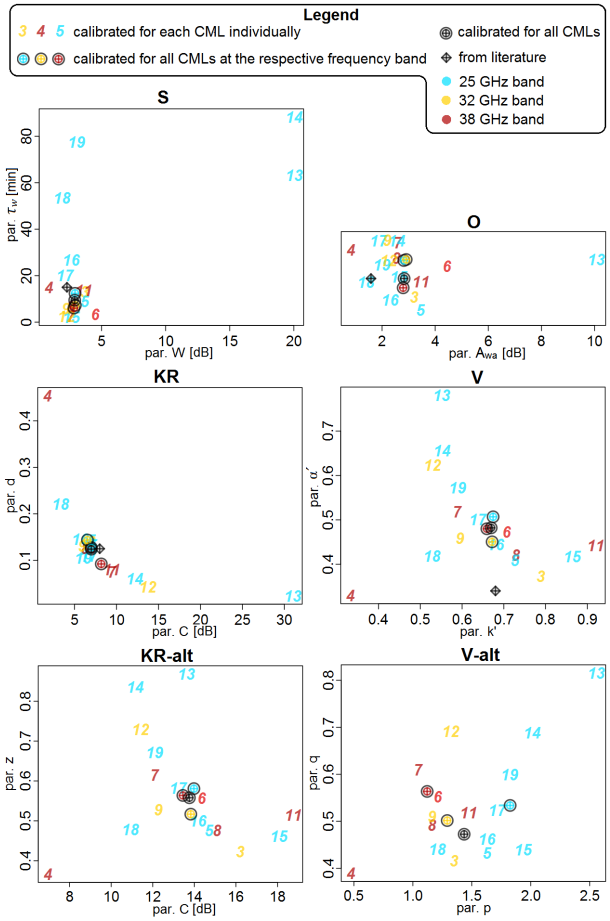


**Figure 7.4:** WAA model parameter values used for WAA model evaluation, both optimized during calibration and taken from literature (if available). The numbers indicate CML IDs and the colors indicate frequency.

## 7.4 Discussion

The best results, in terms of dH and RMSE, are, in general, achieved for the models in which WAA $A_{wa}$ is proportional to rainfall intensity $R$ (KR, V, KR-alt, V-alt). For these models, QPEs of the same high quality can be obtained when calibrating for each CML separately. However, the V model and the newly proposed KR-alt model, which both relate $A_{wa}$ to $R$ explicitly, perform very well, even when using the same parameter set for all CMLs. As the KR model relates $A_{wa}$ to $A$, which is dependent on CML path length, it performs markedly worse when using the same parameter set for more CMLs. The V-alt model performs very well when using the same parameters for CMLs operating at one frequency band and moderately worse when using the same parameter set for all frequency bands. This is in agreement with the calibrated model parameter values (Fig. 7.4) and supports the hypothesis that the parameters of models deriving $A_{wa}$ from $R$ explicitly (V, KR-alt) are more transferrable among CMLs of various frequencies than the parameters of models deriving $A_{wa}$ explicitly from  (V-alt).

The results of calibrating the O and S models resemble each other in terms of estimated rainfalls (Fig. 7.1), optimal model parameters (Fig. 7.4), and WAA levels (Fig. 7.5). The rainfall underestimation (i.e. WAA overestimation) associated with the O and S models is likely caused by different optimal parameter values for *RMSE*, used as the calibration objective function, and *dH* due to the systematic errors in rainfall estimates when modelling WAA $A_{wa}$ as completely or almost constant.

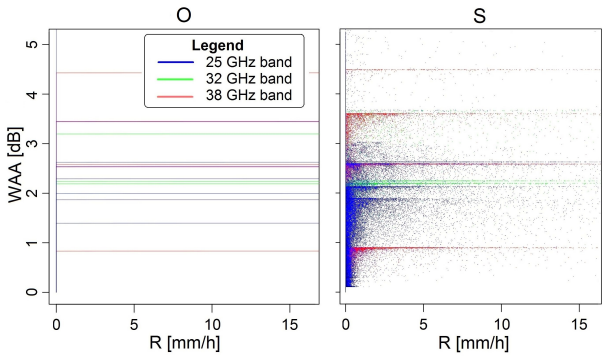


**Figure 7.5:** WAA levels obtained using the O and S WAA models when calibrated separately for each CML in relation to the respective CML QPEs. The vertical line in the left panel at $R = 0$ mm/h is caused by the nature of the O model. If observed attenuation after baseline separation $A$ is lower than a given parameter value of the O model, WAA is considered equal to $A$, i.e. there is no rainfall observed.

In total, our results show that unbiased CML QPEs could be retrieved without the need for extensive additional rainfall monitoring when empirical models for

WAA estimation are calibrated to rainfall data from the permanent municipal rain gauge network. Models in which WAA is dependent on rainfall intensity provide the best WAA estimates. Moreover, models explicitly relating WAA to rainfall intensity can provide optimal results even when using the same set of parameter values for CMLs of different characteristics.

The presented results confirm the importance of appropriately correcting for WAA when deriving QPEs from CMLs which is in agreement with previous research (Chwala & Kunstmann, 2019). In particular, the results imply that modelling WAA as constant (O model) is not satisfying when *TRSL* data in 1-min resolution are available. This is in accordance with Pastorek et al. (2019b); Fencl et al. (2019) and contradicting Ostrometzky et al. (2018), however, it should be noted that the latter study focused on WAA estimation for purposes of CML network design and investigated E-band CMLs. Nonetheless, our findings do not dispute the statement that this approach may be a reasonable choice if only 15-min TRSL maxima and minima are available (Chwala & Kunstmann, 2019).

It is shown that the most accurate rainfall estimates are associated with models relating WAA to rainfall intensity, which is in agreement with the WAA estimation approaches presented in Valtr et al. (2019); Kharadly & Ross (2001); Leijnse et al. (2008); Fencl et al. (2019). On the other hand, having provided a comparison of the performance of different WAA models, Schleiss et al. (2013) came to different conclusions. Although their results correspond to ours in terms of *RMSE*, not only for the scenario without WAA correction (Zero; 3.15 mm/h), but also for the WAA models O (1.34 mm/h) and KR (0.91 mm/h), they observed the best performance for the time-dependent S model (0.72 mm/h). It should be noted that they used data from only a single CML and that the parameter values differed from those used in our study because the models were calibrated to local rainfall data from five disdrometers along the CML path. Since, in our case, the S model has only performed (and generally behaved) very similarly as the constant O model, it seems that, in accordance with van Leth et al. (2018), wetting dynamics play a much smaller role for the antennas used in this study than for those analyzed by Schleiss et al. (2013). Recently, similar behavior was observed by Graf et al. (2020) who found that a semi-empirical WAA model assuming a homogeneous water film on antenna radomes dependent on rain rate through a power law (Leijnse et al., 2008) led to more precise CML QPEs than the S model. As their analysis was based on a large country-wide dataset of around 4000 CMLs, it can be concluded that CML antennas for which WAA is not affected by the wetting dynamics are rather usual.

However, the relevance of our findings for other CML networks should be subject to further research. Firstly, it is likely that the capacity of rainfall data from rain gauge networks for calibrating WAA models will depend on gauge network density as the correlation among the gauges decreases

with increasing distance. Aggregating the data to coarser resolutions for the calibration might improve the results as it would improve the correlation (Villarini et al., 2008). Nevertheless, if the sensors are too far from each other, it might be more appropriate to use long-term (e.g. monthly) precipitation depths.

Secondly, the reference areal rainfall used to evaluate the performance of the WAA models has been derived from the same three rain gauges that had been previously used to calibrate the WAA models. However, the rain gauge network density of one gauge per $20-25$ km$^2$ might not be sufficient to reliably represent areal rainfall for events with high spatial variability, e.g. storms with small convective cells. Therefore, out of the 28 individual rainfall events used for the WAA model evaluation, we have identified 11 events with the highest variability among the rain gauges and repeated our analysis using only the data from the remaining 17 events. Differences between the results for the 17 events and for all 28 events together are subtle. The estimated rainfall depths are slightly higher when evaluating all 28 events together than when using the 17 less variable events only. However, differences in terms of RMSE and SCC are minimal, and mutual relations of the individual WAA models and calibration scenarios are not affected.

Due to the use of only three rain gauges, we are also not able to precisely estimate rainfall starts and ends specifically for each CML. Therefore, the process of wet period identification has been designed to avoid classifying wet timesteps as dry, rather than vice versa. This approach makes wet periods longer, however, as the baseline is relatively stable (Schleiss et al., 2013), the order of errors in the estimated baseline levels is well below 1 dB.

Next, all CMLs used in this study are from the same product family of the same manufacturer (Ericsson, Mini-Link) and have aged similarly due to exposure to similar climatic conditions. However, different behavior might be observed for CML antenna hardware of different producers, exposed to different climates for different time periods, or for other specific conditions (e.g. non-zero antenna elevation angles), and thus, the results of this study might not be directly applicable in such circumstances.

Lastly, it should be noted that the V model was originally derived (Valtr et al., 2019) by using one of our 16 CMLs and data from one of the three summer seasons that we have investigated herein.

## 7.5 Conclusions

We have shown in this study that virtually unbiased QPEs could be retrieved from CMLs without the need for dedicated rainfall monitoring campaigns.

CML QPEs with a bias lower than 5% and *RMSE* of 1 mm/h in the median have been obtained when the empirical models for WAA estimation have been calibrated to rainfall data from the permanent municipal rain gauge network with a spatial resolution of one gauge per $20-25$ km$^2$. It has been shown that such high-quality QPEs can even be derived from short, sub-kilometer CMLs where WAA is relatively large compared to raindrop attenuation. Models relating WAA to rainfall intensity, implicitly or explicitly, have led to the best results. For the latter, parameter sets have been found to be suitable for CMLs of various path lengths operating at various frequency bands, which could thus be transferred to other locations with CMLs of similar antenna hardware characteristics. Moreover, it has been demonstrated how these WAA models can be successfully applied without any auxiliary rainfall observations, i.e. using CML data only.

This study has confirmed both the potential of CMLs as a source of high-quality rainfall data and the importance of appropriate WAA correction when deriving the QPEs. The presented advances in minimizing the requirements on auxiliary data necessary, both during the calibration of WAA models and during their implementation in the CML data processing routine, represent a legitimate step towards the retrieval of reliable QPEs from large CML networks in conditions where rainfall data are scarce. However, since the potential usefulness of CML QPEs increases with the decreasing availability of other rainfall (or other reference) data, further studies are needed, ideally with extensive datasets containing different CML hardware, to advance our capacity to correct for WAA in the data-scarce conditions. This would also be greatly beneficial for the application of CML QPEs in quantitative hydrological tasks such as urban rainfall-runoff predictions.

# Chapter 8

# Assesing CML QPEs by quantifying uncertainties in runoff predictions in a small urban catchment: The final study

This study analyzes the value of state-of-the-art quantitative precipitation estimates (QPEs) from commercial microwave links (CMLs) for rainfall-runoff modelling in a small urban catchment. A model for wet-antenna attenuation (WAA) is calibrated to data which could be commonly available to urban hydrologists. CML QPEs retrieved using such WAA model are then used for runoff predictions. The uncertainty of the predicted runoff is quantified using a stochastic error model. Predictions with CML QPEs derived using the WAA model calibrated to 60-min data from an 8-km distant rain gauge are notably biased. However, such CML QPEs perform better than 1-min data from rain gauges at 2–3 km distances. Calibrating the WAA model to 60-min records from the 3 above gauges, or to observed discharges, leads to CML QPEs predicting discharges almost as well as 1-min records from 3 gauges at the catchment boundaries. These results imply that, for rainfall-runoff modelling in small urban catchments covered by roughly 1 rain gauge per 20–25 km$^2$, CML QPEs represent a notable improvement. For networks with roughly 1 gauge per 0.5–1 km$^2$, CML QPEs are a satisfying alternative.

The bulk of this chapter represents a paper manuscript which is about to be submitted to be considered for publication in *Journal of Hydrology*.

## 8.1 Introduction

Quantitative precipitation estimates (QPEs) retrieved from commercial microwave links (CMLs) have been proven to contain valuable rainfall information which could complement traditional data from rain gauges and weather radars (Chwala & Kunstmann, 2019; Imhoff et al., 2020; Rios Gaona et al.,

2018; Uijlenhoet et al., 2018). Nevertheless, only a few studies, either from rural (Brauer et al., 2016; Cazzaniga et al., 2020; Smiatek et al., 2017) or urban catchments (Disch et al., 2019; Pastorek et al., 2019b; Stránský et al., 2018), have presented application of QPEs derived from real-world CML networks for hydrological modelling. Therefore, in spite of their high potential and recent advances in their retrieval, many questions regarding the suitability of CML QPEs for practical hydrological tasks, such as rainfall-runoff modelling in small urban catchments, remain unresolved.

It has been concluded that CML QPEs could be conveniently used for urban hydrological modelling in combination with other rainfall data, and if available in high temporal resolutions, they can lead to very well predicted temporal dynamics of runoff from a small urban catchment (Disch et al., 2019; Stránský et al., 2018). It has also been shown that, when deriving CML QPEs without using reference rainfall data, systematic errors common in CML QPEs, make them unsuitable for applications where precipitation/runoff volume is of high importance (Pastorek et al., 2019b, Chapter 6). This is unfortunate because CML QPEs could be particularly useful in regions where long-term rainfall monitoring networks are not available, or available only in resolutions which do no not suffice for most purposes of urban hydrological modelling (Gosset et al., 2016). Yet, it is not clear how to make the best use of CML QPEs under such conditions.

It has been argued that ignoring the uncertainty, particularly related to input data, compromises (not only) hydrological modelling (Beven, 2006; Kavetski et al., 2006), or similarly, that quantification of the uncertainty associated with the models in urban stormwater modelling is a must (Dotto et al., 2012). However, extensive quantification of the uncertainties related to applying CML QPEs in urban hydrology, and a comparison with traditional rainfall data uncertainty, has not been presented yet in relevant literature.

We address the above mentioned knowledge gaps and assess the suitability of CML QPEs for rainfall-runoff modelling in small urban catchments. We also try to reduce the systematic errors in the CML QPEs with the help of reference datasets which could be commonly available to urban hydrology professionals. In particular, we aim to optimize the model that estimates the wet-antenna attenuation (WAA) by calibrating it to 60-min data from three rain gauges located 2–3 km outside of the catchment, to 60-min data from a rain gauge located in an 8-km distance from the catchment, and, in combination with a rainfall-runoff model, also to stormwater discharge records. Moreover, the rainfall-runoff modelling performance associated with such CML QPEs is then compared with the performance of traditional rain gauge data while quantifying uncertainties in predicted discharges using a stochastic error model.

## 8.2 Methods

The study is performed using rainfall and runoff data collected during 46 rainfall-runoff events (670 hours) observed over a three-year period in an urban catchment with the area of 1.3 km$^2$ (section 8.2.1). QPEs are derived from CMLs using recent state-of-the-art approaches which could be implemented with the data available (section 8.2.2). We seek to reduce the bias in CML QPEs by calibrating the WAA estimation model to the three reference datasets available, using data from 23 randomly selected events (section 8.2.3). The remaining 23 events are used in the validation stage (section 8.2.5), in which rainfall data retrieved using all observation layouts of interest (section 8.2.4) are propagated through a rainfall-runoff model and the model outputs are evaluated against observed discharges. The model performance is analyzed using a robust prediction uncertainty quantification method.

### 8.2.1 Data used

Both rainfall and runoff observations collected in the investigated small urban catchment (details in chapter 4) are employed in this study. Most importantly, we use signal-level data collected from 16 CMLs located within the catchment and its surroundings (Fig. 4.2). We also use rain gauge data from a permanent monitoring network operated by the municipal sewer authority with the density of 1 gauge per 20–25 km$^2$ (Fig. 4.2). These gauges are referred to as "municipal". Moreover, we observed rainfall using additional rain gauges temporarily installed at three locations around the catchment with the intention of increasing the rain gauge network density in the area (Fig. 4.1). These gauges are referred to as "local". All the rain gauge observations were recorded at a 1-min resolution. For the sake of this study, when the rain gauge data are used as the reference for WAA model optimization, their resolution is aggregated to 60 min. In addition, we use discharges measured at the stormwater drainage system outlet (Fig. 4.2). The temporal resolution of the discharge measurements is 2 min for wet periods and 10 min for dry periods. More details regarding the data retrieval are available in chapter 4.1.

From the three-year observation period, we select data from hydrologically relevant rainfall events (rainfall depth $H > 2$ mm) and only use these in the presented study. After eliminating events with substantial data gaps, 46 rainfall-runoff events (670 hours) are available, from which we randomly select 23 (340 hours) to be used for the WAA model calibration (section 8.2.3). The remaining 23 events (330 hours; basic characteristics are summarized in Table A.2 in Appendix) are then used in the validation stage (section8.2.5).

### 8.2.2 Deriving CML QPEs

CML data processing steps before baseline separation, including a quality check and aggregation to a 1-min resolution, are done in the same way as described in chapter 6.2.2. Baseline is estimated as a moving median with a centered window having the length of 1 week applied on *TRSL* time series averaged over 60-min intervals (Fencl et al., 2020). To estimate WAA, we use the model proposed by (Valtr et al., 2019, see Eq. 7.1). Values of the model parameters $k'$ and $\alpha'$ are obtained by calibration to the individual reference datasets available (details in section 8.2.3).

After subtracting baseline $B$ [dB] and WAA $A_{wa}$ [dB] from the observed *TRSL* (Eq. 2.2), raindrop-induced attenuation $A_r$ [dB] is used to compute rainfall intensity $R$ [mm/h] (Eq. 2.1) with parameters $\alpha$ and $\beta$ according to ITU Radiocommunication Sector (2005), similarly as in chapter 7.2.1.

### 8.2.3 WAA model calibration

WAA estimation models are calibrated using three various reference datasets. We believe that an equivalent of at least one of them could be available to most urban hydrology professionals. The reference datasets include the following:

- 60-min data from the three closest municipal rain gauges located 2–3 km outside of the catchment (Fig. 4.2). A single time series, constructed as the mean of the instantaneous $R$ [mm/h] values of the three gauges, is used.
- 60-min data from a municipal rain gauge located at the Prague central waste water treatment plant (WWTP) in an 8-km distance to the south-west from the catchment (Fig. 4.2).
- Stormwater discharges observed at the catchment's drainage system outlet (Fig. 4.2) with a temporal resolution of 2 min for wet periods and a 10 min for dry ones.

The WAA model is calibrated for each individual reference dataset available. The optimization is performed separately for each single CML.

When using rain gauge data as the reference, the WAA model parameters are optimized by comparing QPEs with the gauge data as described in 7.2.4, however, with CML QPEs aggregated to 60-min resolution to match the reference gauge data resolution. The root mean square error is used as the objective function.

When employing the discharge measurements, we repeatedly propagate the CML QPEs in the original 1-min resolution through a deterministic rainfall-runoff model (details in chapter 4.2) and optimize the WAA model parameters by comparing the modelled and observed discharges. Now, the Nash–Sutcliffe efficiency is the objective function. In the case of both calibration approaches, the objective functions evaluate the QPEs as whole time series consisting of all 23 events.

### 8.2.4 Rainfall observation layouts

In the validation stage, we evaluate several rainfall observation layouts using data collected over 23 rainfall-runoff events not employed in the calibration stage (basic characteristics are summarized in Table A.2 in Appendix). We asses three sets of CML QPEs derived using the calibrated WAA models, corresponding to the three reference datasets used for WAA calibration (section 8.2.3). It has been concluded that only a few very precise CMLs are expected to deliver the most accurate areal QPEs (Fencl et al., 2015) and that the position of CMLs within a small urban catchment affects their ability to capture rainfall-runoff dynamics (Pastorek et al., 2019b, chapter 6). Therefore, for all three CML QPE observation layouts, we evaluate areal QPEs computed as the mean of data from CMLs the paths of which best cover the catchment of interest, i.e. CMLs #3, #7, #8, #12, and #15 (Fig. 4.2). The potential of other CML subsets is discussed in chapter 8.4.

Next, to provide a comparison with capabilities of traditional rain gauge observations, we also asses data from the rain gauges used for the WAA model calibration. In particular, we evaluate 60-min records from the single gauge at an 8-km distance and data from the three gauges at 2–3 km distances (Fig. 4.2) in the original resolution of 1 min. The former layout represents a observations potentially available in data-scarce conditions but clearly not sufficient for urban hydrological modelling, whereas the latter corresponds to the best data usually available in long-term in the context of the Czech Republic. Additionally, we evaluate as well the performance of 1-min observations from the three local rain gauges representing the best-case-scenario regarding the availability of traditional rainfall data (Fig. 4.1).

### 8.2.5 Rainfall data validation by rainfall-runoff modelling

Rainfall data retrieved using the above observation layouts are propagated through a rainfall-runoff model, and the model outputs are evaluated against observed discharges. The deterministic rainfall-runoff model was built in the EPA-SWMM software. It was calibrated in the past and has shown to perform well, except for extreme rainfalls. A detailed description of the rainfall-runoff

model and an analysis of its performance can be found in chapter 4.2. We use the model to simulate discharges at the outlet of the local stormwater drainage system. Except for data from the local rain gauges, rainfall input is implemented in the model as areal rainfall, meaning that rainfall intensity in a given time step has a constant value over all model subcatchments. For the local rain gauges, the catchment is divided into three Thiessen polygons, corresponding to the local gauges at three locations (Fig 4.1).

We decide to quantify uncertainties of the rainfall-runoff model predictions and employ the Bayesian uncertainty analysis framework of Kennedy & O'Hagan (2001) as formulated by Reichert & Schuwirth (2012) and first used in an urban hydrology context by Del Giudice et al. (2013), as introduced in chapter 3.2. More recently, this approach has been successfully applied by Sikorska & Seibert (2018) to analyze the value of different precipitation data for flood prediction in an alpine catchment. The basic principle of the method is to extend the deterministic rainfall-runoff model by a stochastic error model which explicitly accounts for systematic model errors, i.e. bias.

When performing the uncertainty analysis, we follow the same steps as described in chapter 5.2.3, although there are some differences. Most importantly, in this study, we do not calibrate the whole extended (deterministic + stochastic) model. In contrast, we only optimize the stochastic error model parameters, since the deterministic rainfall-runoff model has been calibrated in the past and has shown to perform well (chapter 4.2). The calibration is performed individually for each rainfall observation layout evaluated.

As the model is to be calibrated in a Bayesian framework, prior probability distribution of the model parameters must be first defined (Table 8.1). The part of the error model representing the random noise only has a single parameter - the asymptotic stand. dev. of the random errors $\sigma_E$ [l/s]. The part of the stochastic model representing the bias (Eq. 5.1) has two parameters that are calibrated – the asymptotic stand. dev. of the random fluctuations around the equilibrium $\sigma_B$ [l/s] and the associated correlation time $\tau$ [h]. Compared to the prior distributions used in chapter 5.2.3, the below defined priors aim to better reflect the random measurement errors in our system. Similarly, they address the "severe identifiability problem" between the deterministic model and the bias (Reichert & Schuwirth, 2012, chapter 3.2) and specify that we are seeking for the smallest bias possible.

The calibration by means of Bayesian inference, as well as all the subsequent steps necessary for quantifying the uncertainties in runoff predictions, are performed in the same manner as described in chapter 5.2.3. When calibrating the stochastic error model, data from the same 23 events as when optimizing the WAA estimation model are employed.

| parameter | $\mu$ | $\sigma$ | min. | max. |
|---|---|---|---|---|
| $\sigma_E$ [l/s] | 2 | 2 | 0.01 | 100 |
| $\sigma_B$ [l/s] | 0.001 | 25 | 0 | 1000 |
| $\tau$ [h] | 0.5 | 0.25 | 0.01 | 3 |

**Table 8.1:** Marginal prior distribution of the error model parameters defined as truncated normal distributions with four defining parameters - mean $\mu$, standard deviation $\sigma$, minimum, and maximum. Same as in chapter 5.2.3, $\sigma_E$ and $\sigma_B$ are employed in the analysis in a transformed space (Box-Cox transformation with parameters $\lambda_1 = 0.45$ and $\lambda_2 = 1$) with units $[g(\mathrm{l/s})]$.

To validate the rainfall-runoff modelling performance associated with a given rainfall observation layout, we use data from the 23 events not employed in the calibration stage. We produce hydrographs of each event showing median predictions and 90% confidence intervals. For the median prediction, as well as for every single stochastic model prediction associated with a given event, we quantify the normalized Nash–Sutcliffe efficiency *NNSE* [-] summarizing the overall performance, the relative error of the total runoff volume $dV$ [-], the Spearman rank correlation coefficient *SCC* which quantifies the strength of a monotonic relationship between two variables and is independent of both linear and nonlinear bias, and $dQ_{max}$ [-] which is the relative error of the sum of discharges during eight minutes around the observed maximal discharge (four minutes before and four after). The uncertainty of the performance metrics is analyzed by visualizing the most favorable 90% intervals within their distributions. Next, the discharge prediction reliability is quantified for each event as the fraction of discharge observations falling into the 90% confidence intervals. We also use a metric which takes into account both the prediction accuracy and precision - normalized mean interval skill score *NMISS* [-]. It is based on the interval score (Gneiting & Raftery, 2007; Breinholt et al., 2012) which rewards the forecaster for narrow prediction intervals and, depending on a predefined confidence level, penalizes the forecaster if the observation misses the prediction interval (Eq. 3.6). This concept has been extended into mean interval skill score *MISS* [-] (Bourgin et al., 2015; Bock et al., 2018) which benchmarks the prediction confidence bounds by reference bounds obtained, e.g., from long-term climatological data (Eq. 3.7). We apply this approach and determine *MISS* for each event, however, we benchmark the 90% confidence bounds by the 90% range of the runoff observations for the given event. To confine its values to the interval of [-1, 1], we transform *MISS* into *NMISS* using the equation

$$NMISS = 1/(2 - MISS), \tag{8.1}$$

The 23 events used in the validation stage are classified according to the rainfall spatial variability (Table A.2 in Appendix). This is determined by estimating the variability among records from six rain gauges around the catchment, three local and three nearest municipal gauges, aggregated to 60 min. In particular, for each event, we quantify the arithmetic mean of the coefficients of variation determined for each 60-min time step. When

analyzing the results, we pay special attention to events with high rainfall spatial variability, as they are often associated with a low representativeness of traditional rain gauge observations, and thus represent a promising niche for usage of CML QPEs.

## 8.3 Results

We briefly present precipitation estimates retrieved using all six evaluated rainfall observation layouts (chapter 8.3.1). Next, the effect of various natures of rainfall data from the individual observation layouts on runoff predictions is introduced using the deterministic rainfall-runoff model only (chapter 8.3.2). Subsequently, results based on a quantification of the rainfall-runoff modelling output uncertainty are presented. We pay special attention to events with high rainfall spatial variability (chapter 8.3.3) and then present an exhaustive summary for all events and layouts (chapter 8.3.4).

### 8.3.1 Retrieved rainfall

First, we briefly compare precipitation estimates retrieved using all six evaluated rainfall observation layouts (chapter 8.2.4). Data from the 23 validation events capturing the highest 30% of the records for the individual layouts are plotted in Fig. 8.1. Unsurprisingly, 1-min rain gauge data from three local gauges and from three municipal ones resemble each other much more than 60-min data from the single gauge at the wastewater treatment plant (WWTP). Due to the coarser temporal resolution, records from the WWTP rain gauge contain, relative to the 1-min data from the other gauges, more data points with low ($< 2$ mm/h) rainfall intensities and fewer with high ones ($> 5$ mm/h). Reflecting these imperfections of the WWTP gauge data, CML QPEs derived using a WAA model calibrated to these records also tend to overestimate intensities below ca. 0.7 mm/h and underestimate higher ones, even when compared to the other two CML QPE layouts, which are more alike. Nevertheless, all three CML QPE layouts contain considerably more records of very low (ca. $< 0.3$ mm/h) non-zero intensities than the 1-min gauge data. This is probably due to the high uncertainties when sensing low-intensity rainfall (see chapter 2.4.1), and to the CML QPE retrieval implemented in this study which does not eliminate such low-intensity false positives caused by, e.g., baseline oscillation. However, if not recorded in continual bursts, such low-intensity observations are not likely to affect the runoff above the level of baseflow oscillation at the discharge measuring profile. Thus, as demonstrated in next chapters, CML QPEs retrieved using a WAA model calibrated to records from the three closest municipal gauges, or to the observed discharges, do not lead to practically any bias in runoff predictions.

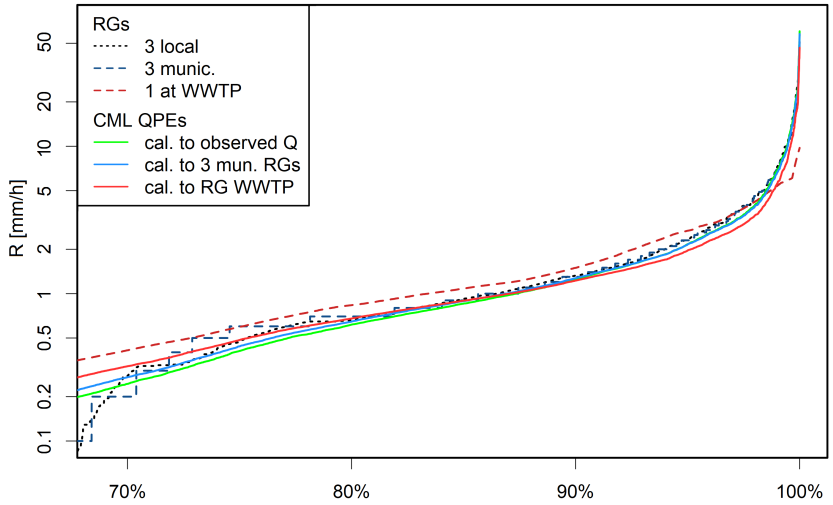


**Figure 8.1:** Rainfall retrieved over the 23 validation events (330 hours) ordered by the rainfall intensity $R$ [mm/h], only showing the highest 30%. Note that the y-axis is in a log scale. All observation layouts evaluated are shown: the mean of the 1-min records from the three local rain gauges (3 local), the mean of the 1-min records from the three muncipal gauges at 2–3 km distances (3 munic.; the "steps" are due to rounding to 1 decimal place), 60-min records from the single gauge at an 8-km distance (1 at WWTP), CML QPEs derived using the WAA model calibrated to observed discharges (cal. to observed Q), to data from the three municipal gagues (cal. to 3 mun. RGs), and to data from the single gauge at an 8-km distance (cal. to RG WWTP).

### 8.3.2 Deterministic rainfall-runoff predictions

Discharges predicted using the deterministic rainfall-runoff model only are summarized in Fig. 8.2. Although this is only a brief analysis, it clearly shows some tendencies present throughout the results. From the four evaluated rainfall observation layouts, records from the local rain gauges lead to the best performance, in terms of both $dV$ (0.009) reflecting the bias and $SCC$ (0.930) reflecting the temporal dynamics reproduction. Next, corresponding to the above rainfall data analysis, CML QPEs derived using the WAA model calibrated to 60-min records from the 8-km distant rain gauge at the WWTP have resulted in the most biased runoff volumes ($dV$ 0.129). When using 1-min data from the three municipal rain gauges, or CML QPEs with the WAA model calibrated to 60-min data from these gauges, the resulting bias is notably lower ($dV$ -0.052 and 0.040 respectively).

Compared to the records from the municipal rain gauges, both CML QPE observation layouts seem to reduce both the amount of outliers associated with rainfall events with high spatial variability and the general point spread perpendicular to the line $x = y$. These is reflected also in the respective values of the $SCC$ performance metric, which are higher for both CML QPE

observation layouts (0.893 and 0.908) than for the municipal rain gauges (0.868), suggesting better reproduction of runoff temporal dynamics by the CML QPEs. This is analyzed more closely in the next section.

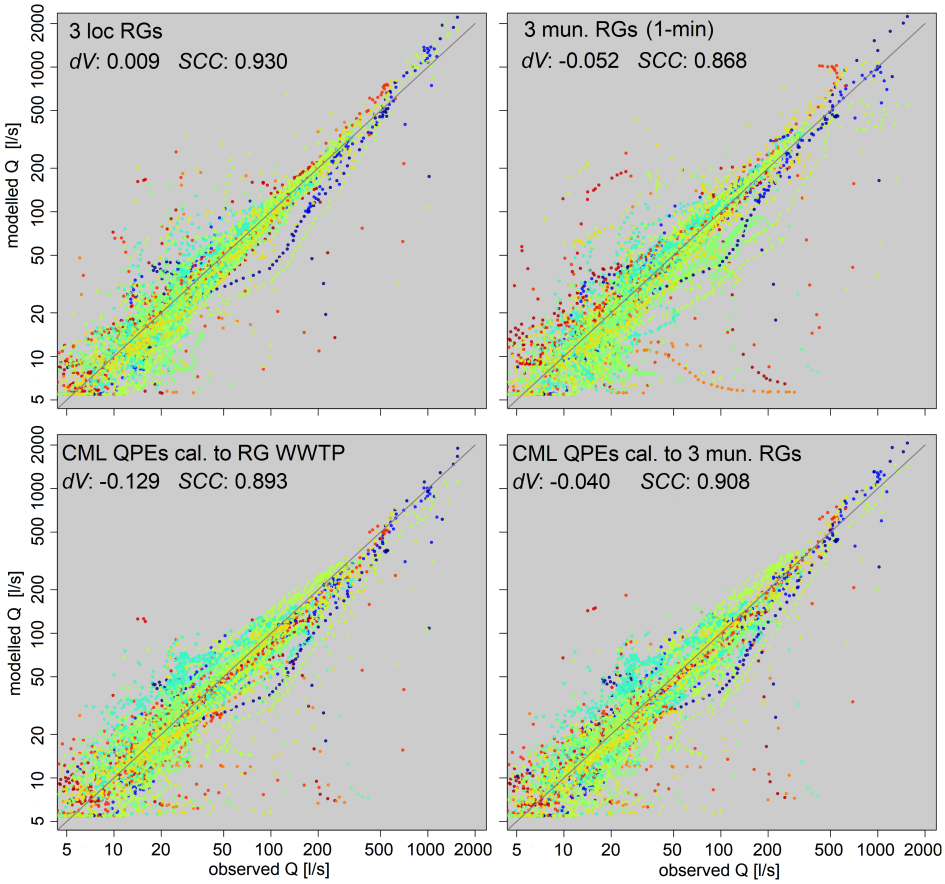


**Figure 8.2:** Scatterplots comparing observed and modelled (using the deterministic rainfall-runoff model only) discharge $Q$ [l/s] at the level of individual data points (time steps) for four rainfall observation layouts: 1-min records from the three local rain gauges (top left), 1-min records from the three municipal gauges at distances of 2–3 km (top right), CML QPEs retrieved with WAA model calibrated to the 60-min records from the gauge at the WWTP (bottom left), and CML QPEs retrieved with WAA model calibrated to the 60-min records from the three municipal gauges (bottom right). Each of the 23 events is displayed in a different colour which represents the rainfall spatial variability during the given event (blue – low variability, red – high variability). Note that the axes are in logarithmic scales. Metrics $dV$ and $SCC$ evaluate the perofrmance for whole time series consisting of all 23 events.

### 8.3.3 Stochastic predictions: Rainfalls with the highest spatial variability

In this section, rainfall-runoff modelling performance when using data from eight events with the highest rainfall spatial variability (see Table A.2 in Appendix) is analyzed. First, we compare the uncertainty of rainfall-runoff modelling predictions only for two rainfall observation layouts: 1-min data from the three nearest municipal rain gauges and QPEs derived from the best-located CMLs with the WAA model calibrated to the 60-min data from the same gauges. For a chosen rainfall-runoff event (Fig. 8.3) with a high spatial rainfall variability, the discharge peak is considerably better reproduced, in terms of both amplitude and timing, when using the CML QPEs. In fact, all modelling performance metrics we quantify reach, in general, better values, in terms of their medians, for the CML QPEs. However, it should be noted that the performance of median discharge predictions (in purple) in terms of *SCC*, reflecting the temporal dynamics, is remarkable in both cases, only slightly higher for the CML QPEs (0.91 vs. 0.87). On the other hand, when the overall uncertainty bound prediction (*NMISS*) is considered and compared with other events, it is above-median for the CML QPEs (0.74), but quite inferior for the rain gauge data (0.53).

If comparing the same two rainfall observation layouts for another event with a high spatial rainfall variability (Fig. 8.4), the aptitude of CML QPEs for rainfall-runoff model predictions is further confirmed. In contrast to the previous event, the rain gauge records rather overestimate the discharges. Most interestingly, they predict a small runoff peak at the event beginning, which is not actually present in the observed discharges. The CML QPEs, correctly, do not predict this peak and, although providing slightly biased predictions ($dV$ median 0.15, $dQ_{max}$ median -0.07), they still lead to considerably better overall performance than the rain gauge data (median *NNSE* 0.74 vs. 0.58). Hydrographs obtained with these two rainfall observation layouts, for all remaining 21 events evaluated, are presented in Appendix A.2.

Summarizing data from all eight events with the highest rainfall spatial variability, the rainfall-runoff modeling performance of all CML QPE observation layouts is compared with the performance of 1-min records from the three local rain gauges in Fig. 8.5. The best-case-scenario rain gauge data outperform the CML QPEs in terms of *SCC*, both for medians (0.72 vs. 0.63–0.667) and variability. Systematic errors in CML QPEs with the WAA model calibrated to records from the rain gauge at the WWTP affect the relative error of maximal discharges $dQ_{max}$, which is -0.292 for this observation layout. However, for the two other CML QPE layouts, $dQ_{max}$ is, in absolute values, lower (-0.127 for calibration to three municipal gauges; -0.103 for calibration to observed discharges) than for the rain gauge records (0.167). The overall uncertainty bound performance in terms of *NMISS* is also very similar for these three layouts, reaching practically the same medians of roughly 0.7 and

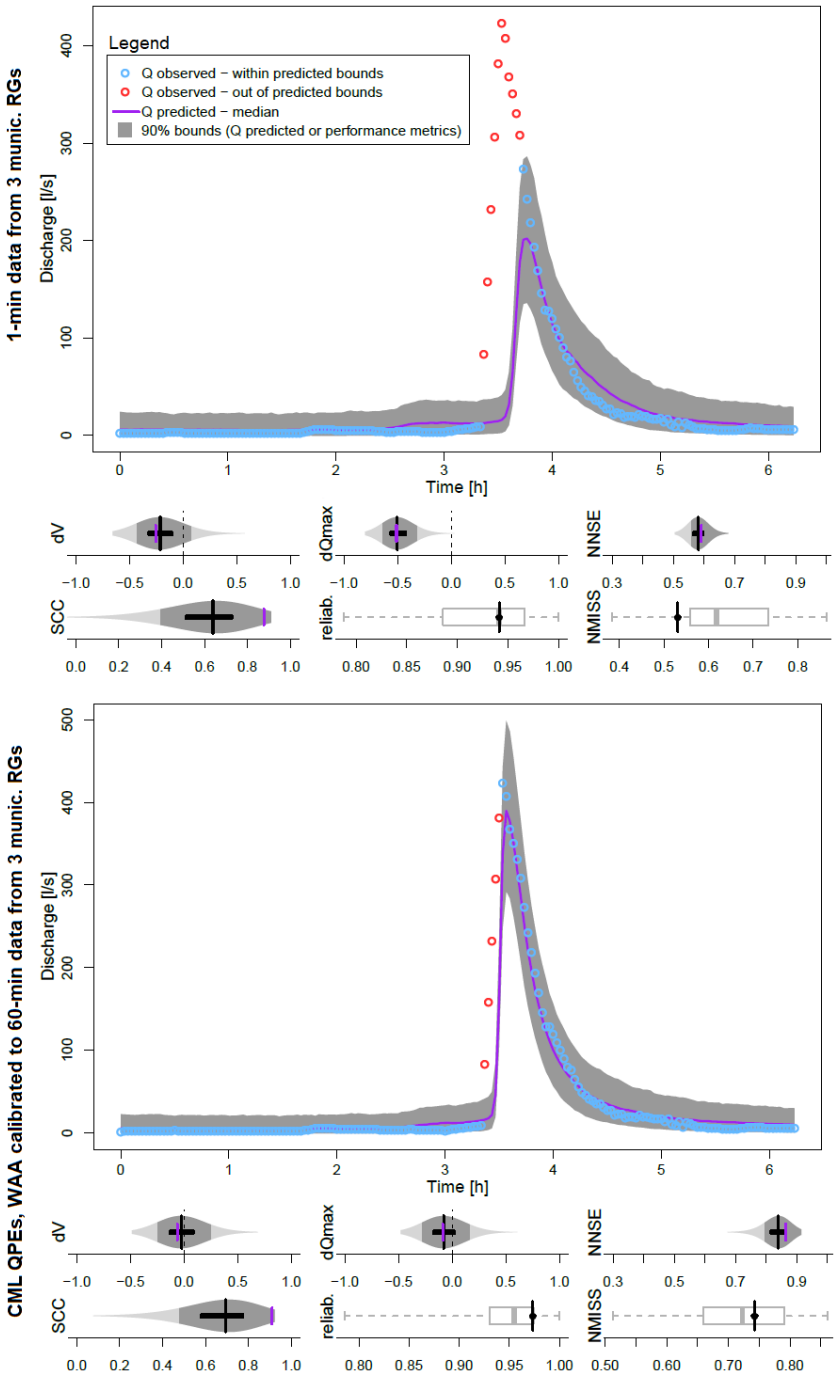


**Figure 8.3:** Hydrographs showing 90% prediction bounds for a chosen rainfall-runoff event (2016-09-05, 12:31) obtained using 1-min data from the three municipal rain gauges (top) and CML QPEs retrieved with the WAA model calibrated using 60-min data from the same gauges (bottom). The violin-plots show the metrics ($dV, dQ_{max}, NNSE, SCC$) which can be evaluated for each individual model prediction within the uncertainty ensemble. The other two metrics (reliability, *NMISS*) show the only value associated with the given event (in black) whereas the background boxplots (in light gray) show the variability among all 23 events used in the validation stage.

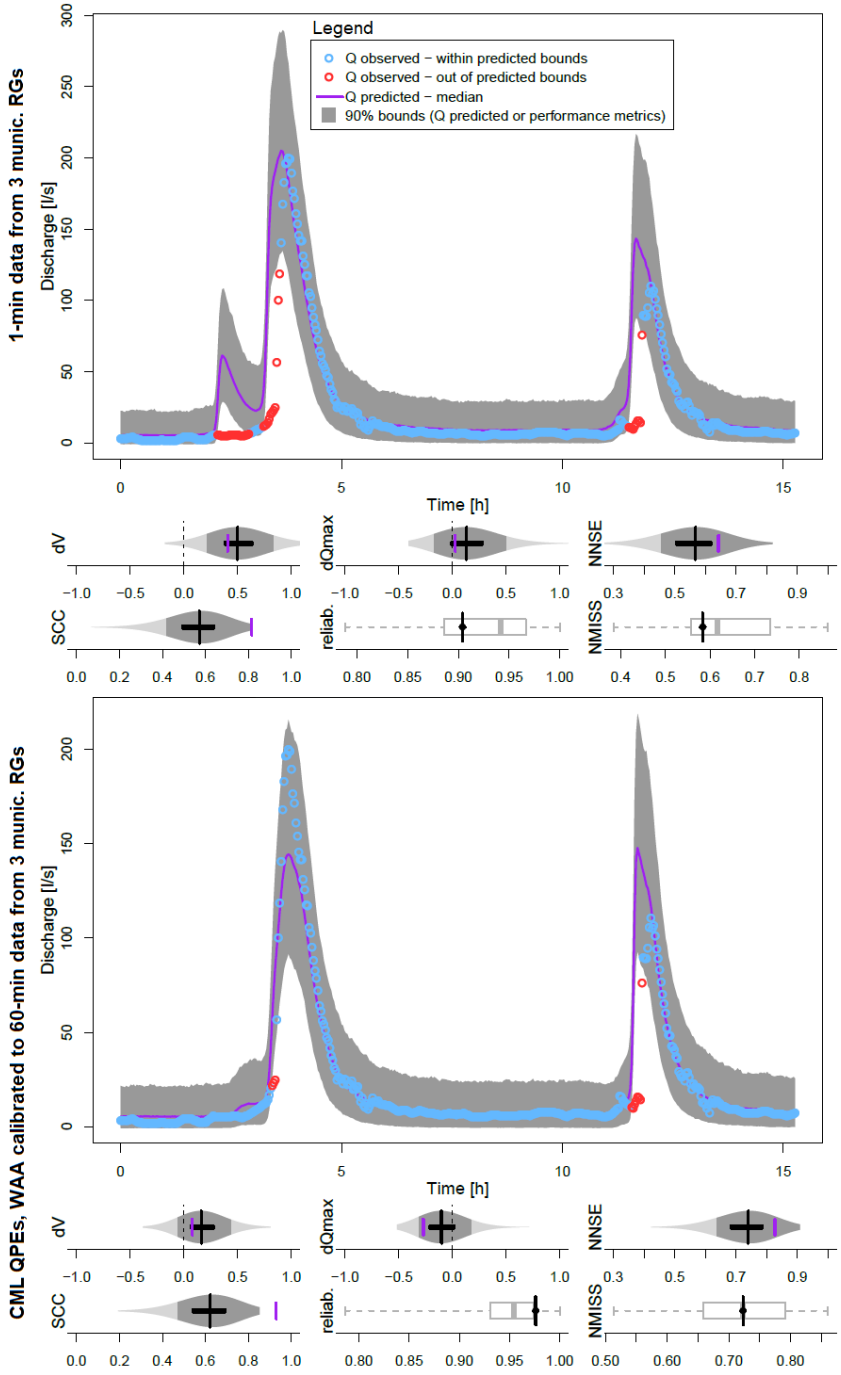


**Figure 8.4:** Hydrographs showing 90% prediction bounds for a chosen rainfall-runoff event (2015-07-25, 03:06) obtained using 1-min data from the three municipal rain gauges (top) and CML QPEs retrieved with the WAA model calibrated using 60-min data from the same gauges (bottom). The violin-plots show the metrics ($dV, dQ_{max}, NNSE, SCC$) which can be evaluated for each individual model prediction within the uncertainty ensemble. The other two metrics (reliability, *NMISS*) show the only value associated with the given event (in black) whereas the background boxplots (in light gray) show the variability among all 23 events used in the validation stage.

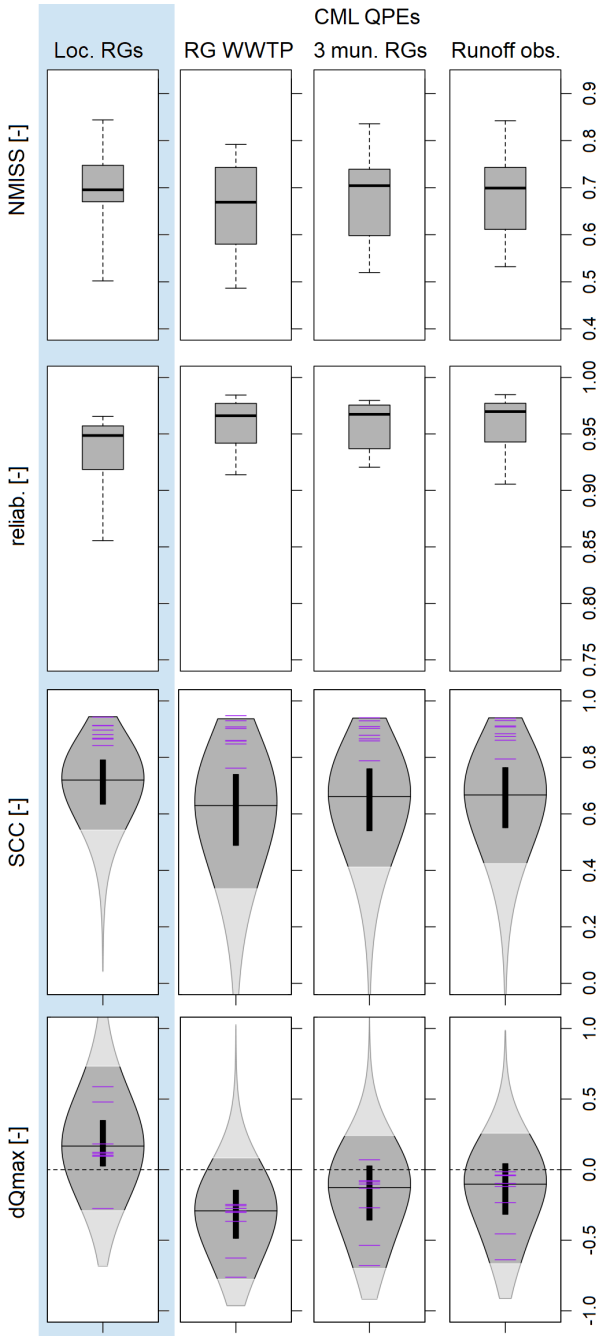


**Figure 8.5:** The output uncertainty of the rainfall-runoff modelling associated with the 1-min records from the three local rain gauges (left) and with all three CML QPE observation layouts, summarized for eight events with the highest rainfall spatial variability. The violin-plots show the metrics ($dQ_{max}, SCC$) which were evaluated for each individual model prediction within the uncertainty ensemble. The purple lines reflect the median predictions for each event. Areas in darker gray highlight the best 90% of the predictions. The boxplots feature metrics (reliability, *NMISS*) which can be calculated only for the band prediction as a whole and thus only visualize the variability among eight values associated with the individual events.

varying between 0.5 and 0.85. Moreover, the rain gauge observations lead to a lower prediction reliability, only 0.95 in median, compared to the medians of circa 0.97 for the CML QPEs.

### 8.3.4 Stochastic predictions: Summary of all events and all observation layouts

In Fig. 8.6, we summarize the rainfall-runoff modelling performance for all evaluated rainfall observation layouts using data from all 23 events. These results confirm the above tendencies that CML QPEs outperform record from the municipal rain gauges and are almost as good as the local rain gauges.

In terms of overall performance *NMISS*, the highest median (0.76) is observed for the local rain gauges, followed by the CML QPE layouts (0.7–0.72), three closest municipal gauges (0.61) and the rain gauge at the WWTP (0.52). The mutual relations are very similar when quantifying the performance in terms of *NNSE*. The highest median (0.82) is reached by the local gauges, followed by the CML QPEs (0.76–0.79), three municipal gauges (0.68) and the WWTP gauge (0.49). The variability of *NNSE* increases accordingly, just like the variability of the relative error of the total discharged volume $dV$. However, $dV$ medians are lower in absolute values for CML QPEs with the WAA model calibrated to records from the three municipal gauges (-0.011) and to discharge observations (-0.007) than for the local rain gauges (0.046). Systematic errors in CML QPEs calibrated to records from the rain gauge at the WWTP affect also the associated $dV$ values, whose median is -0.085. The prediction reliability is above the declared level of 0.9 for most events of all scenarios, except for using data from the WWTP rain gauge, for which the median is 0.89. The associated variability in terms of the interquartile range is lowest for the CML QPE observation layouts.

## 8.4 Discussion

The main finding of the study is that, when using CML QPEs to predict rainfall runoff in the investigated small urban catchment, the rainfall-runoff model performance in terms of the summarizing prediction bound skill score *NMISS* has been better than when using 1-min records from the municipal rain gauge network, and almost as good as when using three local rain gauges installed around the catchment.

From the three CML QPEs observation layouts, the best discharge predictions have been achieved when calibrating the WAA model to the observed discharges and to the 60-min records from the three closest municipal rain

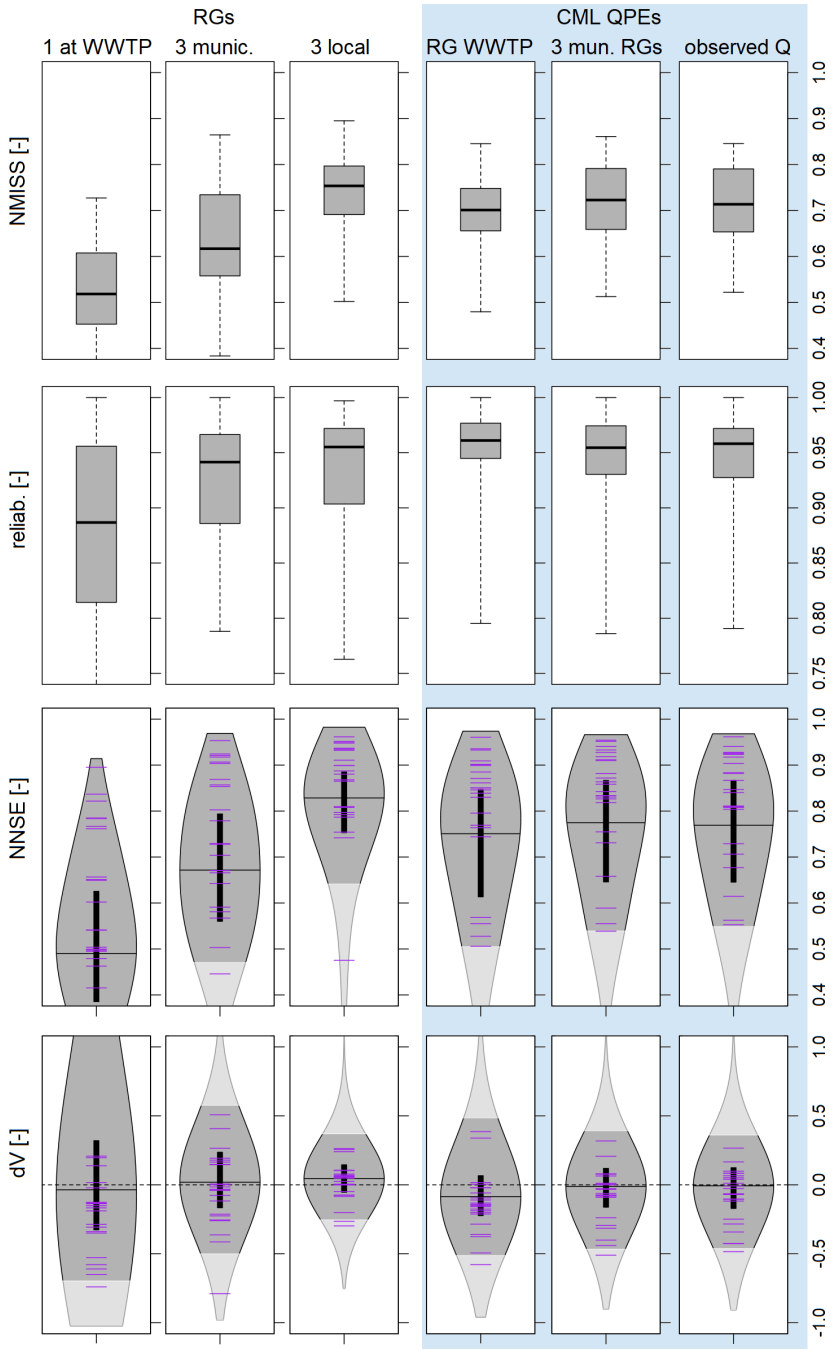


**Figure 8.6:** The output uncertainty of the rainfall-runoff modelling associated with all six rainfall observation layouts evaluated, summarized for all 23 events. The violin-plots show the metrics ($dV, NNSE$) which were evaluated for each individual model prediction within the uncertainty ensemble. The purple lines reflect the median predictions for each event. Areas in darker gray highlight the best 90% of the predictions. The boxplots feature metrics (reliability, *NMISS*) which can be calculated only for the band prediction as a whole and thus only visualize the variability among 23 values associated with the individual events.

gauges. In fact, there has been effectively no difference between the performance of CML QPEs from these two observation layouts. Moreover, the predicted discharges have been biased to a lesser extent than for the local rain gauge data, especially for runoff maxima associated with rainfalls of high spatial variability. In contrast, calibrating the WAA model to 60-min records from the single rain gauge at an 8-km distance has resulted in CML QPEs which underestimate the discharges by 8.5% in median, however, by up to 30% for runoff maxima. Nonetheless, as expected, this performance represents a notable improvement compared to using only the 60-min gauge data themselves.

These results suggest that satisfying rainfall-runoff modelling performance can be achieved with CML QPEs when the availability of data which could be used to optimize the WAA model is considerably limited. This issue has already been addressed in the study of (Pastorek et al., 2022, chapter 7) showing that calibrating the WAA model to 15-min data from the three closest rain gauges from the municipal network can lead to virtually unbiased CML QPEs. However, in that study, the aptitude of CML QPEs to be used in hydrological modelling was not tested. In the presented study, we have used the CML QPEs to predict rainfall runoff, and have shown that practically unbiased CML QPEs and high-quality discharge predictions can be obtained also when calibrating the WAA model to 60-min records from the municipal gauges, or even 1-min discharge observations. We have also shown that CML QPEs with the WAA model calibrated to 60-min records from a rain gauge at an 8-km distance can also lead to reasonable rainfall-runoff modelling performance. The presented results thus confirm the high potential of CML QPEs for rainfall-runoff modelling in small urban catchments where traditional long-term rainfall observations are not available in resolutions suitable for urban hydrology purposes.

The above results also imply that CML QPEs are promising not only for catchments with considerable data scarcity, but also for urban areas already covered by rain gauge networks of densities between 1 gauge per 20—25 $km^2$ and 1 gauge per 0.5–1 $km^2$ (respectively corresponding to the municipal and local gauges). This is in agreement with findings of (Stránský et al., 2018; Disch et al., 2019) who, however, evaluated CML QPEs continuously adjusted to rain gauges. In contrast, we have shown that similar performance can be obtained even when rain gauges are no longer available after the initial WAA model calibration. Moreover, our findings are based on exploiting a larger dataset, spanning over three years, and on employing a robust output uncertainty quantification method. Thus, it seems that CML QPEs can be considered more than a sufficient alternative to rain gauge observations corresponding to the best rainfall data usually available in long-term in the context of the Czech Republic.

Several choices regarding the implemented methods should also be discussed. Firstly, it was concluded that the position of CMLs within a small urban catchment affects their ability to capture rainfall-runoff dynamics and, thus, CMLs used to derive areal rainfall should be selected very carefully (Fencl et al., 2015; Pastorek et al., 2019b, chapter 6). Therefore, from the 16 CMLs available, we have only evaluated the mean QPEs of CMLs the paths of which best cover the catchment of interest, i.e. CMLs #3, #7, #8, #12, and #15 (Fig. 4.2). However, to confirm the validity of this choice, we have analyzed more than 450 additional CML subsets. Due to the high number of all possible subsets of the 16 CMLs (65 535), we have not evaluated each possible combination. Since the effect of adding/subtracting a single CML to a subset is likely to decrease with an increasing number of CMLs in the subset, we have focused primarily on subsets with low numbers of CMLs. In particular, we have evaluated each CML individually (16), all subsets consisting of two CMLs (120), and a randomly selected half of the subsets with three CMLs (280). Next, after having evaluated all individual CMLs, we have sorted them according to their performance in terms of *NNSE*, *dV*, and *SCC*. For each of the metrics, we have created additional CML subsets consisting of two, three, four, (...), fifteen best performing CMLs. Lastly, we have analyzed mean QPEs from all CMLs available. None of the additional CML subsets tested has led to clearly better rainfall-runoff modelling performance than the subset of the "best-located" CMLs. However, several subsets have reached very similar performance, including the mean QPEs from all CMLs. This is in agreement with conclusions of Fencl et al. (2015) that combining QPEs from all available CMLs can very well capture the rainfall and is recommended when no prior information on CML data quality is available. Performance of the subset consisting of all CMLs, in terms of *dV* and *NNSE*, as well as the performance of QPEs from individual CMLs, is presented in Fig. 8.7. The best performing individual CMLs in terms of *NNSE* are #8, #12, and #15 which all make part of the "best-located" subset. When the *dV* metric is concerned, in contrast to previous studies (Pastorek et al., 2019b, chapter 6), no dependence on CML path length is observed, showing that the implemented WAA model can reduce systematic errors also in QPEs from CMLs otherwise prone to bias.

Next, we have quantified the rainfall-runoff modelling output uncertainty by extend the deterministic rainfall-runoff model by a stochastic error model. Prior to that, to ensure reliable uncertainty estimates, we have calibrated stochastic error model parameters for each of the rainfall observation layouts evaluated. However, unlike in chapter 5, the deterministic rainfall-runoff has not been calibrated within this study. In fact, it has been used in the form as resulted from its original calibration to measurements collected from the three local rain gauges before the observation period used in the presented study (see chapter 4.2). It is thus possible that, if the model was calibrated to other data, especially to the CML QPEs themselves, the modelling performance of

individual rainfall observation layouts might change, probably for the worse for the local rain gauges, and for the better for CML QPEs.

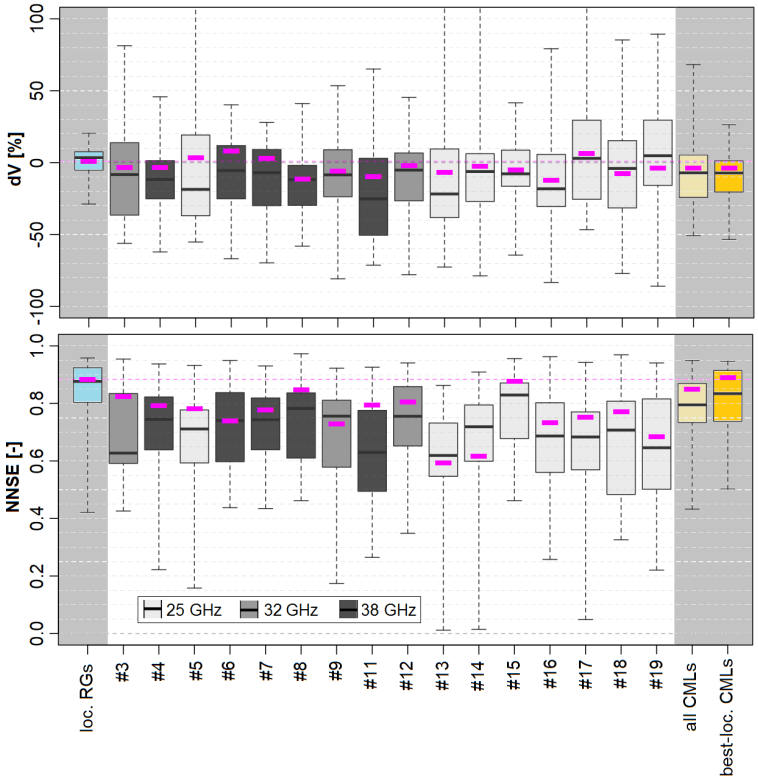


**Figure 8.7:** Deterministic rainfall-runoff modelling performance in terms of *dV* (top) and *NNSE* (bottom) obtained using 1-min records from local rain gauges (loc. RGs), QPEs from individual CMLs (#3, ..., #19), mean QPEs from all CMLs available (all CMLs), and mean QPEs from those CMLs the paths of which best cover the catchment of interest (best-loc. CMLs; see chapter 8.2.4). All CML QPEs were retrieved using the WAA model calibrated to the 60-min data from the three municipal rain gauges. Each boxplot reflects the variability among all 23 events used for the validation. The pink bars show the performance calculated for the time series consisting of the 23 events as a whole. The CMLs are ordered according to the increasing path length, their frequencies are colour-coded.

Nonetheless, the relevance of our findings for other small urban catchments should be subject to further research. Firstly, based on our previous study where we had analyzed several WAA models (Pastorek et al., 2022, chapter 7), we have tested only the WAA model originally derived by using one of our 16 CMLs and data from one of the three summer seasons investigated herein (Valtr et al., 2019). Moreover, all CMLs used in this study are from the same product family of the same manufacturer (Ericsson, Mini-Link) and have aged similarly due to exposure to similar climatic conditions. Nevertheless, CML networks in other areas can consist of antennas of different hardware characteristics exposed to different climates for different time periods. Identi-

fying optimal WAA models might be more complicated in such conditions, especially if the reference data are available only in low resolutions.

## 8.5 Conclusions

In this study, we have assessed the value of quantitative precipitation estimates (QPEs) retrieved from commercial microwave links (CMLs) for rainfall-runoff modelling in a small urban catchment by quantifying model output uncertainties associated both with the CML QPEs and with traditional rain gauge data. Moreover, we have analyzed the possibilities of reducing systematic errors in the CML QPEs with the help of three various reference datasets, equivalents of which might be commonly available to urban hydrology professionals.

It has been shown that, when predicting rainfall runoff with CML QPEs derived using a wet-antenna attenuation (WAA) model calibrated to 60-min records from a single rain gauge at an 8-km distance from the catchment of interest, the simulated discharges have been underestimated by 8.5% in median, and by up to 30% for runoff maxima, due to the low representativeness of the reference gauge data for the catchment's area. However, except for the considerable bias, the performance of these CML QPEs has been an improvement compared to records from the three closest rain gauges from the municipal rainfall monitoring network. These results have confirmed the high potential of CML QPEs for rainfall-runoff modelling in small urban catchments where traditional long-term rainfall observations are not available in resolutions suitable for urban hydrology purposes.

We have also demonstrated that, when calibrating the WAA model to both discharges observed at the catchment's outlet and to 60-min records from the three closest municipal rain gauges, virtually unbiased CML QPEs can be retrieved. These CML QPEs can then reproduce observed discharges almost as well (median *NNSE* 0.79) as three local rain gauges installed around the studied catchment for research purposes (median *NNSE* 0.82). In fact, for rainfall events of high spatial variability, runoff maxima have been biased to a lesser extent when using the CML QPEs (–10%) than for the local rain gauge data (+17%). This shows that CML QPEs can be successfully used for rainfall-runoff modelling also when no reference rainfall data, only runoff observations, are available.

In sum, the presented findings imply that CML QPEs are promising not only for catchments with considerable data scarcity, but also for urban areas already covered by rain gauge networks. For areas with network densities of roughly 1 gauge per 20—25 km$^2$, corresponding to the best rainfall data usually available in long-term in the context of the Czech Republic, CML QPEs represent a notable potential improvement for rainfall-runoff modelling

in small urban catchments. For denser networks with roughly 1 gauge per 0.5–1 $km^2$, CML QPEs can be considered a satisfying alternative, especially for rainfall events with high spatial variability, which are often associated with high rainfall intensities, important for many urban hydrology tasks, e.g. design and evaluation of urban stormwater systems.

# Chapter 9

# Summary

This thesis has aimed to evaluate the potential of quantitative precipitation estimates (QPEs) obtained from commercial microwave links (CMLs) for rainfall-runoff modelling in small urban catchments. It has also investigated which factors (e.g. position relative to the catchment, liability to bias) most affect the suitability of individual CMLs to be used as a source of rainfall data for rainfall-runoff modeling. In order to reach the highest quality of CML QPEs, possibilities of reducing the bias common in CML QPE retrieval have also been addressed. Moreover, as CML QPEs could be most useful when traditional rainfall data are not available in adequate resolutions, which is a common challenge in urban hydrology, a special attention has been payed to CML QPE retrieval in such data-scarce conditions.

In chapter 5, we have first addressed the question whether QPEs from CMLs can be regarded as a viable source of rainfall data in the field of urban rainfall-runoff modelling. Both the CML QPEs and traditional rainfall data have been used for rainfall-runoff modelling in a small urban catchment, the performance of which has been evaluated against observed discharge measurements. The study has shown that stormwater discharges modelled using CML QPEs can very well reproduce the runoff temporal dynamics. However, when using the straightforward QPE retrieval approach, i.e. the mean from all CMLs available and wet-antenna attenuation (WAA) estimated as a constant offset, the runoff predictions were often considerably biased, especially during light rainfall events. In contrast, adjusting QPEs from selected short CMLs to traditional rain gauge data has led to an improvement in the reproduction of both overall volumes during light rainfalls and peak discharges during heavy rainfalls. In fact, for heavy rainfalls, such adjusted CML QPEs has even led to the same rainfall-runoff modelling performance as high-resolution data from the local rain gauges.

The above results have suggested that CML QPEs corrected for systematic errors, e.g. by adjusting to gauges from a low-density network (roughly 1 gauge per 20—25 $km^2$), could represent a relevant rainfall data source for urban hydrology, if traditional rain gauge data in high spatial resolutions (roughly 1 gauge per 0.5–1 $km^2$) are not available in the given catchment. Their value could be especially pronounced for monitoring of heavy rainfalls, which are crucial for design and operation of urban drainage systems. However, at the time of the study, we were able to use data only from three consecutive months covering 15 relevant (rainfall depth over 2 mm) rainfall-runoff events. Similarly, QPEs from only four out of 19 CMLs were available as both unadjusted and adjusted to rain gauge observations. Furthermore, differences among individual CMLs have not been addressed, only the mean of all available CMLs has been examined. This space for improvement have foreshadowed the direction of the subsequent research endeavors.

The study presented in chapter 6 has addressed the combined effect of the CML characteristics (path length, transmission frequency) and their location relative to the catchment on the efficient use of CML QPEs for hydrological applications. In particular, it has investigated ability of individual CMLs to provide relevant QPEs for urban rainfall-runoff modelling in a small urban catchment. An extensive dataset covering a three-year period has been leveraged for the first time. The results have demonstrated that the quality of the retrieved CML QPEs and predicted stormwater runoffs is affected by both characteristics of individual CMLs and their position in respect to the catchment, as well as by CML data pre-processing.

Firstly, the position of a CML in respect to the small urban catchment has been proven to affect the CML's ability to capture rainfall-runoff dynamics, as shorter CMLs with paths within or close to the catchment boundaries have reproduced runoff dynamics better, especially for heavy rainfalls. Interestingly, in terms of capturing the runoff dynamics, mean QPEs of all CMLs have outperformed QPEs from individual CMLs. Secondly, however, it has also been shown that the sensitivity of CMLs to rainfall, given by their frequency, polarization, and length, is the most influential factor affecting the bias in CML QPEs and subsequent runoff, and that the ability of biased CML QPEs to provide reliable flow estimates is predominantly low.

As expected, continuously adjusting the CML QPEs to rain gauge data has minimized the bias for all CMLs. Unfortunately, it has also considerably worsened the ability of CML QPEs to reproduce runoff dynamics during heavy rainfalls. This is, likely, because the adjustment method strongly depends on the rain gauge data reliability, but the gauges are too far from each other to accurately observe small-scale rainfall variability. Moreover, when deriving the CML QPEs using this approach, the rainfall retrieval parameters change in 15-min time steps, which might be too coarse to reflect the underlying

physical processes. Thus, although the adjusting is conceptually promising for eliminating the bias, it requires further development.

In sum, this study has confirmed the potential of CML QPEs for quantitative urban hydrology, especially for those CMLs the position of which corresponds well with the catchment of interest. However, the bias propagated into the runoff predictions has been shown to be inversely proportional to the CML path length. Therefore, to make the best use of these innovative rainfall data when modelling rainfall runoff in small urban catchments, the possibilities of reducing the bias without compromising their ability to reproduce rainfall-runoff dynamics should be better investigated.

The study presented within chapter 7 has addressed the estimation of wet antenna attenuation (WAA), a major source of the bias in CML QPEs. In particular, it has been analyzed how, when deriving QPEs from CMLs, WAA can be reliably estimated without dedicated rainfall monitoring. Various WAA estimation model based on considerably different assumptions have been tested, including a newly formulated one. Their performance has been evaluated both when calibrated to rainfall observations from a municipal rain gauge network and when using model parameters from the literature. We have also analyzed which of the studied models can provide reliable WAA estimates without being calibrated for each individual CML.

The results have shown that virtually unbiased CML QPEs could be retrieved when calibrating the WAA estimation models to rainfall data from the permanent municipal rain gauge network with a spatial resolution of one gauge per $20-25$ km$^2$ and a temporal resolution of 15 minutes. Such high-quality QPEs have been derived even from short, sub-kilometer CMLs which are in general very prone to bias. It has also been demonstrated how models relating WAA to rainfall intensity, implicitly or explicitly, can be successfully applied without any auxiliary rainfall observations, i.e. using CML data only. In fact, out of all models evaluated, these have led to the best WAA estimation. In contrast, modeling WAA as a constant offset has been shown to be unsatisfying for CML data available in a 1-min resolution. Next, for models relating WAA to rainfall intensity explicitly, we have found sets of model parameters which are suitable for CMLs of various path lengths operating at various frequency bands, and which could thus be transferred to other locations with CMLs of similar antenna hardware characteristics.

In short, it has been presented how high-quality QPEs can be derived from CMLs of all path lengths while minimizing the requirements on auxiliary data necessary. The importance of adequate WAA correction when deriving CML QPEs in the 1-min resolution has been confirmed. This study thus represents a legitimate step towards the retrieval and application of CML QPEs, especially in conditions when the availability of auxiliary rainfall data

is an important limiting factor, e.g. in areas where traditional rainfall data are scarce, or when employing large CML networks.

In chapter 8, we have assessed the value of state-of-the-art CML QPEs for rainfall-runoff modelling in a small urban catchment by quantifying model output uncertainties associated both with the CML QPEs and with traditional rain gauge data. Moreover, we have explored the possibilities to calibrate WAA estimation models using data that could be more commonly available to urban hydrology specialists than the 15-min data from the three closest rain gauges from the municipal network which were used in chapter 7. In particular, we have calibrated the WAA model to 60-min records from the same three gauges, to 60-min records from a single rain gauge at an 8-km distance from the catchment of interest, and to discharges observed at the catchment's outlet. CML QPEs retrieved using such calibrated WAA models have been then used to predict rainfall runoff in the investigated small urban catchment. The uncertainty of the predicted runoffs has been quantified using a stochastic error model, and the rainfall-runoff modelling performance has been evaluated by comparing observed and simulated discharges.

It has been shown that, when predicting rainfall runoff with CML QPEs derived using a WAA model calibrated to 60-min records from the 8-km distant rain gauge, the simulated discharges have been considerably biased, due to the low representativeness of the reference gauge data for the catchment's area. However, except for that, the performance of these CML QPEs has been an improvement compared to the performance of 1-min records from the three closest municipal rain gauges. We have also demonstrated that, when calibrating the WAA model both to 60-min records from the three municipal gauges or to observed discharges, practically unbiased CML QPEs can be retrieved. Moreover, such CML QPEs have been shown to reproduce observed discharges almost as well as 1-min records from three local rain gauges temporarily installed around the studied catchment for research purposes. In fact, for rainfall events of high spatial variability, runoff maxima have been biased to a lesser extent when using the CML QPEs.

Research presented in 8 has demonstrated that CML QPEs can be successfully used for rainfall-runoff modelling when no reference rainfall data, only runoff observations, are available. Moreover, the above findings imply that CML QPEs are promising also for urban catchments already covered by rain gauge networks. For areas with network densities of roughly 1 gauge per 20–25 $km^2$, corresponding to the best rainfall data usually available in long-term in the context of the Czech Republic, CML QPEs represent a notable improvement for rainfall-runoff modelling in small urban catchments. For denser networks with roughly 1 gauge per 0.5–1 $km^2$, CML QPEs can be considered as a satisfying alternative. This is especially true for rainfall events with high spatial variability, which are often associated with high rainfall intensities, important for urban hydrology tasks such as design and evaluation of urban stormwater management systems.

# Appendix

This Appendix contains additional information on rainfall data as used in chapter 6 as well as information on rainfall characteristics and hydrographs with simulated and observed discharges from chapter 8. More additional material is available in the "Supplementary material" document published with the study of (Pastorek et al., 2019b, chapter 6), where hydrographs for all rainfall layouts evaluated in that study are presented, including those for rainfall data from the local rain gauges, which were used to verify the rainfall-runoff model reliability.

## A.1 Rainfall from chapter 6

The following material presents additional information on rainfall event characteristics (Table A.1) and CML data availability (Fig. A.1). It is based on rainfall-runoff events as defined and used for the study presented in chapter 6 (see 6.2.1). Although the underlying observations are the same (see chapter 4.1), the exact number of rainfall (or rainfall-runoff) events differs for each study presented in the thesis due to various availability of data from various devices used, or differences in the event definition.

| start (id) | end | duration [min] | depth [mm] | $R_{max}$ [mm/h] | $R_{max,10}$ [mm/h] |
|---|---|---|---|---|---|
| 2014-09-19 15:41 | 2014-09-20 00:45 | 544 | 5.7 | 33.9 | 24.3 |
| 2014-09-20 14:46 | 2014-09-20 17:19 | 153 | 2 | 10.8 | 7.3 |
| 2014-09-21 19:16 | 2014-09-22 02:27 | 431 | 7.5 | 9.5 | 6.3 |
| 2014-10-13 22:55 | 2014-10-14 10:15 | 680 | 18.1 | 19.1 | 17.4 |
| 2014-10-15 16:36 | 2014-10-16 11:25 | 1129 | 8.2 | 24.5 | 10.1 |
| 2014-10-16 17:02 | 2014-10-16 19:31 | 149 | 2.1 | 35.3 | 12.5 |
| 2014-10-21 21:58 | 2014-10-22 02:51 | 293 | 6.2 | 12.9 | 8 |
| 2014-10-22 10:36 | 2014-10-23 08:31 | 1315 | 11.6 | 5.9 | 3.9 |
| 2015-04-27 18:41 | 2015-04-28 00:21 | 340 | 8.9 | 30.8 | 18.3 |
| 2015-04-28 07:35 | 2015-04-28 17:11 | 576 | 8.9 | 10.7 | 7.3 |
| 2015-05-03 20:36 | 2015-05-04 01:15 | 279 | 2.4 | 5 | 2.4 |
| 2015-05-05 21:07 | 2015-05-06 12:09 | 902 | 6.9 | 6 | 3.2 |
| 2015-05-09 06:19 | 2015-05-09 09:15 | 176 | 2.5 | 10.3 | 8.6 |
| 2015-05-29 22:06 | 2015-05-30 02:47 | 281 | 10.4 | 54.4 | 39.3 |
| 2015-06-08 19:54 | 2015-06-09 13:11 | 1037 | 29.2 | 34.5 | 21 |
| 2015-06-13 13:50 | 2015-06-13 20:31 | 401 | 3.8 | 14.8 | 7.2 |
| 2015-06-23 00:22 | 2015-06-23 05:51 | 329 | 4.1 | 5.1 | 3.6 |
| 2015-07-07 02:12 | 2015-07-08 03:45 | 1533 | 6.8 | 35.1 | 18 |
| 2015-07-25 04:23 | 2015-07-25 17:20 | 777 | 4.5 | 9.8 | 6 |
| 2015-07-27 13:51 | 2015-07-27 18:01 | 250 | 5.6 | 43.7 | 28.2 |
| 2015-07-29 14:48 | 2015-07-29 20:23 | 335 | 3.2 | 16.4 | 8.2 |
| 2015-08-17 06:08 | 2015-08-19 14:28 | 3380 | 49.9 | 22.8 | 13.5 |
| 2015-09-01 16:45 | 2015-09-02 04:11 | 686 | 4.1 | 6 | 4.7 |
| 2015-09-07 11:03 | 2015-09-07 15:55 | 292 | 2.2 | 14 | 6.7 |
| 2015-09-09 12:05 | 2015-09-09 17:05 | 300 | 2.5 | 22.9 | 13 |
| 2015-10-07 00:55 | 2015-10-07 07:59 | 424 | 7.8 | 10.1 | 7.8 |
| 2015-10-07 10:15 | 2015-10-07 16:31 | 376 | 5 | 9 | 6.9 |
| 2015-10-07 17:17 | 2015-10-08 16:33 | 1396 | 10.5 | 4 | 2.3 |
| 2015-10-14 01:20 | 2015-10-14 18:39 | 1039 | 10.3 | 5.9 | 4.8 |

Table continues on the next page.

Table starts on the previous page.

| start (id) | end | duration [min] | depth [mm] | $R_{max}$ [mm/h] | $R_{max,10}$ [mm/h] |
|---|---|---|---|---|---|
| 2015-10-14 20:48 | 2015-10-15 13:21 | 993 | 8.1 | 4.8 | 3.1 |
| 2015-11-15 04:02 | 2015-11-15 15:51 | 709 | 2.7 | 3.4 | 2 |
| 2015-11-19 16:36 | 2015-11-20 06:41 | 845 | 15.1 | 23 | 18.6 |
| 2015-11-20 10:48 | 2015-11-21 01:31 | 883 | 4.7 | 5.1 | 1.7 |
| 2015-11-30 03:28 | 2015-12-01 02:29 | 1381 | 11 | 23.8 | 14 |
| 2015-12-01 04:41 | 2015-12-01 12:11 | 450 | 3.1 | 7.7 | 4.2 |
| 2015-12-09 14:49 | 2015-12-09 20:35 | 346 | 2.1 | 3.4 | 1.8 |
| 2016-05-03 18:25 | 2016-05-04 19:36 | 1511 | 5.4 | 3 | 1.3 |
| 2016-05-24 13:53 | 2016-05-25 03:07 | 794 | 13.9 | 31.6 | 22.4 |
| 2016-05-31 04:41 | 2016-05-31 09:25 | 284 | 6.2 | 18.1 | 9.3 |
| 2016-06-02 13:19 | 2016-06-02 21:41 | 502 | 5.1 | 18 | 9.8 |
| 2016-06-02 23:03 | 2016-06-03 10:41 | 698 | 6.4 | 6 | 4.3 |
| 2016-06-12 15:47 | 2016-06-12 21:59 | 372 | 15.7 | 49.9 | 38.7 |
| 2016-06-16 19:20 | 2016-06-17 01:33 | 373 | 4.2 | 10.8 | 5.6 |
| 2016-06-17 04:36 | 2016-06-17 13:24 | 528 | 6.5 | 35.8 | 15.6 |
| 2016-06-25 13:54 | 2016-06-26 02:07 | 733 | 4.7 | 23 | 9.6 |
| 2016-07-01 01:55 | 2016-07-01 06:01 | 246 | 15.5 | 51.9 | 43.2 |
| 2016-07-12 04:46 | 2016-07-12 10:00 | 314 | 3.1 | 5.1 | 3.9 |
| 2016-07-13 12:45 | 2016-07-14 17:45 | 1740 | 18.2 | 14.5 | 10.2 |
| 2016-08-10 13:46 | 2016-08-10 17:03 | 197 | 3.1 | 8 | 7.2 |
| 2016-08-29 11:38 | 2016-08-29 19:31 | 473 | 7.4 | 21.6 | 16.7 |
| 2016-09-05 13:38 | 2016-09-05 17:45 | 247 | 2.4 | 18.7 | 8.7 |
| 2016-09-16 15:52 | 2016-09-17 12:03 | 1211 | 45.3 | 62.3 | 33.8 |
| 2016-10-02 11:35 | 2016-10-02 23:38 | 723 | 4.2 | 5.1 | 2.5 |
| 2016-10-03 08:56 | 2016-10-03 22:03 | 787 | 15.8 | 36.2 | 23 |
| 2016-10-03 23:59 | 2016-10-04 11:05 | 666 | 10.7 | 6.9 | 4.8 |
| 2016-10-11 13:37 | 2016-10-12 00:03 | 626 | 2.3 | 6.9 | 4.5 |
| 2016-10-12 01:05 | 2016-10-12 10:41 | 576 | 2.3 | 2.6 | 0.9 |
| 2016-10-19 05:59 | 2016-10-19 12:17 | 378 | 5.1 | 15.8 | 8.8 |
| 2016-10-25 02:45 | 2016-10-25 08:51 | 366 | 4.5 | 6.1 | 4.8 |

**Table A.1:** Basic characteristics of the 56 rainfalls events data from which are evaluated in chapter 6 (see 6.2.1). The characteristics were estimated on the basis of data from the local rain gauges (Fig. 4.1), in particular, a single time series obtained as the mean value of the three gauges. $R_{max}$ stands for the maximal 1-min rainfall intensity and $R_{max,10}$ for the maximal 10-min rainfall intensity.

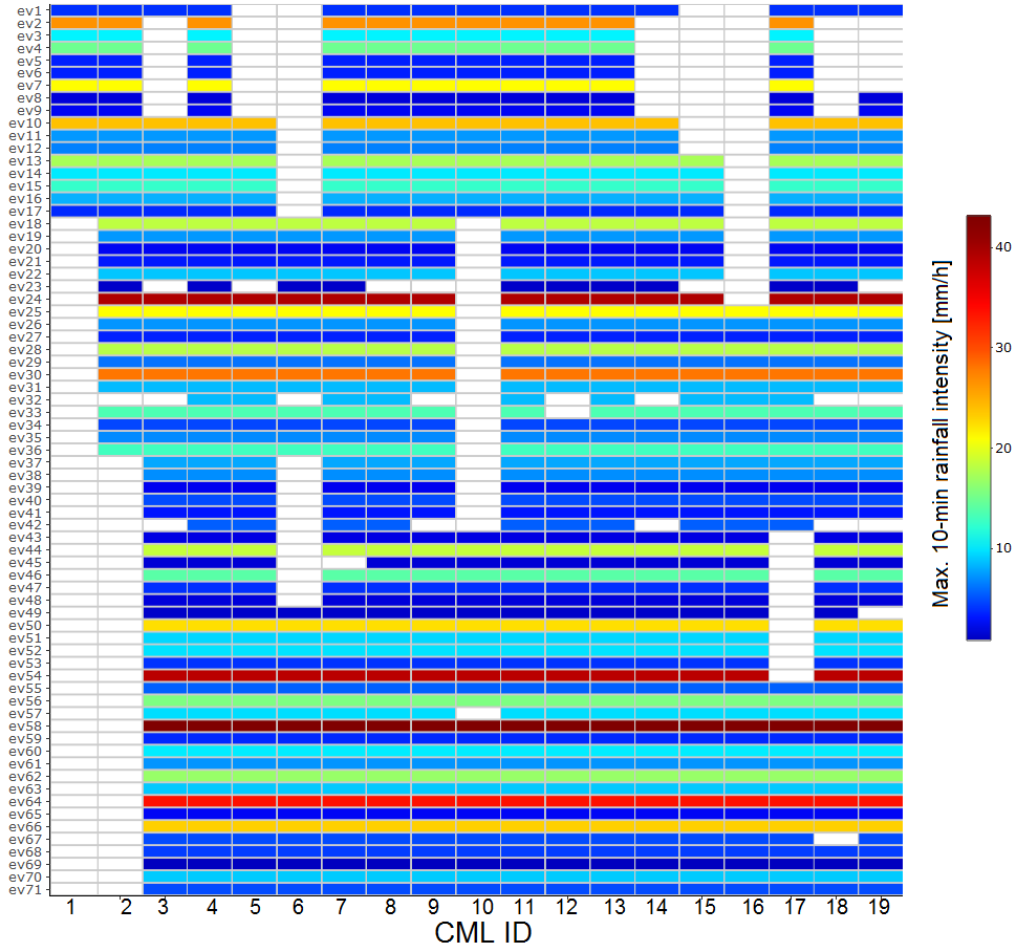


**Figure A.1:** Overall availability of CML data for individual CMLs and 71 events for which it was possible to perform rainfall-runoff simulations within the study presented in chapter 6 (see 6.2.1).

## A.2 Rainfall events and hydrographs from chapter 8

The following material presents additional information on rainfall event characteristics (Table A.2) based on rainfall-runoff events as defined and used for the study presented in chapter 8. Next, hydrographs showing 90% prediction bounds obtained with two rainfall observation layouts for all 23 events evaluated, are also presented. The selected rainfall layouts are 1-min data from the three nearest municipal rain gauges and QPEs derived from the best-located CMLs with the WAA model calibrated to the 60-min data from the same gauges.

| start (id) | duration [min] | depth [mm] | $R_{max}$ [mm/h] | $R_{max,10}$ [mm/h] | spatial var. [-] |
|---|---|---|---|---|---|
| 2014-09-20 13:31 | 288 | 2.0 | 9.8 | 7.2 | 1.84 |
| 2014-09-21 17:58 | 569 | 7.5 | 9.0 | 6.2 | 0.89 |
| 2014-10-13 21:27 | 828 | 18.1 | 19.1 | 17.4 | 0.35 |
| 2014-10-16 15:32 | 299 | 2.2 | 36.3 | 12.5 | 1.17 |
| 2014-10-22 09:09 | 1462 | 11.6 | 5.1 | 3.7 | 0.74 |
| 2015-05-03 19:18 | 417 | 2.4 | 2.8 | 2.3 | 0.76 |
| 2015-05-05 15:44 | 1285 | 7.2 | 4.3 | 3.0 | 0.59 |
| 2015-05-29 20:40 | 427 | 10.4 | 54.4 | 39.2 | 0.26 |
| 2015-06-23 09:00 | 639 | 2.9 | 14.7 | 7.2 | 1.45 |
| 2015-07-07 22:48 | 357 | 6.8 | 35.1 | 18.0 | 1.42 |
| 2015-07-25 03:06 | 914 | 4.6 | 8.6 | 5.9 | 1.75 |
| 2015-09-07 10:03 | 412 | 2.2 | 13.1 | 6.5 | 1.16 |
| 2015-09-09 12:48 | 317 | 2.5 | 22.0 | 13.0 | 0.65 |
| 2015-10-14 00:07 | 3344 | 20.4 | 5.4 | 4.7 | 0.59 |
| 2015-11-20 09:27 | 1024 | 4.7 | 1.7 | 1.5 | 0.71 |
| 2015-12-09 10:29 | 666 | 2.2 | 1.8 | 1.7 | 0.80 |
| 2016-05-24 13:04 | 903 | 13.9 | 31.6 | 22.3 | 0.85 |
| 2016-06-25 20:05 | 364 | 4.7 | 23.3 | 9.7 | 0.70 |
| 2016-08-29 02:28 | 1023 | 8.9 | 21.6 | 16.5 | 0.95 |
| 2016-09-05 12:31 | 374 | 2.4 | 18.9 | 8.5 | 1.45 |
| 2016-10-03 07:33 | 1712 | 26.6 | 36.2 | 23.0 | 0.79 |
| 2016-10-11 12:35 | 1469 | 4.7 | 5.7 | 4.4 | 0.70 |
| 2016-10-19 00:13 | 784 | 6.0 | 15.4 | 8.8 | 0.97 |

**Table A.2:** Basic characteristics of the 23 rainfalls events used to validate the rainfall observation layouts in chapter 8. $R_{max}$ stands for the maximal 1-min rainfall intensity and $R_{max,10}$ for the maximal 10-min rainfall intensity. Except for the last column reflecting the spatial rainfall variability, the characteristics were estimated on the basis of data from the local rain gauges, in particular, a single time series obtained as the mean value of the three gauges. The spatial variability is determined by estimating the variability among 60-min rainfall data from six rain gauges around the catchment - three local and three nearest municipal gauges. In particular, we quantify the arithmetic mean of the coefficients of variation determined for each 60-min time step. Higher values indicate higher spatial variability.

# 1-min data from the three municipal rain gauges (1/4)

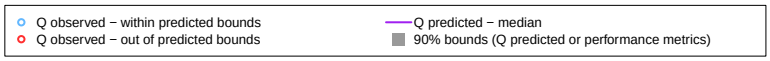


**2014–09–20 13:31:00, Rmax10 = 7.2 mm/h**

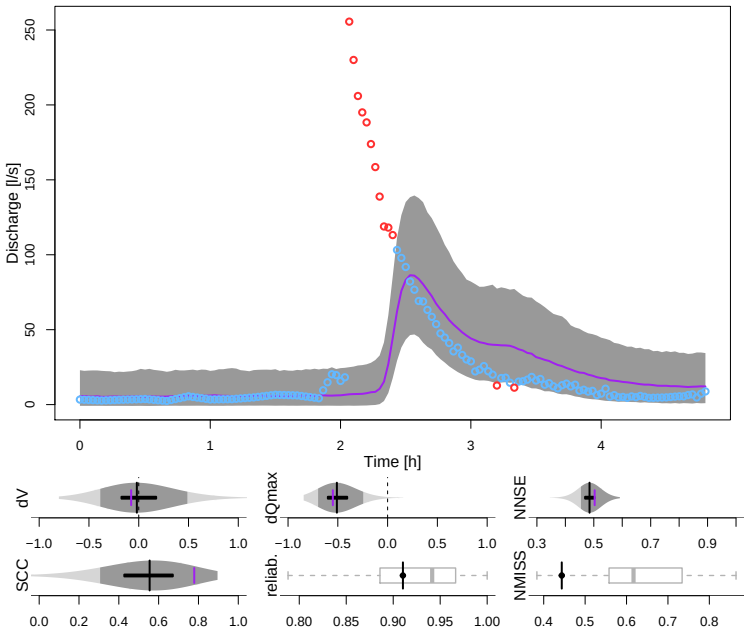





**2014–09–21 17:58:00, Rmax10 = 6.2 mm/h**

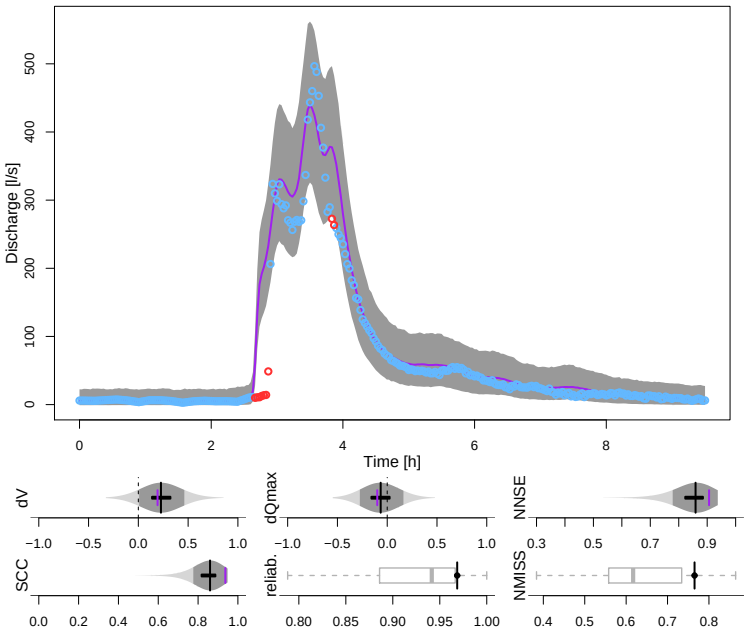





**2014–10–13 21:27:00, Rmax10 = 17.4 mm/h**

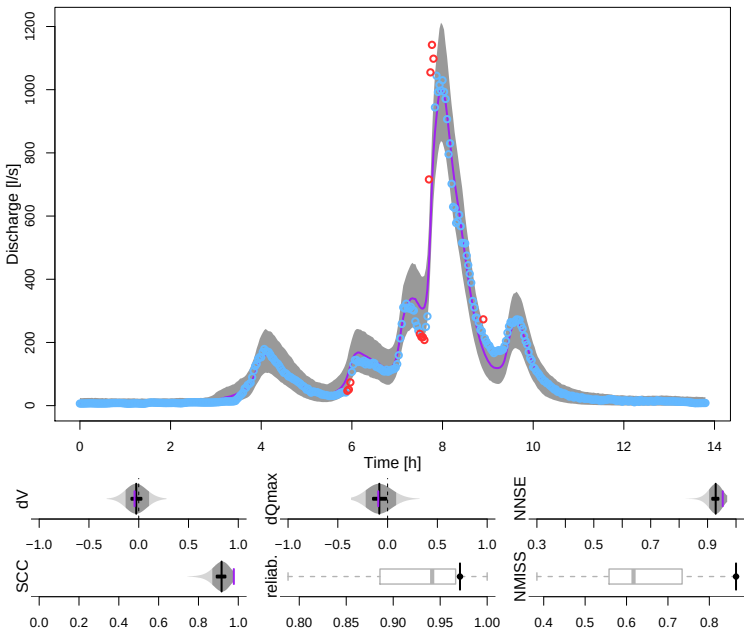





**2014–10–16 15:32:00, Rmax10 = 12.5 mm/h**

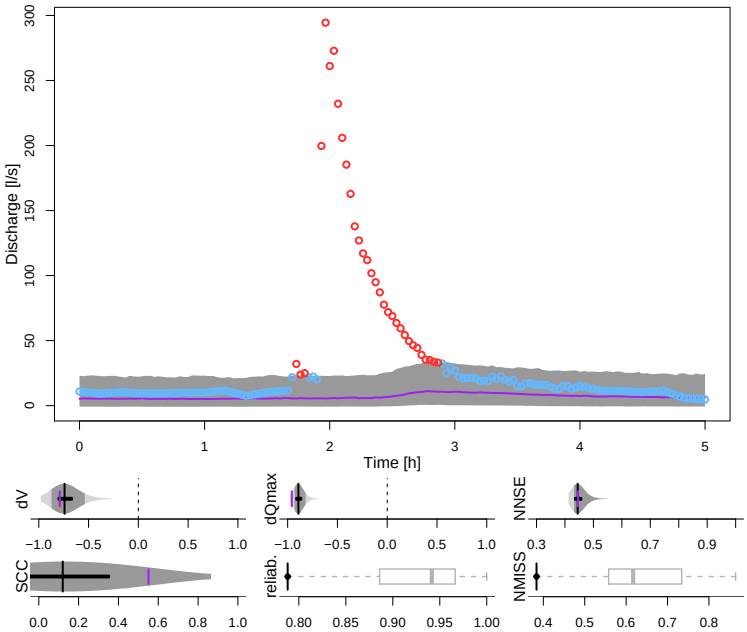





**2014–10–22 09:09:00, Rmax10 = 3.7 mm/h**

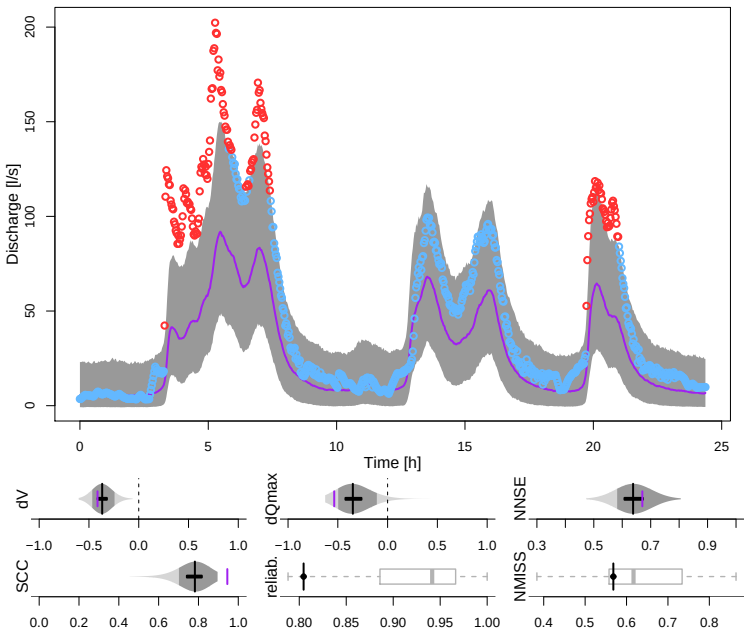





**2015–05–03 19:18:00, Rmax10 = 2.3 mm/h**

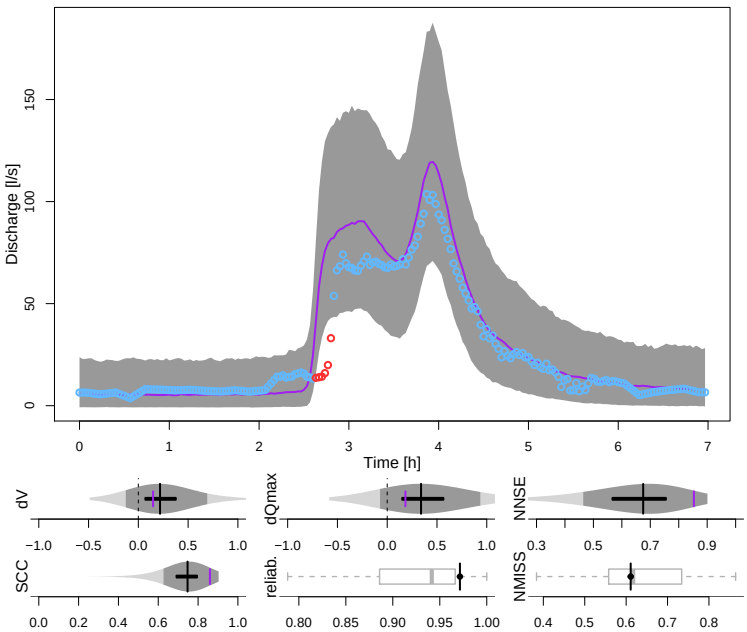

# 1-min data from the three municipal rain gauges (2/4)

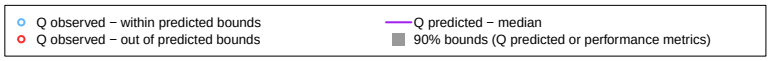


**2015–05–05 15:44:00, Rmax10 = 3 mm/h**

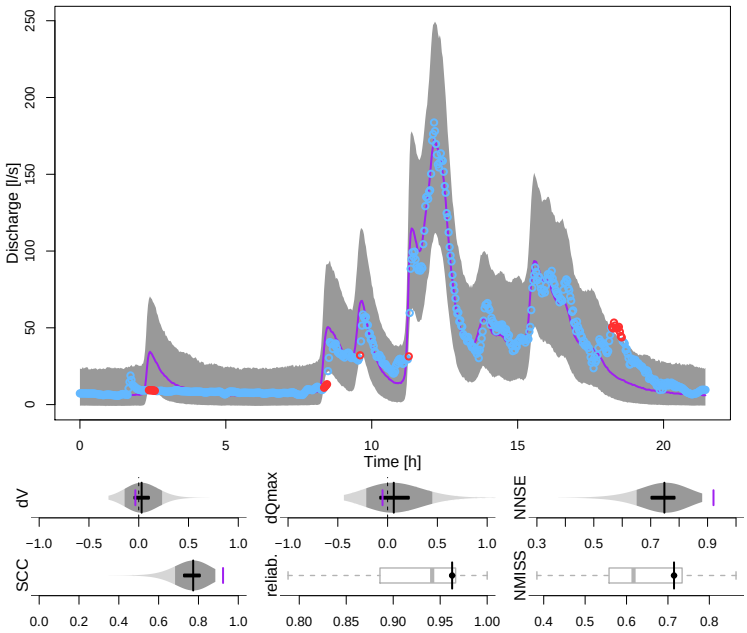


**2015–05–29 20:40:00, Rmax10 = 39.2 mm/h**

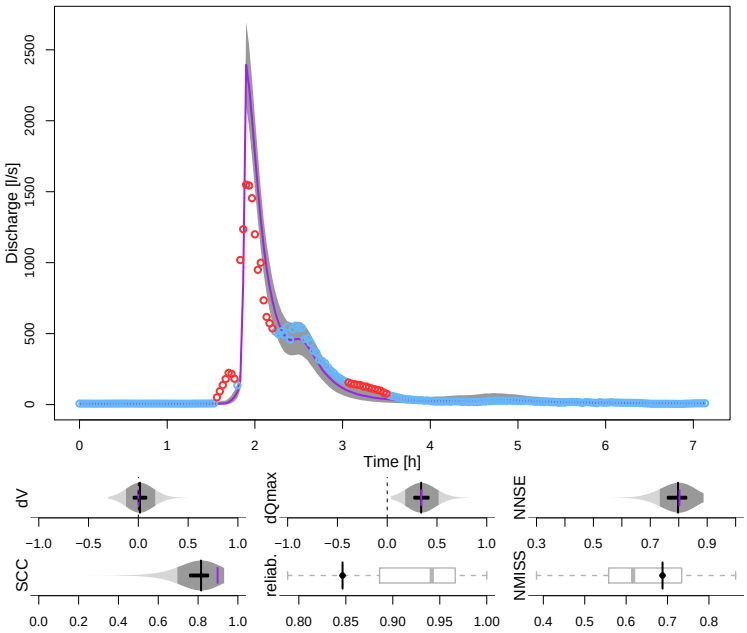


**2015–06–23 09:00:00, Rmax10 = 7.2 mm/h**

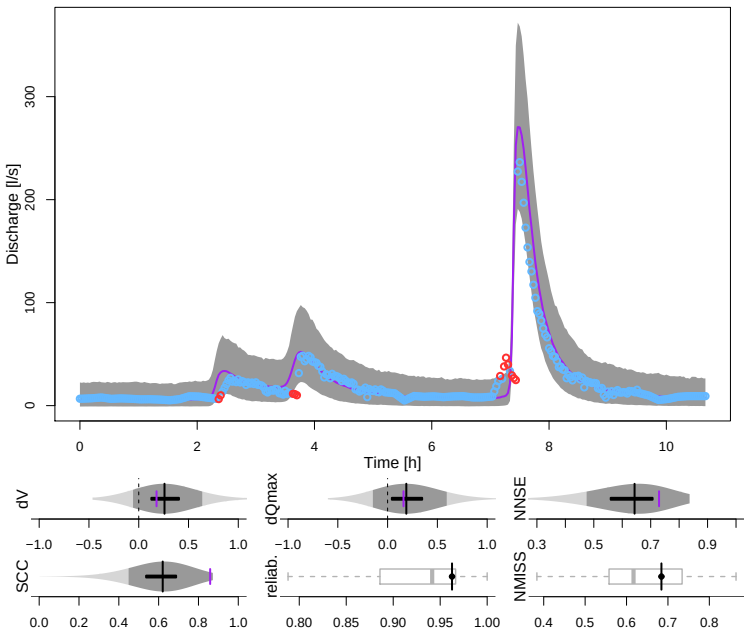


**2015–07–07 22:48:00, Rmax10 = 18 mm/h**

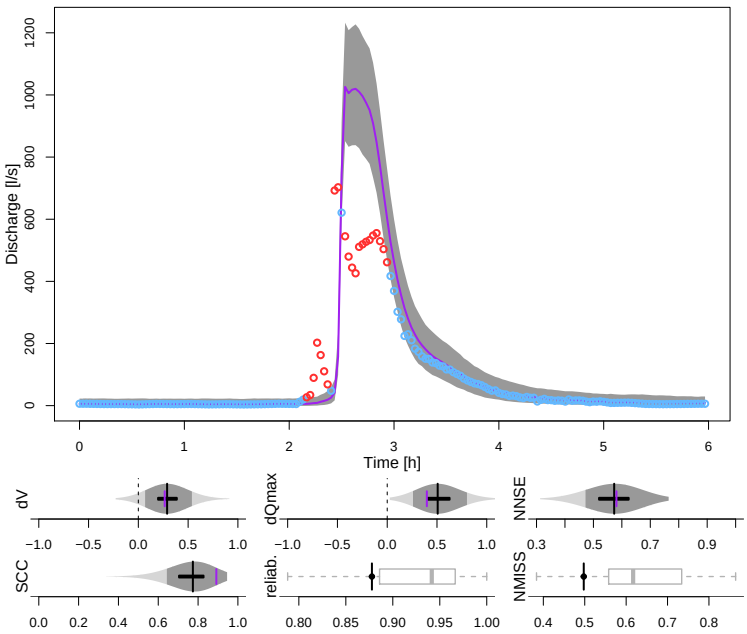


**2015–07–25 03:06:00, Rmax10 = 5.9 mm/h**

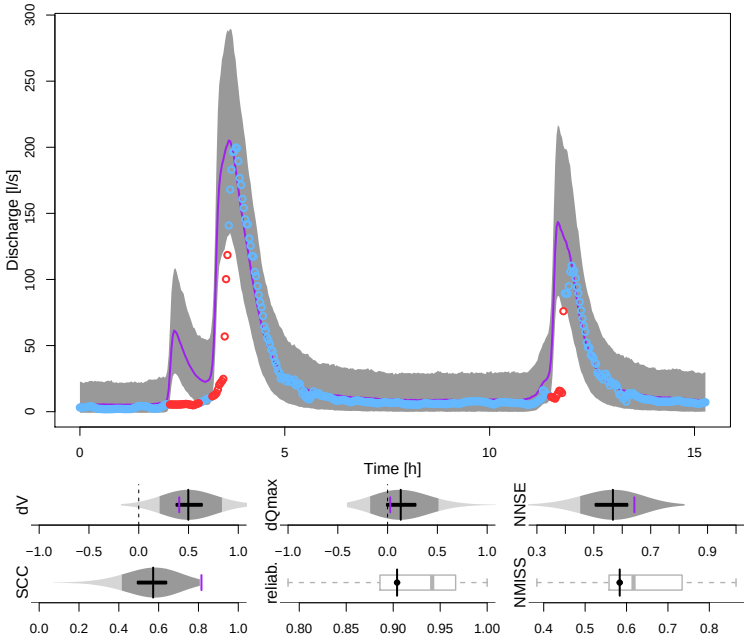


**2015–09–07 10:03:00, Rmax10 = 6.5 mm/h**

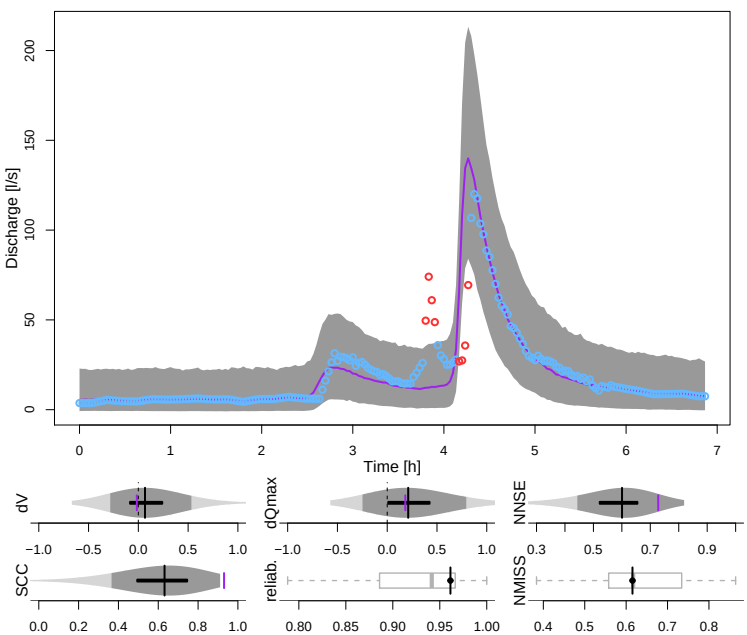

# 1-min data from the three municipal rain gauges (3/4)

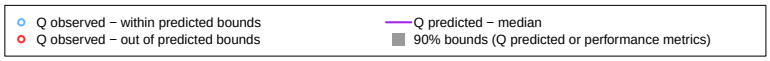


**2015−09−09 12:48:00, Rmax10 = 13 mm/h**

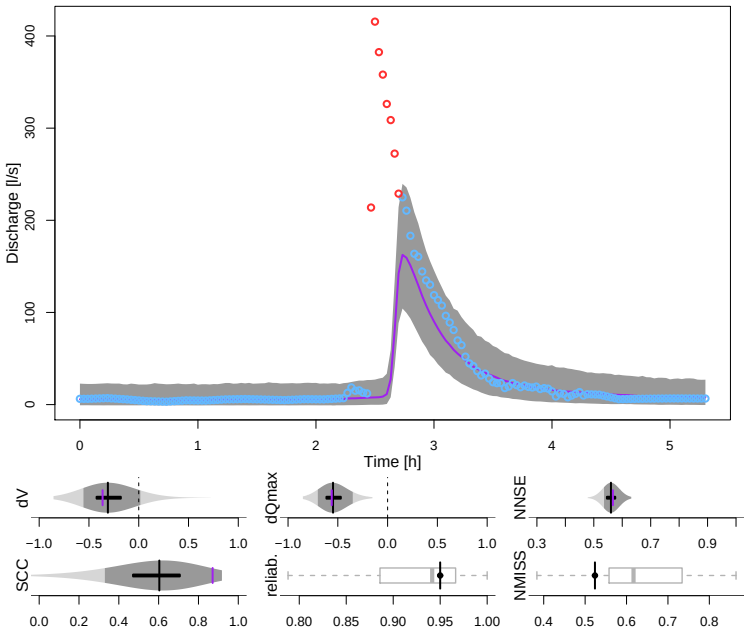


**2015−10−14 00:07:00, Rmax10 = 4.7 mm/h**

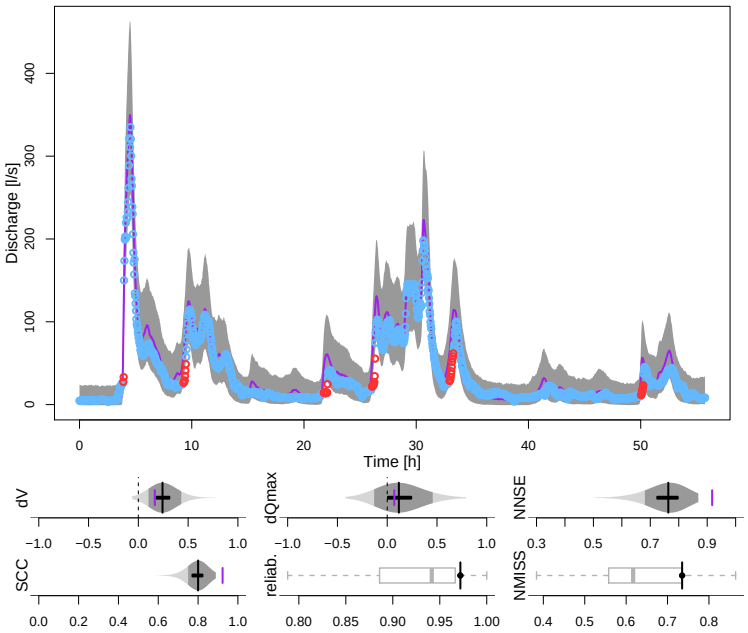


**2015−11−20 09:27:00, Rmax10 = 1.5 mm/h**

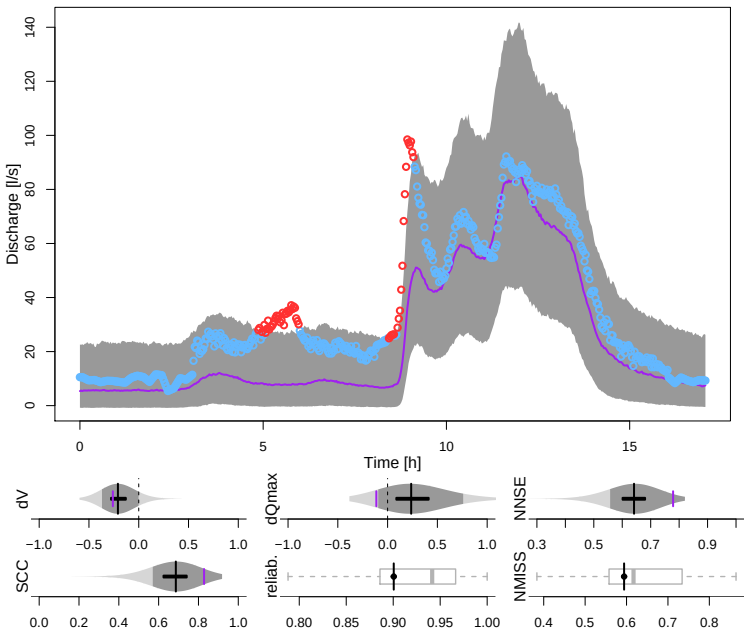


**2015−12−09 10:29:00, Rmax10 = 1.7 mm/h**

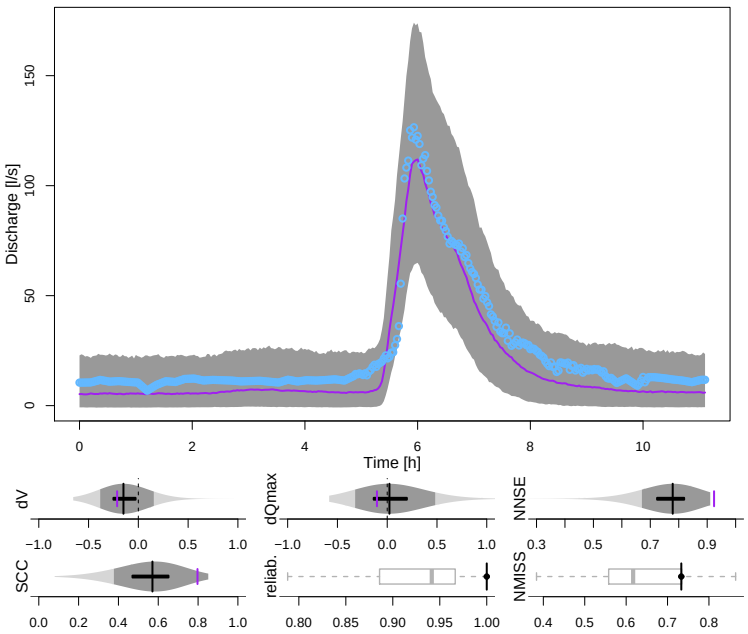


**2016−05−24 13:04:00, Rmax10 = 22.3 mm/h**

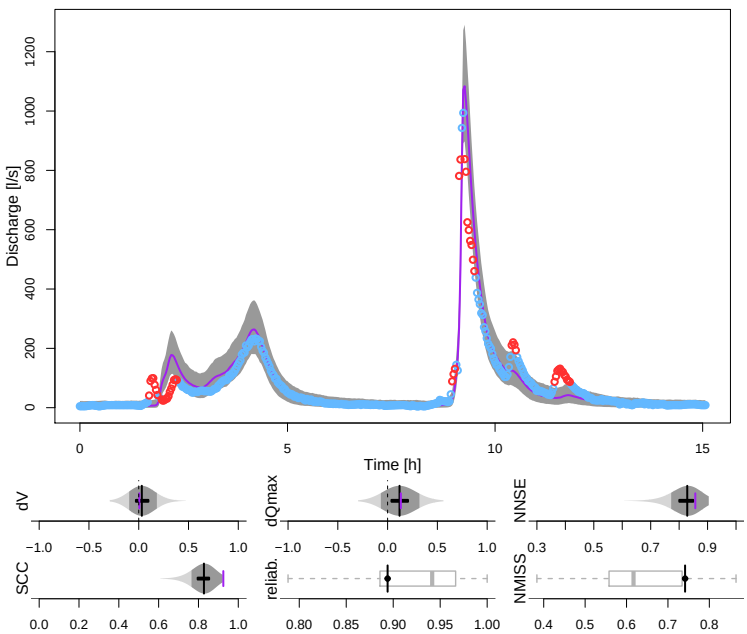


**2016−06−25 20:05:00, Rmax10 = 9.7 mm/h**

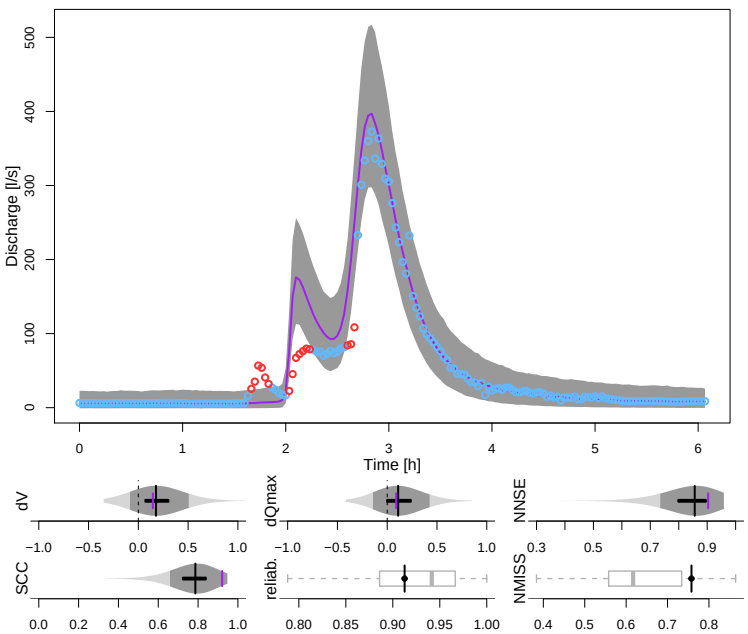

# 1-min data from the three municipal rain gauges (4/4)

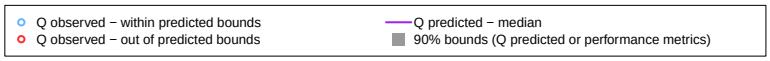


**2016−08−29 02:28:00, Rmax10 = 16.5 mm/h**

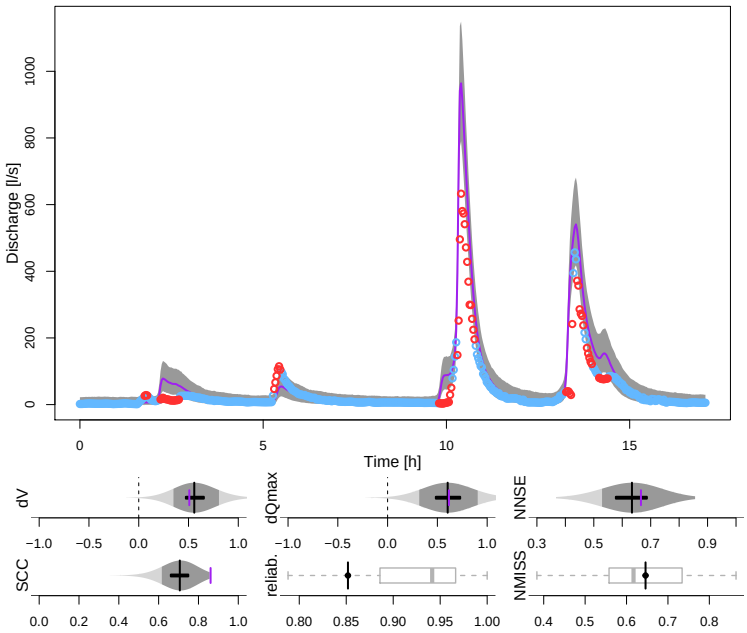





**2016−09−05 12:31:00, Rmax10 = 8.5 mm/h**

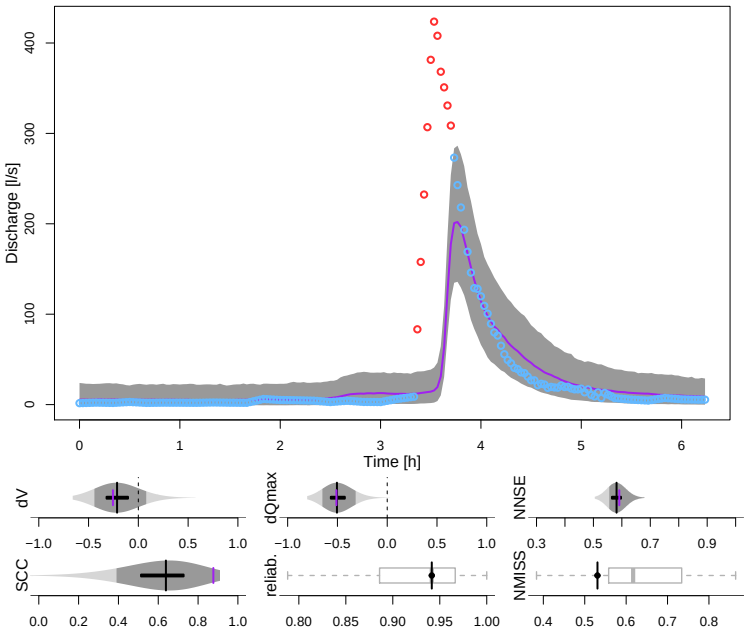





**2016−10−03 07:33:00, Rmax10 = 23 mm/h**

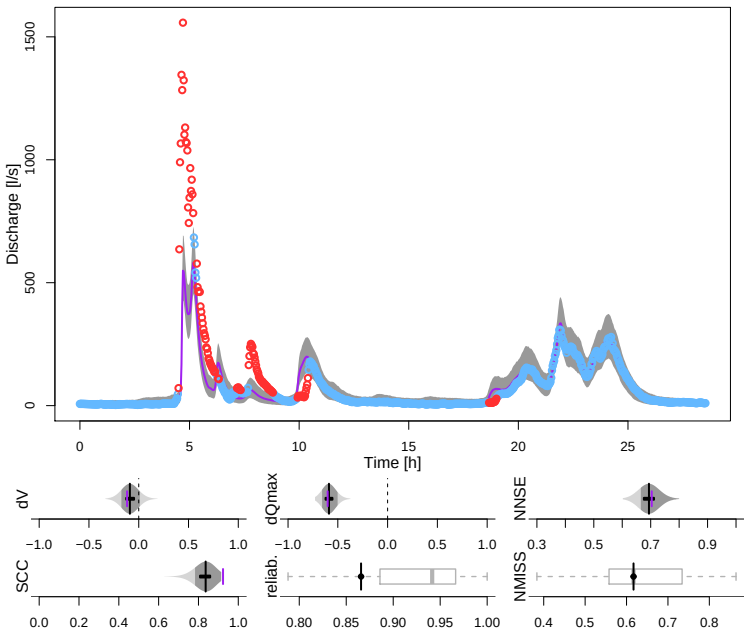





**2016−10−11 12:35:00, Rmax10 = 4.4 mm/h**

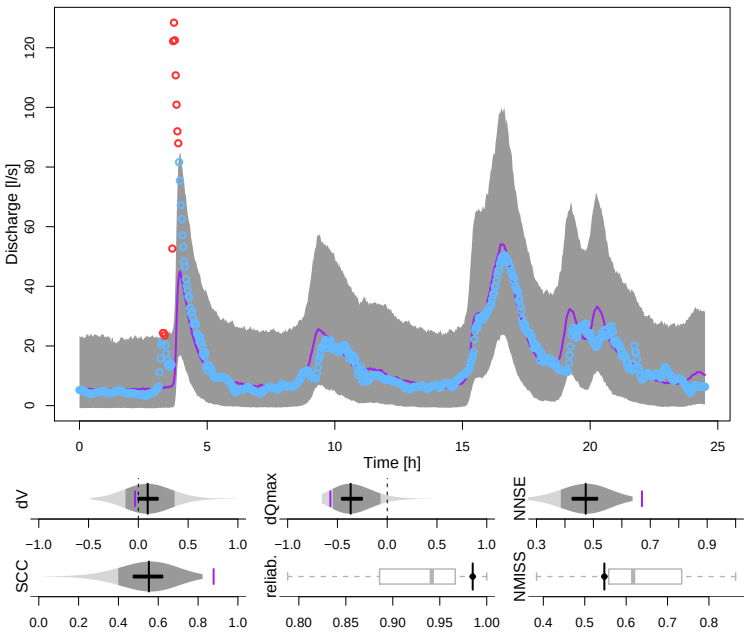





**2016−10−19 00:13:00, Rmax10 = 8.8 mm/h**

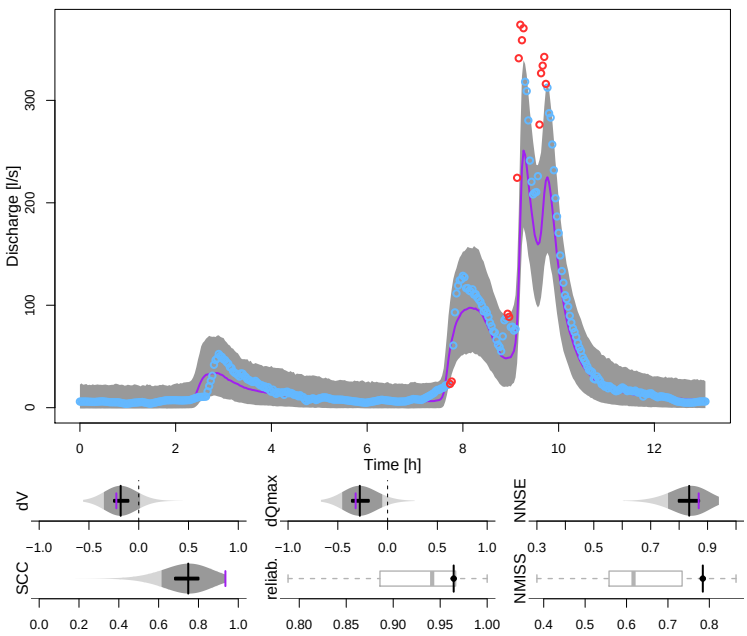

# CML QPEs, WAA calibrated to 60-min data from the 3 municipal gauges (1/4)

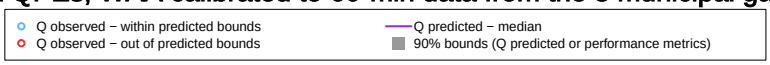


**2014–09–20 13:31:00, Rmax10 = 7.2 mm/h**

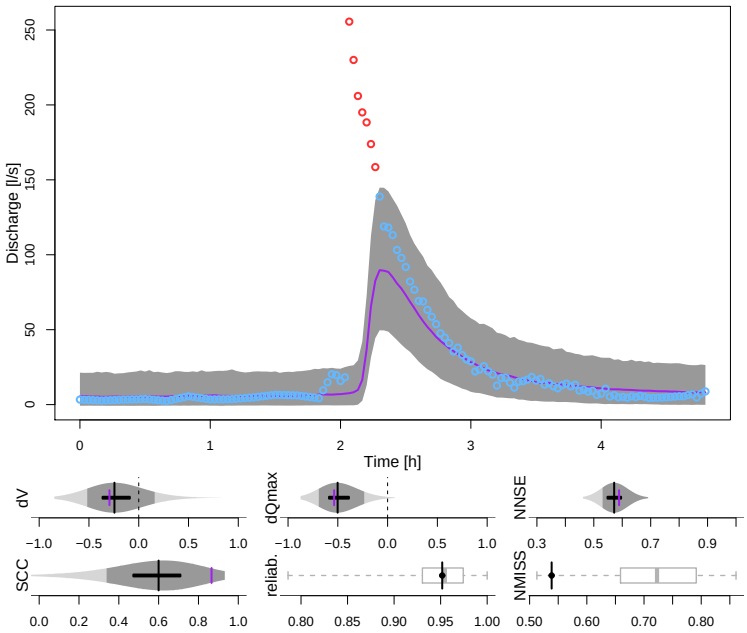





**2014–09–21 17:58:00, Rmax10 = 6.2 mm/h**

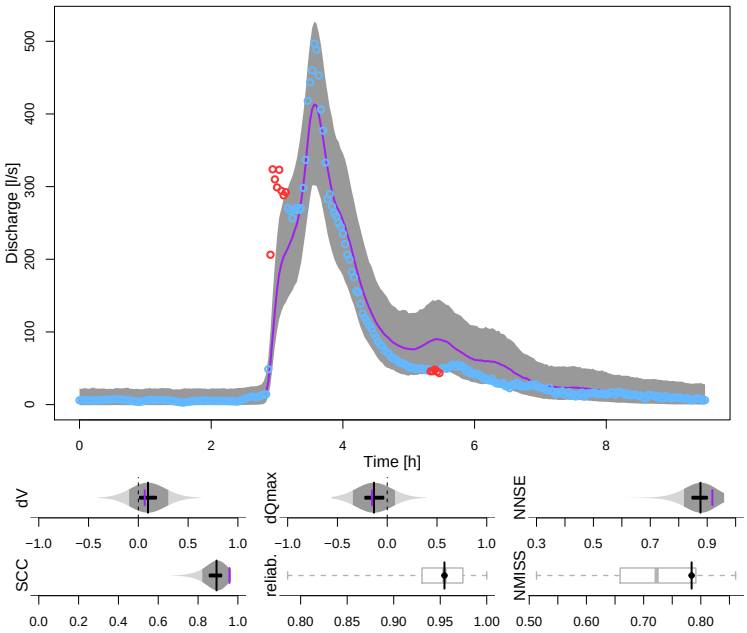





**2014–10–13 21:27:00, Rmax10 = 17.4 mm/h**

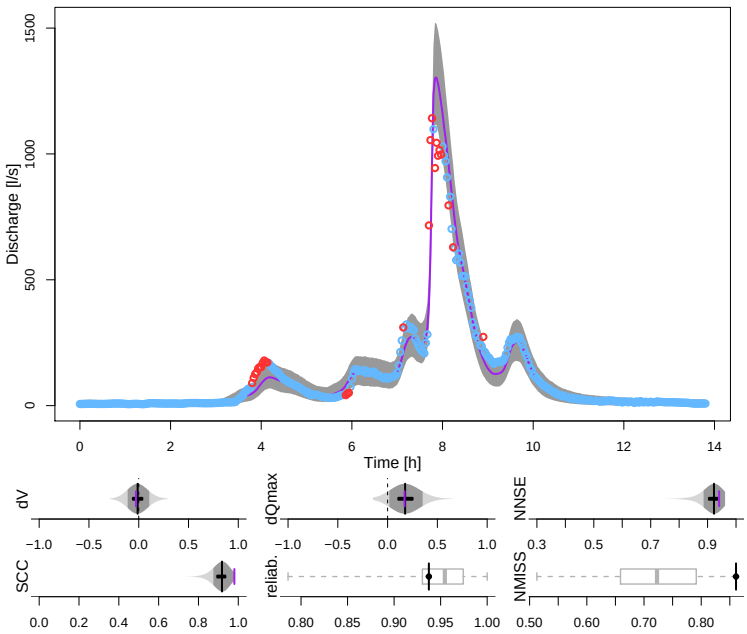





**2014–10–16 15:32:00, Rmax10 = 12.5 mm/h**

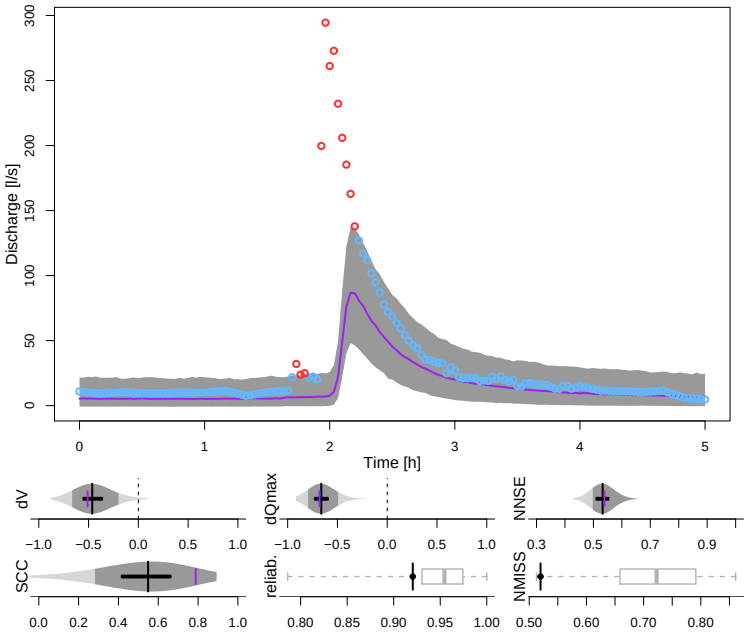





**2014–10–22 09:09:00, Rmax10 = 3.7 mm/h**

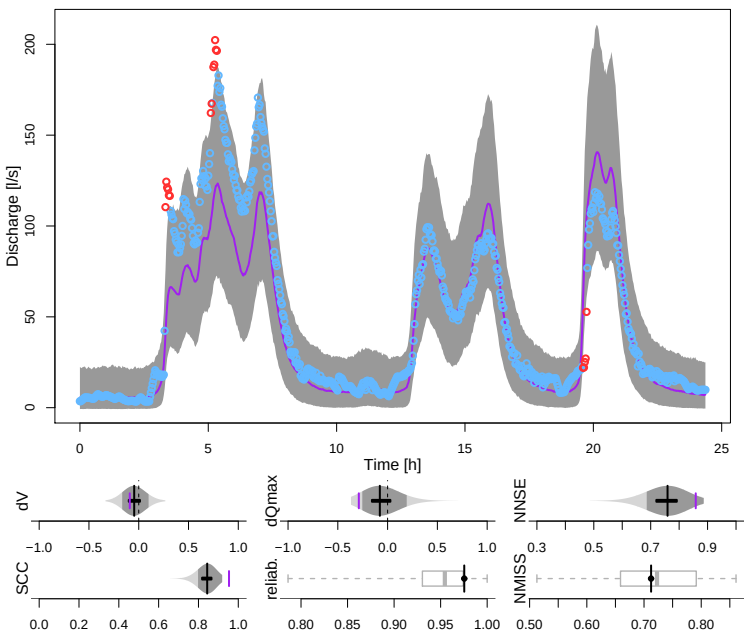





**2015–05–03 19:18:00, Rmax10 = 2.3 mm/h**

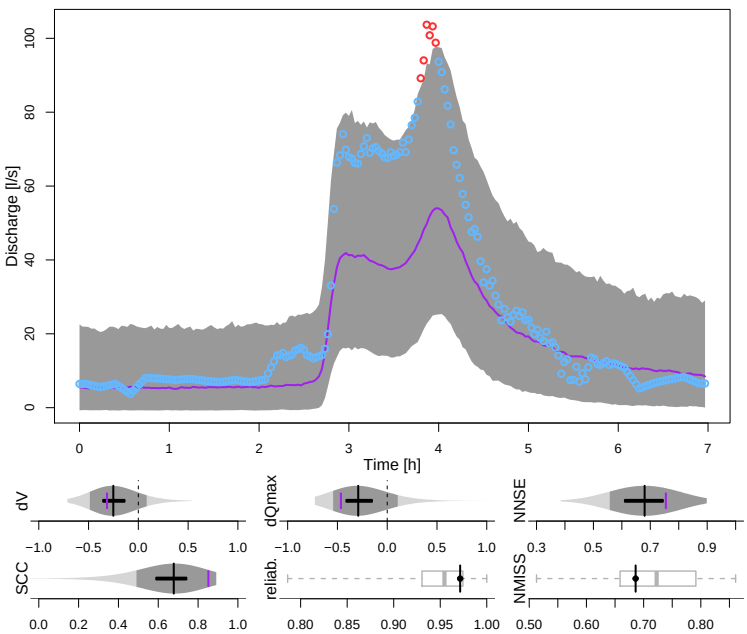

# CML QPEs, WAA calibrated to 60-min data from the 3 municipal gauges (2/4)

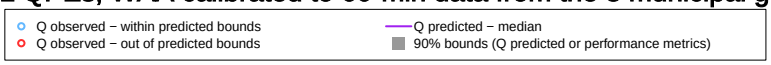


**2015–05–05 15:44:00, Rmax10 = 3 mm/h**

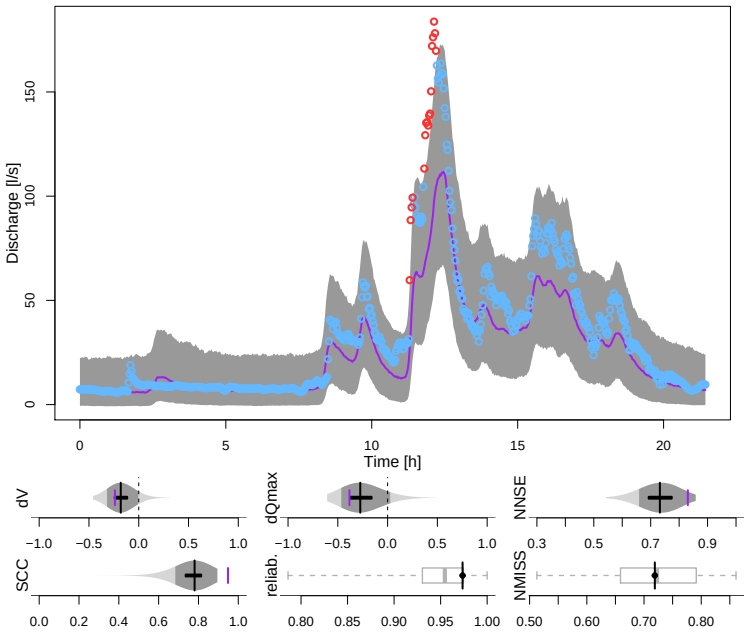





**2015–05–29 20:40:00, Rmax10 = 39.2 mm/h**

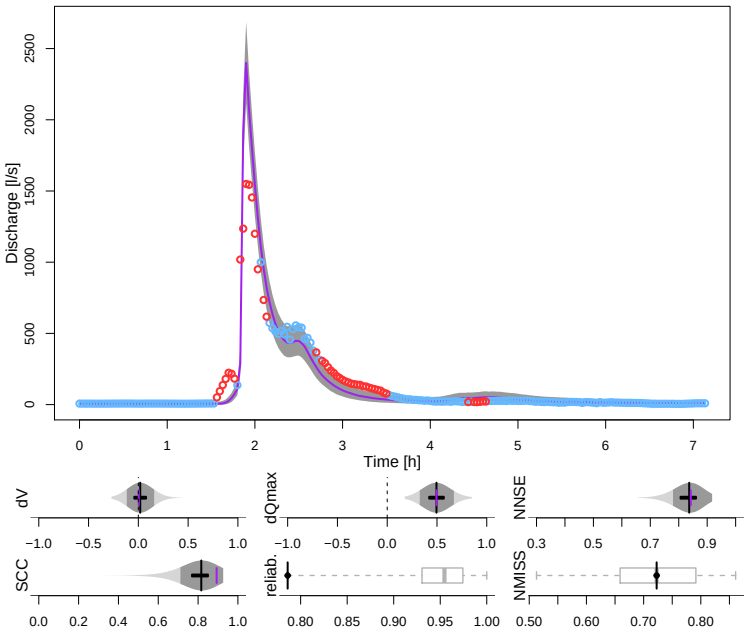





**2015–06–23 09:00:00, Rmax10 = 7.2 mm/h**

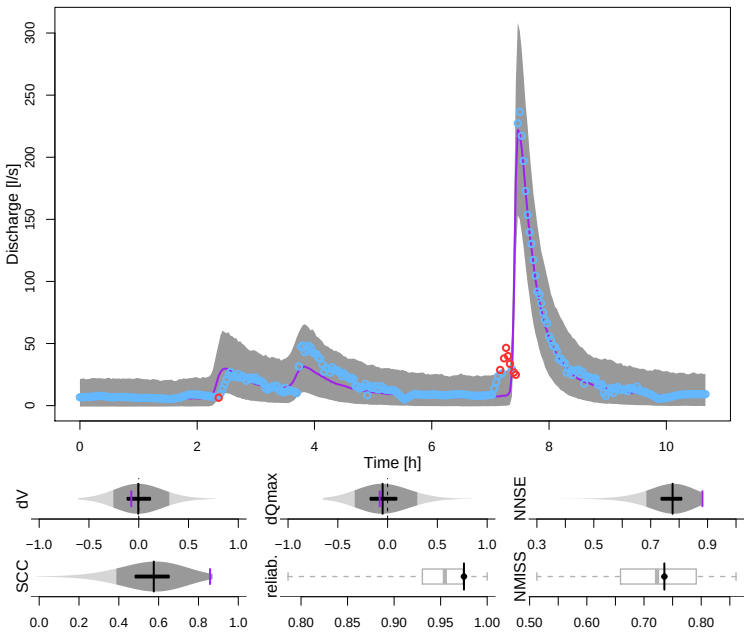





**2015–07–07 22:48:00, Rmax10 = 18 mm/h**

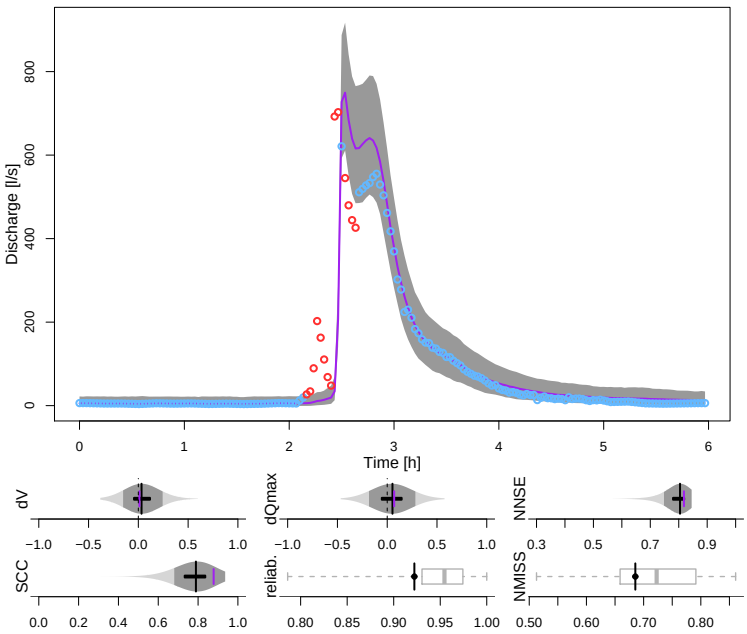





**2015–07–25 03:06:00, Rmax10 = 5.9 mm/h**

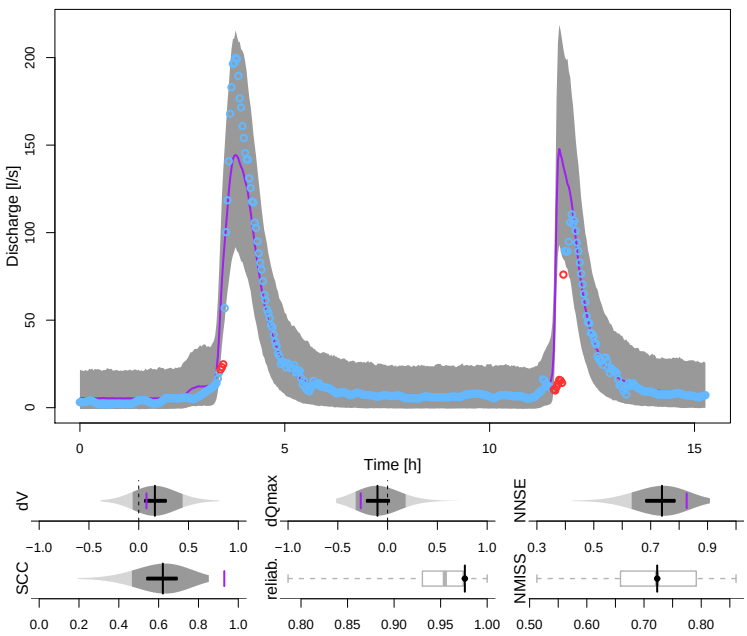





**2015–09–07 10:03:00, Rmax10 = 6.5 mm/h**

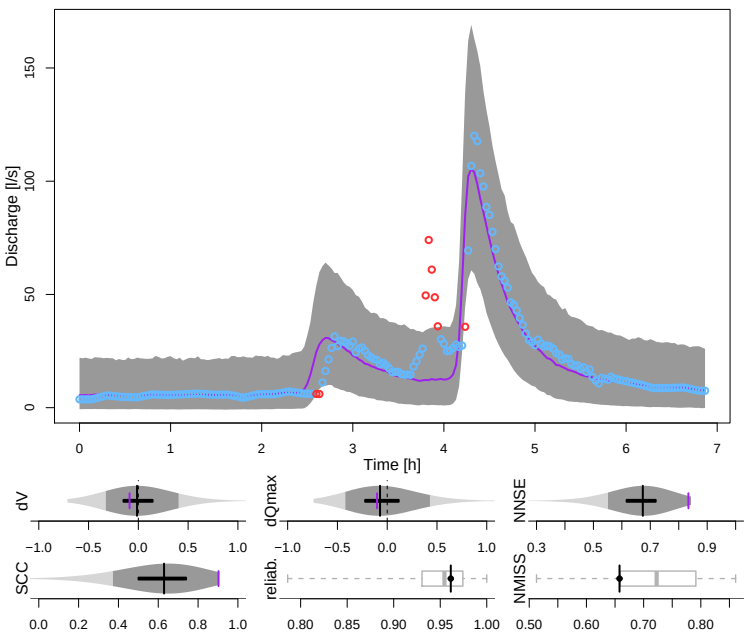

# CML QPEs, WAA calibrated to 60-min data from the 3 municipal gauges (3/4)

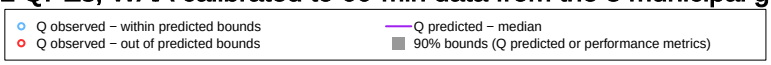


**2015−09−09 12:48:00, Rmax10 = 13 mm/h**

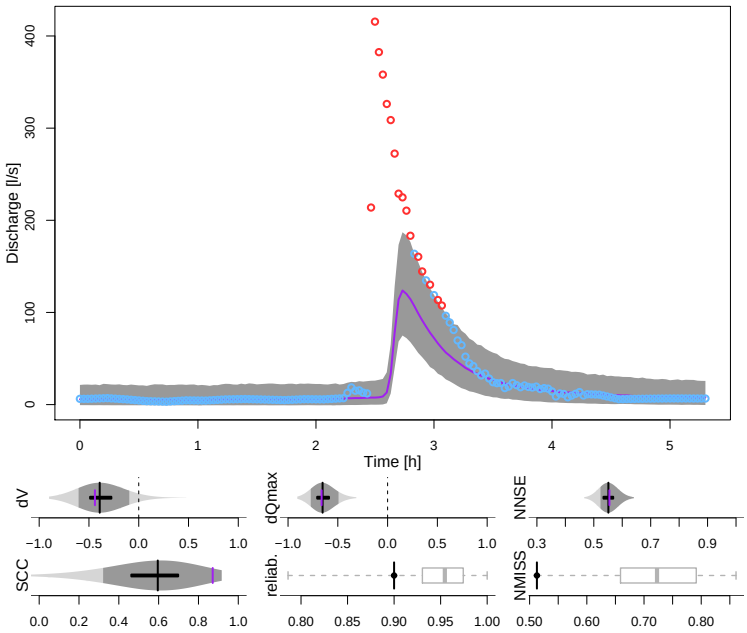





**2015−10−14 00:07:00, Rmax10 = 4.7 mm/h**

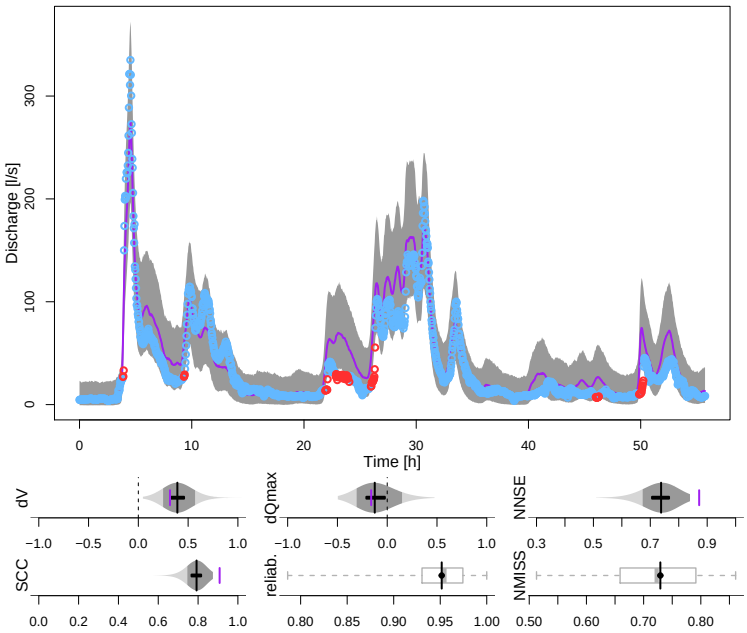





**2015−11−20 09:27:00, Rmax10 = 1.5 mm/h**

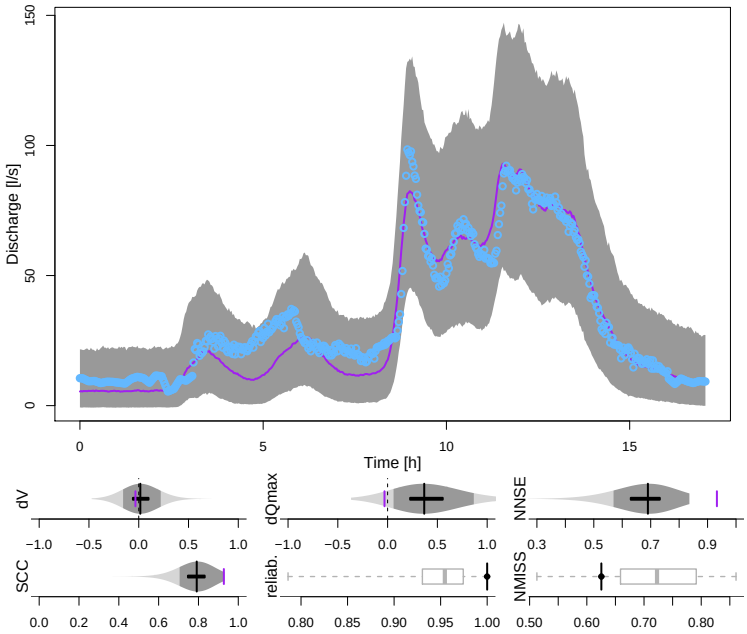





**2015−12−09 10:29:00, Rmax10 = 1.7 mm/h**

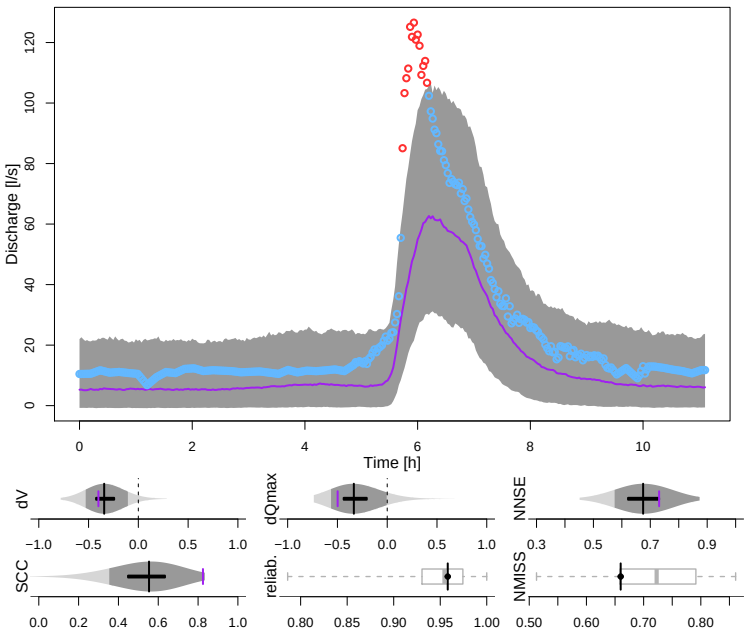





**2016−05−24 13:04:00, Rmax10 = 22.3 mm/h**

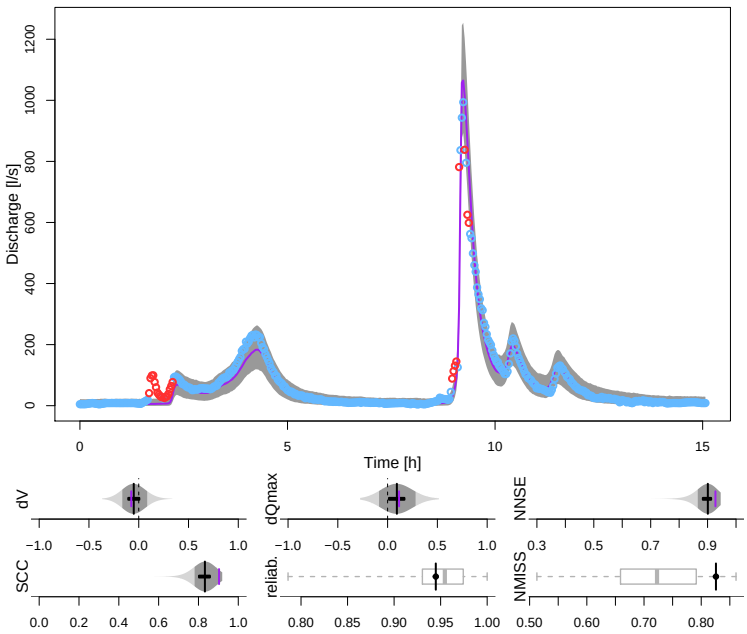





**2016−06−25 20:05:00, Rmax10 = 9.7 mm/h**

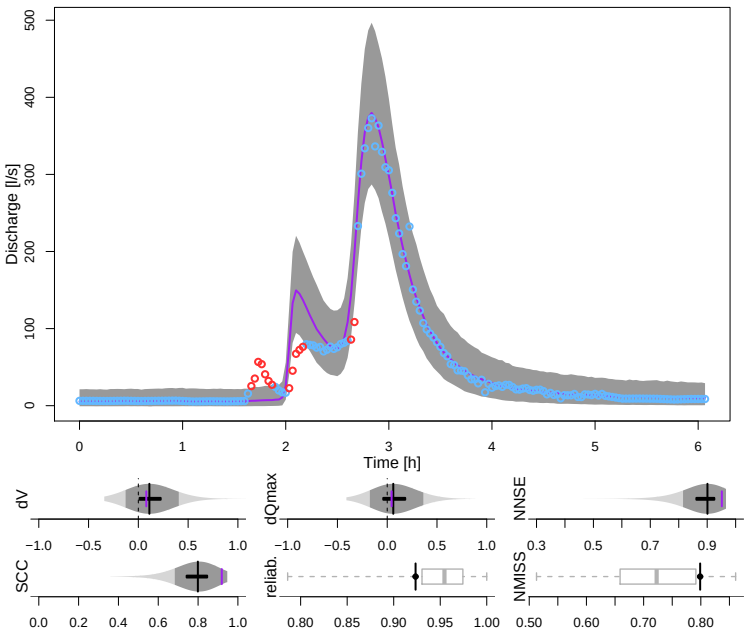

# CML QPEs, WAA calibrated to 60-min data from the 3 municipal gauges (4/4)

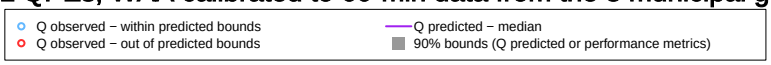


**2016−08−29 02:28:00, Rmax10 = 16.5 mm/h**

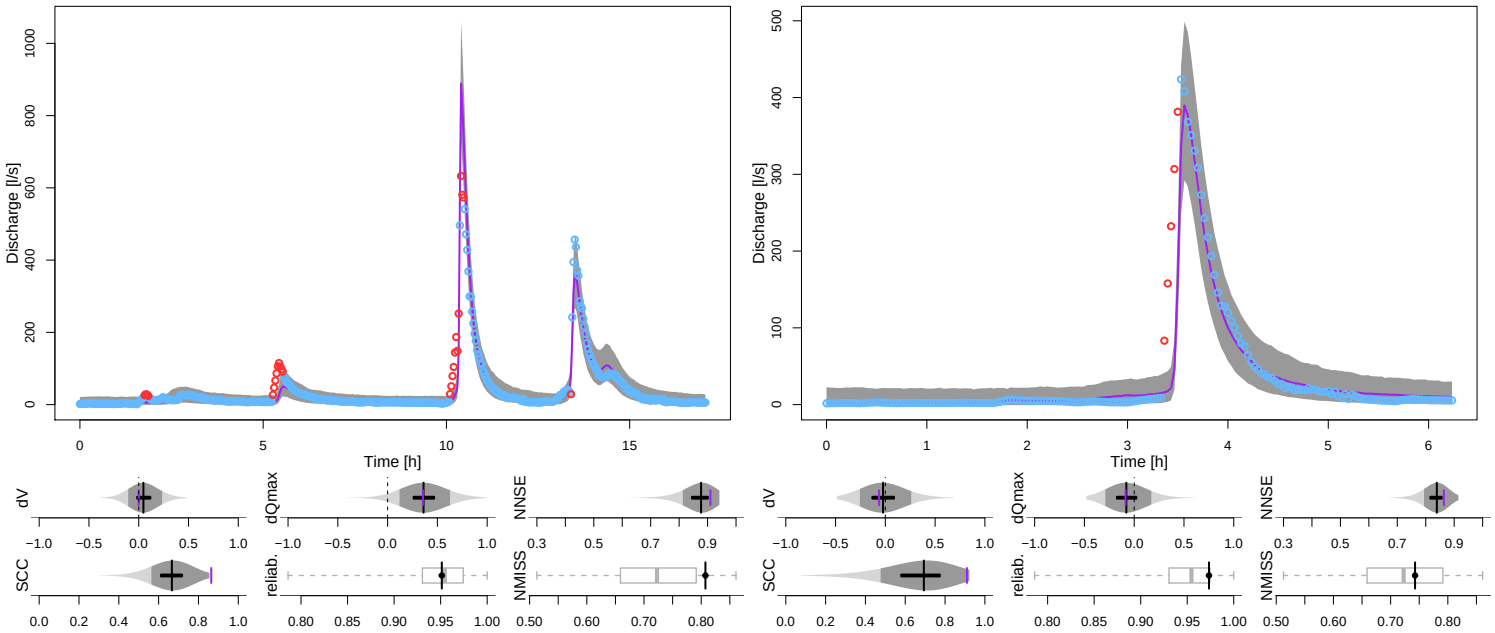


**2016−09−05 12:31:00, Rmax10 = 8.5 mm/h**




**2016−10−03 07:33:00, Rmax10 = 23 mm/h**

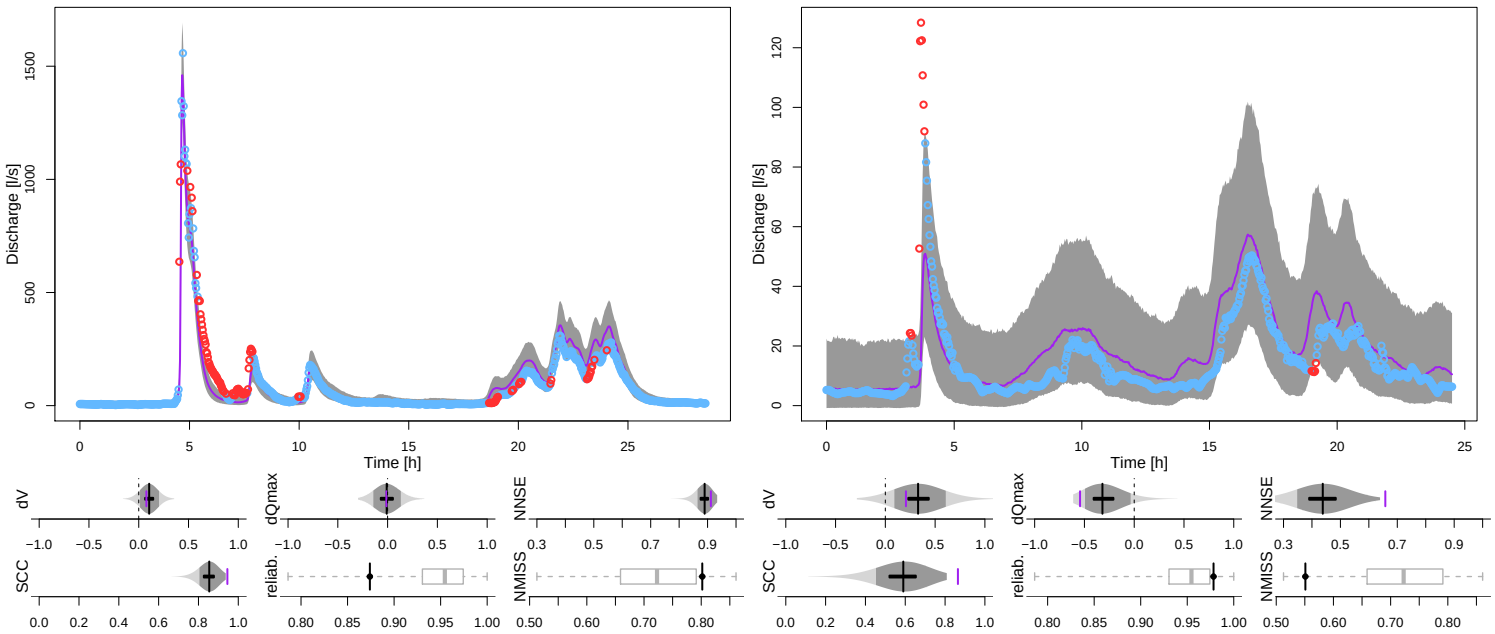


**2016−10−11 12:35:00, Rmax10 = 4.4 mm/h**




**2016−10−19 00:13:00, Rmax10 = 8.8 mm/h**

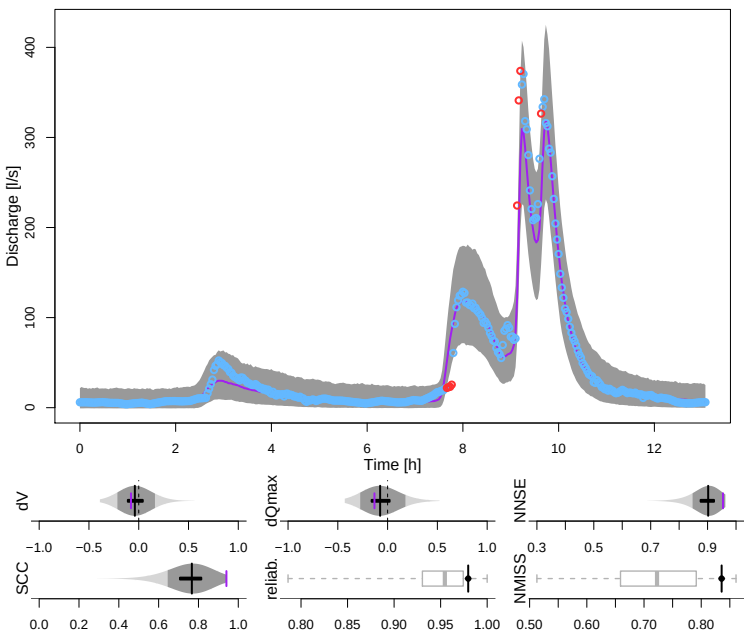

# Bibliography


Ahm, M. & Rasmussen, M. R. (2017). Weather Radar Adjustment Using Runoff from Urban Surfaces. *Journal of Hydrologic Engineering*, 22(5).

Anagnostou, E. N., Krajewski, W. F., & Smith, J. (1999). Uncertainty Quantification of Mean-Areal Radar-Rainfall Estimates. *Journal of Atmospheric and Oceanic Technology*, 16(2), 206–215.

Atlas, D. & Ulbrich, C. W. (1977). Path- and Area-Integrated Rainfall Measurement by Microwave Attenuation in the 1–3 cm Band. *Journal of Applied Meteorology*, 16(12), 1322–1331.

Bárdossy, A. & Pegram, G. (2017). Combination of radar and daily precipitation data to estimate meaningful sub-daily point precipitation extremes. *Journal of Hydrology*, 544, 397–406.

Berne, A., Delrieu, G., Creutin, J.-D., & Obled, C. (2004). Temporal and spatial resolution of rainfall measurements required for urban hydrology. *Journal of Hydrology*, 299(3-4), 166–179.

Berne, A. & Krajewski, W. (2013). Radar for hydrology: Unfulfilled promise or unrecognized potential? *Advances in Water Resources*, 51, 357–366.

Beven, K. (2006). On undermining the science? *Hydrological processes*, 20, 3141–3146.

Bock, A. R., Farmer, W. H., & Hay, L. E. (2018). Quantifying uncertainty in simulated streamflow and runoff from a continental-scale monthly water balance model. *Advances in Water Resources*, 122, 166–175.

Borup, M., Grum, M., Linde, J. J., & Mikkelsen, P. S. (2016). Dynamic gauge adjustment of high-resolution X-band radar data for convective rain storms: Model-based evaluation against measured combined sewer overflow. *Journal of Hydrology*, 539, 687–699.

Bourgin, F., Andréassian, V., Perrin, C., & Oudin, L. (2015). Transferring global uncertainty estimates from gauged to ungauged catchments. *Hydrology and Earth System Sciences*, 19(5), 2535–2546.

Box, G. E. & Cox, D. R. (1964). An analysis of transformations. *Journal of the Royal Statistical Society. Series B (Methodological)*, (pp. 211–252).

Brauer, C. C., Overeem, A., Leijnse, H., & Uijlenhoet, R. (2016). The effect of differences between rainfall measurement techniques on groundwater and discharge simulations in a lowland catchment: Rainfall Measurement Techniques for Hydrological Simulations. *Hydrological Processes*, 30(21), 3885–3900.

Breinholt, A., Møller, J. K., Madsen, H., & Mikkelsen, P. S. (2012). A formal statistical approach to representing uncertainty in rainfall–runoff modelling with focus on residual analysis and probabilistic output evaluation – Distinguishing simulation and prediction. *Journal of Hydrology*, 472–473, 36–52.

Cazzaniga, G., De Michele, C., Deidda, C., D'Amico, M., Ghezzi, A., Nebuloni, R., & Sileo, A. (2020). Calculating the hydrological response of a mountain catchment using conventional and unconventional (CML) rainfall observations: The case study of Mallero catchment. In *EGU General Assembly 2020* (pp. EGU2020–16368).

Chen, H. & Chandrasekar, V. (2015). The quantitative precipitation estimation system for Dallas–Fort Worth (DFW) urban remote sensing network. *Journal of Hydrology*, 531, 259–271.

Chwala, C., Gmeiner, A., Qiu, W., Hipp, S., Nienaber, D., Siart, U., Eibert, T., Pohl, M., Seltmann, J., Fritz, J., & Kunstmann, H. (2012). Precipitation observation using microwave backhaul links in the alpine and pre-alpine region of Southern Germany. *Hydrology and Earth System Sciences*, 16(8), 2647–2661.

Chwala, C., Keis, F., & Kunstmann, H. (2016). Real-time data acquisition of commercial microwave link networks for hydrometeorological applications. *Atmospheric Measurement Techniques*, 9(3), 991–999.

Chwala, C. & Kunstmann, H. (2019). Commercial microwave link networks for rainfall observation: Assessment of the current status and future challenges. *Wiley Interdisciplinary Reviews: Water*, 6(2), e1337.

Cristiano, E., ten Veldhuis, M.-C., & van de Giesen, N. (2017). Spatial and temporal variability of rainfall and their effects on hydrological response in urban areas – a review. *Hydrology and Earth System Sciences*, 21(7), 3859–3878.

D'Amico, M., Manzoni, A., & Solazzi, G. L. (2016). Use of Operational Microwave Link Measurements for the Tomographic Reconstruction of 2-D Maps of Accumulated Rainfall. *IEEE Geoscience and Remote Sensing Letters*, 13(12), 1827–1831.

de Vos, L., Leijnse, H., Overeem, A., & Uijlenhoet, R. (2017). The potential of urban rainfall monitoring with crowdsourced automatic weather stations in Amsterdam. *Hydrology and Earth System Sciences*, 21(2), 765–777.

Del Giudice, D., Albert, C., Rieckermann, J., & Reichert, P. (2016). Describing the catchment-averaged precipitation as a stochastic process improves parameter and input estimation. *Water Resources Research*, 52(4), 3162–3186.

Del Giudice, D., Honti, M., Scheidegger, A., Albert, C., Reichert, P., & Rieckermann, J. (2013). Improving uncertainty estimation in urban hydrological modeling by statistically describing bias. *Hydrology and Earth System Sciences*, 17, 4209–4225.

Deletic, A., Dotto, C., McCarthy, D., Kleidorfer, M., Freni, G., Mannina, G., Uhl, M., Henrichs, M., Fletcher, T., Rauch, W., Bertrand-Krajewski, J., & Tait, S. (2012). Assessing uncertainties in urban drainage models. *Physics and Chemistry of the Earth, Parts A/B/C*, 42–44, 3–10.

Disch, A., Scheidegger, A., Wani, O. F., & Rieckermann, J. (2019). Impact of different sources of precipitation data on urban rainfall-runoff predictions: A comparison of rain gauges, commercial microwave links and radar. *Rainfall monitoring, modelling and forecasting in urban environments. UrbanRain18: 11th International Workshop on Precipitation in Urban Areas. Conference Proceedings.*

Dotto, C. B., Mannina, G., Kleidorfer, M., Vezzaro, L., Henrichs, M., McCarthy, D. T., Freni, G., Rauch, W., & Deletic, A. (2012). Comparison of different uncertainty techniques in urban stormwater quantity and quality modelling. *Water research*, 46, 2545–2558.

Ehret, U. & Zehe, E. (2011). Series distance – an intuitive metric to quantify hydrograph similarity in terms of occurrence, amplitude and timing of hydrological events. *Hydrology and Earth System Sciences*, 15(3), 877–896.

Einfalt, T., Arnbjergnielsen, K., Golz, C., Jensen, N., Quirmbach, M., Vaes, G., & Vieux, B. (2004). Towards a roadmap for use of radar rainfall data in urban drainage. *Journal of Hydrology*, 299(3-4), 186–202.

Ericsson (2018). Ericsson Microwave Outlook. https://www.ericsson.com/4a312c/assets/local/reports-papers/microwave-outlook/2018/ericsson-microwave-outlook-report-2018.pdf.

Fencl, M., Dohnal, M., Rieckermann, J., & Bareš, V. (2017). Gauge-adjusted rainfall estimates from commercial microwave links. *Hydrology and Earth System Sciences*, 21(1), 617–634.

Fencl, M., Dohnal, M., Valtr, P., Grabner, M., & Bareš, V. (2020). Atmospheric observations with E-band microwave links – challenges and opportunities. *Atmospheric Measurement Techniques*, 13(12), 6559–6578.

Fencl, M., Rieckermann, J., Schleiss, M., Stránský, D., & Bareš, V. (2013). Assessing the potential of using telecommunication microwave links in urban drainage modelling. *Water Science & Technology*, 68.

Fencl, M., Rieckermann, J., Sýkora, P., Stránský, D., & Bareš, V. (2015). Commercial microwave links instead of rain gauges: Fiction or reality? *Water Science and Technology*, 71(1), 31–37.

Fencl, M., Valtr, P., Kvičera, M., & Bareš, V. (2019). Quantifying Wet Antenna Attenuation in 38-GHz Commercial Microwave Links of Cellular Backhaul. *IEEE Geoscience and Remote Sensing Letters*, 16(4), 514–518.

Fenicia, F., Pfister, L., Kavetski, D., Matgen, P., Iffly, J.-F., Hoffmann, L., & Uijlenhoet, R. (2012). Microwave links for rainfall estimation in an urban environment: Insights from an experimental setup in Luxembourg-City. *Journal of Hydrology*, 464–465, 69–78.

Gharesifard, M., Wehn, U., & van der Zaag, P. (2017). Towards benchmarking citizen observatories: Features and functioning of online amateur weather networks. *Journal of Environmental Management*, 193, 381–393.

Gires, A., Giangola-Murzyn, A., Abbes, J.-B., Tchiguirinskaia, I., Schertzer, D., & Lovejoy, S. (2015). Impacts of small scale rainfall variability in urban areas: A case study with 1D and 1D/2D hydrological models in a multifractal framework. *Urban Water Journal*, 12(8), 607–617.

Gneiting, T. & Raftery, A. E. (2007). Strictly proper scoring rules, prediction, and estimation. *Journal of the American Statistical Association*, 102, 359–378.

Goldshtein, O., Messer, H., & Zinevich, A. (2009). Rain Rate Estimation Using Measurements From Commercial Telecommunications Links. *IEEE Transactions on Signal Processing*, 57(4), 1616–1625.

Goormans, T. & Willems, P. (2013). Using Local Weather Radar Data for Sewer System Modeling: Case Study in Flanders, Belgium. *Journal of Hydrologic Engineering*, 18(2), 269–278.

Gosset, M., Kunstmann, H., Zougmore, F., Cazenave, F., Leijnse, H., Uijlenhoet, R., Chwala, C., Keis, F., Doumounia, A., Boubacar, B., Kacou, M., Alpert, P., Messer, H., Rieckermann, J., & Hoedjes, J. (2016). Improving Rainfall Measurement in Gauge Poor Regions Thanks to Mobile Telecommunication Networks. *Bulletin of the American Meteorological Society*, 97(3), ES49–ES51.

Graf, M., Chwala, C., Polz, J., & Kunstmann, H. (2020). Rainfall estimation from a German-wide commercial microwave link network: Optimized processing and validation for 1 year of data. *Hydrology and Earth System Sciences*, 24(6), 2931–2950.

Gupta, H. V., Kling, H., Yilmaz, K. K., & Martinez, G. F. (2009). Decomposition of the mean squared error and NSE performance criteria: Implications for improving hydrological modelling. *Journal of Hydrology*, 377(1-2), 80–91.

Haese, B., Hörning, S., Chwala, C., Bárdossy, A., Schalge, B., & Kunstmann, H. (2017). Stochastic Reconstruction and Interpolation of Precipitation Fields Using Combined Information of Commercial Microwave Links and Rain Gauges. *Water Resources Research*, 53(12), 10740–10756.

Harrison, D. L., Scovell, R. W., & Kitchen, M. (2009). High-resolution precipitation estimates for hydrological uses. *Proceedings of the Institution of Civil Engineers - Water Management*, 162(2), 125–135.

Heistermann, M., Jacobi, S., & Pfaff, T. (2013). Technical Note: An open source library for processing weather radar data (wradlib). *Hydrology and Earth System Sciences*, 17(2), 863–871.

Honti, M., Stamm, C., & Reichert, P. (2013). Integrated uncertainty assessment of discharge predictions with a statistical error model. *Water Resources Research*, 49, 4866–4884.

Humphrey, M. D., Istok, J. D., Lee, J. Y., Hevesi, J. A., & Flint, A. L. (1997). A New Method for Automated Dynamic Calibration of Tipping-Bucket Rain Gauges. *Journal of Atmospheric and Oceanic Technology*, 14(6), 1513–1519.

Ichiba, A., Gires, A., Tchiguirinskaia, I., Schertzer, D., Bompard, P., & Ten Veldhuis, M.-C. (2018). Scale effect challenges in urban hydrology highlighted with a distributed hydrological model. *Hydrology and Earth System Sciences*, 22(1), 331–350.

Imhoff, R. O., Overeem, A., Brauer, C. C., Leijnse, H., Weerts, A. H., & Uijlenhoet, R. (2020). Rainfall Nowcasting Using Commercial Microwave Links. *Geophysical Research Letters*, 47(19).

ITU Radiocommunication Sector (2005). Recommendation 838-3: Specific attenuation model for rain for use in prediction methods.

Kavetski, D., Kuczera, G., & Franks, S. W. (2006). Bayesian analysis of input uncertainty in hydrological modeling: 1. Theory: INPUT UNCERTAINTY IN HYDROLOGY, 1. *Water Resources Research*, 42(3).

Kendall, M., Stuart, A., & Ord, J. (1994). *The Advanced Theory of Statistics: Distribution Theory (Vol. 1)*. Arnold, London.

Kennedy, M. C. & O'Hagan, A. (2001). Bayesian calibration of computer models. *Journal of the Royal Statistical Society: Series B (Statistical Methodology)*, 63, 425–464.

Kharadly, M. M. Z. & Ross, R. (2001). Effect of wet antenna attenuation on propagation data statistics. *IEEE Transactions on Antennas and Propagation*, 49(8), 1183–1191.

Kidd, C. & Huffman, G. (2011). Global precipitation measurement: Global precipitation measurement. *Meteorological Applications*, 18(3), 334–353.

Kleidorfer, M., Deletic, A., Fletcher, T. D., & Rauch, W. (2009). Impact of input data uncertainties on urban stormwater model parameters. *Water Science and Technology*, 60(6), 1545–1554.

Kollo, T. & von Rosen, D. (2006). *Advanced Multivariate Statistics with Matrices*, volume 579. Springer Science & Business Media.

Leijnse, H., Uijlenhoet, R., & Berne, A. (2010). Errors and Uncertainties in Microwave Link Rainfall Estimation Explored Using Drop Size Measurements and High-Resolution Radar Data. *Journal of Hydrometeorology*, 11(6), 1330–1344.

Leijnse, H., Uijlenhoet, R., & Stricker, J. N. M. (2007). Rainfall measurement using radio links from cellular communication networks: RAPID COMMUNICATION. *Water Resources Research*, 43(3).

Leijnse, H., Uijlenhoet, R., & Stricker, J. N. M. (2008). Microwave link rainfall estimation: Effects of link length and frequency, temporal sampling, power resolution, and wet antenna attenuation. *Advances in Water Resources*, 31(11), 1481–1493.

Lorenz, C. & Kunstmann, H. (2012). The Hydrological Cycle in Three State-of-the-Art Reanalyses: Intercomparison and Performance Analysis. *Journal of Hydrometeorology*, 13(5), 1397–1420.

Mancini, A., Lebron, R. M., & Salazar, J. L. (2019). The Impact of a Wet S-Band Radome on Dual-Polarized Phased-Array Radar System Performance. *IEEE Transactions on Antennas and Propagation*, 67(1), 207–220.

McKee, J. L. & Binns, A. D. (2016). A review of gauge–radar merging methods for quantitative precipitation estimation in hydrology. *Canadian Water Resources Journal / Revue canadienne des ressources hydriques*, 41(1-2), 186–203.

Messer, H., Zinevich, A., & Alpert, P. (2006). Environmental monitoring by wireless communication networks. *Science*, 312, 713–713.

Montesarchio, V., Lombardo, F., & Napolitano, F. (2009). Rainfall thresholds and flood warning: An operative case study. *Natural Hazards and Earth System Sciences*, 9(1), 135–144.

Moroder, C., Siart, U., Chwala, C., & Kunstmann, H. (2019). Modeling of Wet Antenna Attenuation for Precipitation Estimation From Microwave Links. *IEEE Geoscience and Remote Sensing Letters*, (pp. 1–5).

Muste, M., Lee, K., & Bertrand-Krajewski, J.-L. (2012). Standardized uncertainty analysis for hydrometry: A review of relevant approaches and implementation examples. *Hydrological Sciences Journal*, 57(4), 643–667.

Nešpor, V. & Sevruk, B. (1999). Estimation of Wind-Induced Error of Rainfall Gauge Measurements Using a Numerical Simulation. *Journal of Atmospheric and Oceanic Technology*, 16(4), 450–464.

Notaro, V., Fontanazza, C. M., Freni, G., & Puleo, V. (2013). Impact of rainfall data resolution in time and space on the urban flooding evaluation. *Water Science and Technology*, 68(9), 1984–1993.

Obled, C., Wendling, J., & Beven, K. (1994). The sensitivity of hydrological models to spatial rainfall patterns: An evaluation using observed data. *Journal of Hydrology*, 159(1-4), 305–333.

Ochoa-Rodriguez, S., Wang, L.-P., Gires, A., Pina, R. D., Reinoso-Rondinel, R., Bruni, G., Ichiba, A., Gaitan, S., Cristiano, E., van Assel, J., Kroll, S., Murlà-Tuyls, D., Tisserand, B., Schertzer, D., Tchiguirinskaia, I., Onof, C., Willems, P., & ten Veldhuis, M.-C. (2015). Impact of spatial and temporal resolution of rainfall inputs on urban hydrodynamic modelling outputs: A multi-catchment investigation. *Journal of Hydrology*, 531, 389–407.

Ochoa-Rodriguez, S., Wang, L.-P., Willems, P., & Onof, C. (2019). A Review of Radar-Rain Gauge Data Merging Methods and Their Potential for Urban Hydrological Applications. *Water Resources Research*, 55(8), 6356–6391.

Olsen, R., Rogers, D., & Hodge, D. (1978). The aRb relation in the calculation of rain attenuation. *IEEE Transactions on Antennas and Propagation*, 26(2), 318–329.

Ostrometzky, J., Raich, R., Bao, L., Hansryd, J., & Messer, H. (2018). The Wet-Antenna Effect—A Factor to be Considered in Future Communication Networks. *IEEE Transactions on Antennas and Propagation*, 66(1), 315–322.

Overeem, A., Leijnse, H., & Uijlenhoet, R. (2011). Measuring urban rainfall using microwave links from commercial cellular communication networks. *Water Resources Research*, 47(12).

Overeem, A., Leijnse, H., & Uijlenhoet, R. (2013). Country-wide rainfall maps from cellular communication networks. *Proceedings of the National Academy of Sciences*, 110(8), 2741–2745.

Pastorek, J. (2014). *Návrh a kalibrácia zrážko-odtokového modelu urbanizovaného povodia Praha Letňany v prostredí SWMM [Design and calibration of a dynamic rainfall-runoff model of an urbanized catchment using the SWMM simulator]*. Bachelor Thesis, Czech Technical University in Prague.

Pastorek, J. (2016). The effect of different rainfall information on uncertainty in urban runoff modelling. Master's thesis, Czech Technical University in Prague.

Pastorek, J., Fencl, M., & Bareš, V. (2019a). Calibrating microwave link rainfall retrieval model using runoff observations. In *Geophysical Research Abstracts*, volume 21.

Pastorek, J., Fencl, M., Rieckermann, J., & Bareš, V. (2019b). Commercial microwave links for urban drainage modelling: The effect of link characteristics and their position on runoff simulations. *Journal of Environmental Management*, 251, 109522.

Pastorek, J., Fencl, M., Rieckermann, J., & Bareš, V. (2022). Precipitation Estimates From Commercial Microwave Links: Practical Approaches to Wet-Antenna Correction. *IEEE Transactions on Geoscience and Remote Sensing*, 60, 1–9.

Pastorek, J., Fencl, M., Rieckermann, J., Sýkora, P., Stránský, D., Dohnal, M., & Bareš, V. (2018). Posouzení srážkových dat z mikrovlnných spojů v městském povodí pomocí analýzy nejistot hydrologického modelu [The Evaluation of CML Rainfall Data in Urban Catchment by Means of Hydrologic Model Uncertainty]. *SOVAK: Časopis oboru vodovodů a kanalizací*, 27, 16–22.

Pastorek, J., Fencl, M., Stránský, D., Rieckermann, J., & Bareš, V. (2017). Reliability of microwave link rainfall data for urban runoff modelling. In *Proceedings of the 14th IWA/IAHR International Conference on Urban Drainage* (pp. 1340–1343). Prague, Czech Republic.

Peleg, N., Ben-Asher, M., & Morin, E. (2013). Radar subpixel-scale rainfall variability and uncertainty: Lessons learned from observations of a dense rain-gauge network. *Hydrology and Earth System Sciences*, 17(6), 2195–2208.

Reichert, P. & Schuwirth, N. (2012). Linking statistical bias description to multiobjective model calibration. *Water Resources Research*, 48.

Rico-Ramirez, M., Liguori, S., & Schellart, A. (2015). Quantifying radar-rainfall uncertainties in urban drainage flow modelling. *Journal of Hydrology*, 528, 17–28.

Rios Gaona, M. F., Overeem, A., Leijnse, H., & Uijlenhoet, R. (2015). Measurement and interpolation uncertainties in rainfall maps from cellular communication networks. *Hydrology and Earth System Sciences*, 19(8), 3571–3584.

Rios Gaona, M. F., Overeem, A., Raupach, T. H., Leijnse, H., & Uijlenhoet, R. (2018). Rainfall retrieval with commercial microwave links in São Paulo, Brazil. *Atmospheric Measurement Techniques*, 11(7), 4465–4476.

Roversi, G., Alberoni, P. P., Fornasiero, A., & Porcù, F. (2020). Commercial microwave links as a tool for operational rainfall monitoring in Northern Italy. *Atmospheric Measurement Techniques*, 13(11), 5779–5797.

Saltikoff, E., Friedrich, K., Soderholm, J., Lengfeld, K., Nelson, B., Becker, A., Hollmann, R., Urban, B., Heistermann, M., & Tassone, C. (2019). An Overview of Using Weather Radar for Climatological Studies: Successes, Challenges, and Potential. *Bulletin of the American Meteorological Society*, 100(9), 1739–1752.

Salvadore, E., Bronders, J., & Batelaan, O. (2015). Hydrological modelling of urbanized catchments: A review and future directions. *Journal of Hydrology*, 529, 62–81.

Scheidegger, A. (2012). adaptMCMC: Implementation of a generic adaptive monte carlo markov chain sampler. R package version 1.1.

Schellart, A., Shepherd, W., & Saul, A. (2012). Influence of rainfall estimation error and spatial variability on sewer flow prediction at a small urban scale. *Advances in Water Resources*, 45, 65–75.

Schilling, W. (1991). Rainfall data for urban hydrology: What do we need? *Atmospheric Research*, 27(1), 5–21.

Schleiss, M. & Berne, A. (2010). Identification of Dry and Rainy Periods Using Telecommunication Microwave Links. *IEEE Geoscience and Remote Sensing Letters*, 7(3), 611–615.

Schleiss, M., Olsson, J., Berg, P., Niemi, T., Kokkonen, T., Thorndahl, S., Nielsen, R., Ellerbæk Nielsen, J., Bozhinova, D., & Pulkkinen, S. (2020). The accuracy of weather radar in heavy rain: A comparative study for Denmark, the Netherlands, Finland and Sweden. *Hydrology and Earth System Sciences*, 24(6), 3157–3188.

Schleiss, M., Rieckermann, J., & Berne, A. (2013). Quantification and Modeling of Wet-Antenna Attenuation for Commercial Microwave Links. *IEEE Geoscience and Remote Sensing Letters*, 10(5), 1195–1199.

Schütze, M., Campisano, A., Colas, H., Schilling, W., & Vanrolleghem, P. (2004). Real time control of urban wastewater systems - Where do we stand today? *Journal of Hydrology*, 299(3-4), 335–348.

Segond, M.-L., Wheater, H. S., & Onof, C. (2007). The significance of spatial rainfall representation for flood runoff estimation: A numerical evaluation based on the Lee catchment, UK. *Journal of Hydrology*, 347(1-2), 116–131.

Sikorska, A. & Seibert, J. (2018). Value of different precipitation data for flood prediction in an alpine catchment: A Bayesian approach. *Journal of Hydrology*, 556, 961–971.

Sikorska, A. E., Scheidegger, A., Banasik, K., & Rieckermann, J. (2012). Bayesian uncertainty assessment of flood predictions in ungauged urban basins for conceptual rainfall-runoff models. *Hydrology and Earth System Sciences*, 16(4), 1221–1236.

Smiatek, G., Keis, F., Chwala, C., Fersch, B., & Kunstmann, H. (2017). Potential of commercial microwave link network derived rainfall for river runoff simulations. *Environmental Research Letters*, 12(3), 034026.

Spekkers, M. H., Kok, M., Clemens, F. H. L. R., & ten Veldhuis, J. A. E. (2013). A statistical analysis of insurance damage claims related to rainfall extremes. *Hydrology and Earth System Sciences*, 17(3), 913–922.

Stránský, D., Fencl, M., & Bareš, V. (2018). Runoff prediction using rainfall data from microwave links: Tabor case study. *Water Science and Technology*, 2017(2), 351–359.

Sun, Q., Miao, C., Duan, Q., Ashouri, H., Sorooshian, S., & Hsu, K.-L. (2018). A Review of Global Precipitation Data Sets: Data Sources, Estimation, and Intercomparisons. *Reviews of Geophysics*, 56(1), 79–107.

Swan, M. (2012). Sensor Mania! The Internet of Things, Wearable Computing, Objective Metrics, and the Quantified Self 2.0. *Journal of Sensor and Actuator Networks*, 1(3), 217–253.

Tauro, F., Selker, J., van de Giesen, N., Abrate, T., Uijlenhoet, R., Porfiri, M., Manfreda, S., Caylor, K., Moramarco, T., Benveniste, J., Ciraolo, G., Estes, L., Domeneghetti, A., Perks, M. T., Corbari, C., Rabiei, E., Ravazzani, G., Bogena, H., Harfouche, A., Brocca, L., Maltese, A., Wickert, A., Tarpanelli, A., Good, S., Lopez Alcala, J. M., Petroselli, A., Cudennec, C., Blume, T., Hut, R., & Grimaldi, S. (2018). Measurements and Observations in the XXI century (MOXXI): Innovation and multi-disciplinarity to sense the hydrological cycle. *Hydrological Sciences Journal*, 63(2), 169–196.

Thorndahl, S., Beven, K., Jensen, J., & Schaarup-Jensen, K. (2008). Event based uncertainty assessment in urban drainage modelling, applying the GLUE methodology. *Journal of Hydrology*, 357(3-4), 421–437.

Thorndahl, S., Einfalt, T., Willems, P., Nielsen, J. E., ten Veldhuis, M.-C., Arnbjerg-Nielsen, K., Rasmussen, M. R., & Molnar, P. (2017). Weather radar rainfall data in urban hydrology. *Hydrology and Earth System Sciences*, 21(3), 1359–1380.

Tsihrintzis, V. A. & Hamid, R. (1997). Modeling and Management of Urban Stormwater Runoff Quality: A Review. *Water Resources Management*, 11(2), 136–164.

Uhlenbeck, G. E. & Ornstein, L. S. (1930). On the theory of the Brownian motion. *Physical review*, 36, 823.

Uijlenhoet, R., Overeem, A., & Leijnse, H. (2018). Opportunistic remote sensing of rainfall using microwave links from cellular communication networks. *Wiley Interdisciplinary Reviews: Water*, 5(4), e1289.

Valtr, P., Fencl, M., & Bareš, V. (2019). Excess Attenuation Caused by Antenna Wetting of Terrestrial Microwave Links at 32 GHz. *IEEE Antennas and Wireless Propagation Letters*, 18(8), 1636–1640.

van der Pol, T., van Ierland, E., Gabbert, S., Weikard, H.-P., & Hendrix, E. (2015). Impacts of rainfall variability and expected rainfall changes on cost-effective adaptation of water systems to climate change. *Journal of Environmental Management*, 154, 40–47.

van Leth, T. C., Overeem, A., Leijnse, H., & Uijlenhoet, R. (2018). A measurement campaign to assess sources of error in microwave link rainfall estimation. *Atmospheric Measurement Techniques*, 11(8), 4645–4669.

Vezzaro, L. & Grum, M. (2014). A generalised Dynamic Overflow Risk Assessment (DORA) for Real Time Control of urban drainage systems. *Journal of Hydrology*, 515, 292–303.

Vihola, M. (2012). Robust adaptive Metropolis algorithm with coerced acceptance rate. *Statistics and Computing*, 22, 997–1008.

Villarini, G., Mandapaka, P. V., Krajewski, W. F., & Moore, R. J. (2008). Rainfall and sampling uncertainties: A rain gauge perspective. *Journal of Geophysical Research*, 113(D11), D11102.

Vrugt, J. A., ter Braak, C. J. F., Clark, M. P., Hyman, J. M., & Robinson, B. A. (2008). Treatment of input uncertainty in hydrologic modeling: Doing hydrology backward with Markov chain Monte Carlo simulation: FORCING DATA ERROR USING MCMC SAMPLING. *Water Resources Research*, 44(12).

Wang, L.-P., Ochoa-Rodríguez, S., Onof, C., & Willems, P. (2015). Singularity-sensitive gauge-based radar rainfall adjustment methods for urban hydrological applications. *Hydrol. Earth Syst. Sci.*, 19(9), 4001–4021.

Wang, L.-P., Ochoa-Rodríguez, S., Simões, N. E., Onof, C., & Maksimović, Č. (2013). Radar–raingauge data combination techniques: A revision and analysis of their suitability for urban hydrology. *Water Science and Technology*, 68(4), 737–747.

Wang, Q., Shrestha, D. L., Robertson, D., & Pokhrel, P. (2012). A log-sinh transformation for data normalization and variance stabilization. *Water Resources Research*, 48.

Willems, P., Arnbjerg-Nielsen, K., Olsson, J., & Nguyen, V. (2012). Climate change impact assessment on urban rainfall extremes and urban drainage: Methods and shortcomings. *Atmospheric Research*, 103, 106–118.

Wood, S. J., Jones, D. A., & Moore, R. J. (2000). Accuracy of rainfall measurement for scales of hydrological interest. *Hydrology and Earth System Sciences*, 4(4), 531–543.

Xiang, Y., Gubian, S., Suomela, B., & Hoeng, J. (2013). Generalized Simulated Annealing for Efficient Global Optimization: The GenSA Package for R. *The R Journal*, 5(1).

Zinevich, A., Messer, H., & Alpert, P. (2010). Prediction of rainfall intensity measurement errors using commercial microwave communication links. *Atmospheric Measurement Techniques*, 3(5), 1385–1402.

# Author's publications

The following list includes all author's publications associated with the research presented in the doctoral thesis. References to the most relevant citing research works are also included.

## Peer-reviewed journal papers

Pastorek, J., Fencl, M., Rieckermann, J., Sýkora, P., Stránský, D., Dohnal, M., and Bareš, V. (2018). **Posouzení srážkových dat z mikrovlnných spojů v městském povodí pomocí analýzy nejistot hydrologického modelu**. [The Evaluation of CML Rainfall Data in an Urban Catchment by Means of Hydrological Model Uncertainty]. *SOVAK: Časopis oboru vodovodů a kanalizací* 27, 16–22.

Pastorek, J., Fencl, M., Rieckermann, J., and Bareš, V. (2019). **Commercial microwave links for urban drainage modelling: The effect of link characteristics and their position on runoff simulations**. *Journal of Environmental Management* 251, 109522. https://doi.org/10.1016/j.jenvman.2019.109522. Cited by:

- Diba, F., Samad, M., Ghimire, J., and Choi, D. (2021). **Wireless Telecommunication Links for Rainfall Monitoring: Deep Learning Approach and Experimental Results**. *IEEE Access* 9, 66769–66780.
- Polz, J., Chwala, C., Graf, M., and Kunstmann, H. (2020). **Rain event detection in commercial microwave link attenuation data using convolutional neural networks**. *Atmospheric Measurement Techniques* 13, 3835–3853.
- Pudashine, J., Guyot, A., Overeem, A., Pauwels, Valentijn R. N., Seed, A., Uijlenhoet, R., Prakash, M., Walker, and Jeffrey P. (2021). **Rainfall retrieval using commercial microwave links: Effect of sampling strategy on retrieval accuracy**. *Journal of Hydrology* 603, 126909.
- Troemel, S., Chwala, C., Furusho-Percot, C., Henken, C., Polz, J., Potthast, R., Reinoso-Rondinel, R., and Simmer, C. (2021). **Near-Realtime Quanti-**

**tative Precipitation Estimation and Prediction (RealPEP)**. *Bulletin of the American Meteorological Society* 102, E1591–E1596.

Turko, M., Gosset, M., Kacou, M., Bouvier, C., Chahinian, N., Boone, A., and Alcoba, M. (2021). **Rainfall Measurement from Commercial Microwave Links for Urban Hydrology in Africa: A Simulation Framework for Sensitivity Analysis**. *Journal of Hydrometeorology* 22, 1819–1834.

Moroder, C. (2021). **Untersuchung des Wet-Antenna-Effekts bei Richtfunkstrecken**. Doctoral thesis, Technische Universität München. [online] http://mediatum.ub.tum.de/?id=1559781.

Riechel, M. (2022). **Integrated Modelling of Stormwater Management Strategies and CSO Impacts on Urban Rivers**. Doctoral thesis, Technische Universität Berlin. [online] https://doi.org/10.14279/depositonce-15263.

Cazzaniga, G., De Michele, C., D'Amico, M., Deidda, C., Ghezzi, A. and Nebuloni, R. **Hydrological response of a peri-urban catchment exploiting conventional and unconventional rainfall observations: the case study of Lambro catchment**. Accepted for publication in *Hydrology and Earth System Sciences*. [online] https://doi.org/10.5194/hess-2021-389.

Eshel, A., Alpert., P., and Messer, H. **Estimating the Parameters of the Spatial Autocorrelation of Rainfall Fields by Measurements from Commercial Microwave Links**. Accepted for publication in *IEEE Transactions on Geoscience and Remote Sensing*. [online] https://doi.org/10.1109/TGRS.2022.3165309.

Pastorek, J., Fencl, M., Rieckermann, J., and Bareš, V. (2022). **Precipitation Estimates from Commercial Microwave Links: Practical Approaches to Wet-Antenna Correction**. *IEEE Transactions on Geoscience and Remote Sensing* 60, 1–9. https://doi.org/10.1109/TGRS.2021.3110004. Cited by:

Špačková, A., Bareš, V., Fencl, M., Schleiss, M., Jaffrain, J., Berne, A., and Rieckermann, J. (2021). **A year of attenuation data from a commercial dual-polarized duplex microwave link with concurrent disdrometer, rain gauge, and weather observations**. *Earth System Science Data* 13, 4219–4240.

## Conference contributions

Pastorek, J., Fencl, M., Rieckermann, J., Sýkora, P., Stránský, D., Dohnal, M., and Bareš, V. (2016). "The effect of innovative rainfall data on urban drainage modelling by means of model uncertainty" in Sborník přednášek konference s mezinárodní učastí Městské vody 2016. Brno, Czech Rep., ARDEC s.r.o.

Pastorek, J., Fencl, M., Stránský, D., Rieckermann, J., and Bareš, V. (2017). "Predicting urban stormwater runoff with quantitative precipitation estimates from commercial microwave links" in Geophysical Research Abstracts. EGU General Assembly 2017. Goettingen, Germany, Copernicus GmbH. [online] http://meetingorganizer.copernicus.org/EGU2017/EGU2017-1525.pdf. Cited by:

Disch, A., Scheidegger, A., Wani, O., Rieckermann, J. (2018). "Impact of different sources of precipitation data on urban rainfall-runoff predictions: A comparison of rain gauges, commercial microwave links and radar" in Proceedings of 11th International Workshop on Precipitation in Urban Areas. Zurich, Switzerland, ETH Zurich. [online] https://www.research-collection.ethz.ch/handle/20.500.11850/347531.

Pastorek, J., Fencl, M., Stránský, D., Rieckermann, J., and Bareš, V. (2017). "Použitie zrážkových dát z mikrovlnných spojov v zrážko-odtokovom modelovaní mestských povodí" in Sborník konference Hydrologie malého povodí 2017. Praha, Czech Rep., Ústav pro hydrodynamiku AV ČR, v. v. i.

Pastorek, J., Fencl, M., Stránský, D., Rieckermann, J., and Bareš, V. (2017). "Reliability of microwave link rainfall data for urban runoff modelling" in Conference Proceedings - 14th IWA/IAHR International Conference on Urban Drainage (ICUD). Praha, Czech Rep., C-IN. Cited by:

Ochoa-Rodriguez, S., Wang, L. -P., Willems, P., and Onof, C. (2019). **A Review of Radar-Rain Gauge Data Merging Methods and Their Potential for Urban Hydrological Applications**. *Water Resources Research* 55, 6356–6391.

Zheng, F., Tao, R., Maier, Holger R., See, L., Savic, D., Zhang, T., Chen, Q., Assumpcao, Thaine H. et al. (2018). **Crowdsourcing Methods for Data Collection in Geophysics: State of the Art, Issues, and Future Directions**. *Reviews of Geophysics* 56, 698–740.

Pastorek, J., Fencl, M., Stránský, D., Rieckermann, J., and Bareš, V. (2018). "CML precipitation estimates for hydrological modelling: A three-year experiment" in Geophysical Research Abstracts. EGU General Assembly 2018. Munich, Germany, European Geosciences Union. [online] https://meetingorganizer.copernicus.org/EGU2018 /EGU2018-18667.pdf.

Pastorek, J., Fencl, M., Rieckermann, J., and Bareš, V. (2018). "Commercial Microwave Links in Urban Drainage Modelling: On Deriving Precipitation Estimates for Various Link Lengths" in Proceedings of 11th International Conference on Urban Drainage Modelling. Palermo, Italy, Ingegneria Civile, Amb., Aerosp., dei Materiali University of Palermo.

Bareš, V., Fencl, M., Stránský, D., and Pastorek, J. (2018). "Validace srážkových dat z mikrovlnných spojů pro potřeby městské hydrologie: Výsledky z pilotních lokalit" in Sborník přednášek konference s mezinárodní učastí Městské vody 2018. Brno, Czech Rep., ARDEC s.r.o.

Pastorek, J., Fencl, M., and Bareš, V. (2018). "The suitability of precipitation estimates from short CMLs for urban hydrological predictions" in Proceedings of 11th International Workshop on Precipitation in Urban Areas. Zurich, Switzerland, ETH Zurich. [online] https://www.research-collection.ethz.ch/handle/20.500.11850/347556. Cited by:

Špačková, A., Bareš, V., Fencl, M., Schleiss, M., Jaffrain, J., Berne, A., and Rieckermann, J. (2021). **A year of attenuation data from a commercial dual-polarized duplex microwave link with concurrent disdrometer, rain gauge, and weather observations**. *Earth System Science Data* 13, 4219–4240.

Pastorek, J., Fencl, M., and Bareš, V. (2019). "Calibrating microwave link rainfall retrieval model using runoff observations" in Geophysical Research Abstracts. EGU General Assembly 2019. Goettingen, Germany, Copernicus GmbH. [online] https://meetingorganizer.copernicus.org/EGU2019/EGU2019-10072.pdf.

Pastorek, J., Fencl, M., Rieckermann, J., and Bareš, V. (2019). "Long-term rainfall-runoff experiment at a small urban catchment using dense CML network" in Proceedings of Symposium on the hydrometeorological usage of data from commercial microwave link networks. Garmisch- Partenkirchen, Germany, Karlsruhe Institute of Technology. [online] https://indico.scc.kit.edu/event/570/contributions/5713/contribution.pdf.

Pastorek, J., Fencl, M., Rieckermann, J., and Bareš, V. (2020). "Commercial microwave links in urban rainfall-runoff modelling: Two different approaches to removing the bias" in EGU General Assembly 2020. Goettingen, Germany, Copernicus Publications. [online] https://meetingorganizer.copernicus.org/EGU2020/EGU2020-9384.html.

Fencl, M., Bareš, V., Pastorek, J., Mudroch, M., and Pechač, P. (2020). "Commercial Microwave Links forUrban Rainfall-runoff Modelling" in RealPeP - Precipitation and Flash Flood Prediction from Minutes to Days. Berlin, Germany, European Meteorological Society. [online] https://indico.scc.kit.edu/event/883/contributions/7568.

Pastorek, J., Fencl, M., Rieckermann, J., and Bareš, V. (2020). "The importance of adequate correction for the wet antenna effect when predicting urban rainfall-runoff using microwave link data" in AGU Fall Meeting 2020 Abstracts. Washington, USA, American Geophysical Union.

Pastorek, J., Fencl, M., Rieckermann, J., and Bareš, V. (2021). "Microwave link rainfall data for urban drainage modelling: Reducing the systematic errors under data-scarce conditions" in Conference Proceedings - 15th International Conference on Urban Drainage. Oxford, GB, International Water Association.

Pastorek, J., Fencl, M., Rieckermann, J., and Bareš, V. (2021). "Precipitation Estimates from Microwave Links for Urban Hydrology: Improving the Accuracy Using Wet-Antenna Calibration" in Proceedings of CELLular ENvironment MONitoring (CELLENMON) Workshop. Tel-Aviv, Israel, Tel-Aviv University.